

MODELING OF HYDRONIC AND ELECTRIC-CABLE
SNOW-MELTING SYSTEMS FOR PAVEMENTS
AND BRIDGE DECKS

By

XIA XIAO

Bachelor of Engineering

Tsinghua University

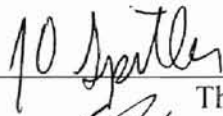
Beijing, P.R.China

2000

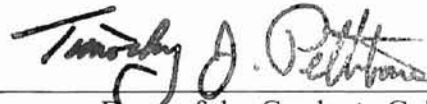
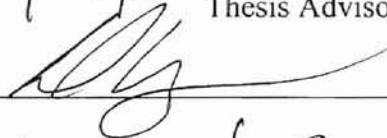
Submitted to the Faculty of the
Graduate College of the
Oklahoma State University
in partial fulfillment of
the requirements for
the Degree of
MASTER of SCIENCE
December, 2002

MODELING OF HYDRONIC AND ELECTRIC-CABLE
SNOW-MELTING SYSTEMS FOR PAVEMENTS
AND BRIDGE DECKS

Thesis Approved:



Thesis Advisor



Dean of the Graduate College

ACKNOWLEDGEMENTS

First, I wish to thank my advisor Dr. Jeffery Spitzer for his constructive guidance. His intelligent insights have given me a new perspective. Without his timely encouragement, this work would not have been done. I would like to extend my sincere gratitude and appreciation to Dr. Simon Rees who serves as the co-advisor along the course of the research and this thesis. His expertise in computational methods was quite valuable in helping me to achieve the project goals.

My sincere appreciation also extends to Dr. Strand who provided transfer functions generation program for this work. Thanks for the guidance, and his valuable suggestions to improve this work. Thanks also to my committee members for their time and patience.

A special thanks to my family. I would like to thank my parents Yuli Jia and Zhizhen Xiao for their continued support and patience throughout my life that has enabled me to be where I am today.

Last, but not least, I thank my colleagues, namely Manoj Chulliparambil, Zheng Deng, Xiaobing Liu, and Dongyi Xiao, for their ideas and suggestions along the way.

This work was partially supported by the ASHRAE RP-1090, and partially supported by the Geothermal Smart Bridge Research Project at the Oklahoma State University with the close cooperation of the Oklahoma Department of Transportation. Support from the ASHRAE and the Oklahoma Department of Transportation is gratefully acknowledged.

TABLE OF CONTENTS

Chapter	Page
1. INTRODUCTION	1
1.1. Background	1
1.2. Literature Review	2
1.2.1. Steady State Modeling	2
1.2.2. Transient Modeling	12
1.3. Thesis Objective and Scope	45
2. PARAMETRIC STUDY OF SNOW-MELTING SYSTEM	47
2.1. Introduction	47
2.2. Methodology of Parametric Study	50
2.2.1. Organization and Methodology of Parametric Study	50
2.2.2. Methodology of Center Zone Parametric Study	52
2.2.3. Methodology of Edge Zone Parametric Study	57
2.3. Results and Discussion	57
2.3.1. Center Zone Parametric Study	57
2.3.2. Edge Zone Parametric Study	74
2.4. Conclusion of Parametric Study	78
3. MODELING THE BRIDGE DECK BY TRANSFER FUNCTION METHOD	80
3.1. Introduction	80
3.2. Modeling by Transfer Function Method	81
3.2.1. Heat Transfer in Bridge Decks	81
3.2.2. Boundary Conditions	84
3.2.3. Heat Transfer at the Source Location	91
3.3. Implementing in HVACSIM+ Environment	98
3.4. Results and Discussion	99
3.4.1. One Dimensional Comparative Studies	99
3.4.2. Two Dimensional Comparative Studies	112
3.4.3. Error Analysis	115
3.5. Summary	125

4. VALIDATION OF THE QTF MODEL BY EXPERIMENTAL DATA	127
4.1. Introduction	127
4.2. Previous Work	127
4.3. System Simulation Results and Discussion	131
4.3.1. Thermal Resistance Error	132
4.3.2. Summer Recharge	133
4.3.3. Winter Heating	138
4.4. Summary	152
5. CONCLUSIONS AND RECOMMENDATIONS	154
5.1. Conclusions	154
5.2. Recommendations	156
REFERENCES	158
APPENDIXES	161
Appendix A: Description of the QTF model in <i>TYPAR.DAT</i>	162

LIST OF TABLES

Table	Page
Table 1.1: Possible Slab Surface Conditions vs. Different Initial Conditions	33
Table 2.1: Center Zone Parametric Study	51
Table 2.2: Edge Zone Parametric Study.....	52
Table 2.3: Tolerance of Minimum Fluxes.....	56
Table 2.4: Minimum Required Heat Flux (BTU/hr-ft ²) for Transient Conditions with Back Losses (Free Area Ratio = 1.0)	60
Table 2.5: Normalized Minimum Required Heat Flux for Transient Conditions with Back Losses (Free Area Ratio = 1.0)	61
Table 2.6: Minimum Required Heat Flux (BTU/hr-ft ²) for Transient Conditions with Back Losses (Free Area Ratio = 0.0)	68
Table 2.7: Normalized Minimum Required Heat Flux for Transient Conditions with Back Losses (Free Area Ratio = 0.0)	69
Table 2.8: Maximum Percentage Back Loss (BTU/hr-ft ²) for Transient Conditions (Free Area Ratio = 1.0).....	72
Table 2.9: Maximum Percentage Back Loss for Transient Conditions (Free Area Ratio = 0.0)	73
Table 2.10: Minimum Free Area Ratio near the Edge for Transient Conditions (Free Area Ratio = 1.0)	76
Table 2.11: Maximum Percentage Edge Losses for Transient Conditions (Free Area Ratio = 1.0).....	77
Table 3.1: Parameters Used for One-dimensional Analytical and Numerical Testing ...	100
Table 3.2: Parameters Used for Two-dimensional Study	112
Table 3.3: Tests Summary for Two Dimensional Hydronic Heating Cases	117

Table 3.4: Summary of Thermal Resistances [K-m ² /W]	121
Table 4.1: Comparison of Simulation Results of OSU Bridge Deck under Simplified Boundary Conditions	132
Table 4.2: List of Thermal Resistances in the Numerical Simulation of OSU Bridge Deck [K-m ² /W]	132

LIST OF FIGURES

Figure	Page
Figure 1.1: Solution domain for 2-D transient heat conduction equation.....	15
Figure 1.2: Finite difference cell geometry and notation (by Chiasson, et al. 2000).....	17
Figure 1.3: Local coordinate systems at the east face of a typical finite volume cell.....	19
Figure 1.4: The finite-difference model grid and boundary conditions	21
Figure 1.5: An example of a boundary fitted grid for 1090-RP.....	22
Figure 1.6: Four-block definition of the slab containing a pipe.....	23
Figure 1.7: Mass transfer to/from the snow layer.	36
Figure 1.8: Mass transfer to/from the slush layer.....	36
Figure 1.9: Schematic representation of heat transfer in the snowmelt model	37
Figure 2.1: Representation of soil and slab for edge and center zone.....	49
Figure 2.2: The Flow Chart for the Minimum Flux Search	55
Figure 2.3: Weather conditions and loads for Spokane, $A_r=1$	62
Figure 2.4: Weather conditions and loads for OKC, $A_r=1$	62
Figure 2.5: Weather Conditions and Loads for Salt Lack City, $A_r=1$	64
Figure 2.6: Artificially Modified Storm in Salt Lake City, $A_r=1$	64
Figure 2.7: Distribution of the surface heat flux (Buffalo, 12" spacing)	67
Figure 2.8: Surface conditions at the controlling hour (Buffalo, 12" spacing).....	67
Figure 2.9: Colorado Springs Storm with Warm Conditions prior to Snowfall	70
Figure 2.10: Grid Sample for Edge Zone Simulation	74
Figure 3.1: Typical arrangement of bridge deck heating pipe loop.	82
Figure 3.2: Flow chart for the NTU method	97
Figure 3.3: Profile of the ambient air temperature	100

Figure 3.4: Comparison of numerical and analytical solutions for top and bottom surface temperatures (Test TC2).....	101
Figure 3.5: Profile of the top ambient air temperature.....	102
Figure 3.6: Comparison of numerical and analytical solutions for bottom surface fluxes (Test TC3).....	102
Figure 3.7: Comparison of numerical and analytical solutions for top and bottom surface fluxes (step change in the input function).....	105
Figure 3.8: Comparison of numerical and analytical solutions for temperature at source location (step change in the input function).....	105
Figure 3.9: Comparison of numerical and analytical solutions for top and bottom surface fluxes (input function period of 24 hours).....	107
Figure 3.10: Comparison of numerical and analytical solutions for temperature at source location (input function period of 24 hours).....	107
Figure 3.11: Comparison of numerical and analytical solutions for top and bottom surface fluxes (input function period of 3 hours).....	109
Figure 3.12: Comparison of numerical and analytical solutions for temperature at source location (input function period of 3 hours).....	109
Figure 3.13: Comparison of numerical and analytical solutions for the temperature and the heat flux at the source location.....	111
Figure 3.14: Comparison for the temperature at the bottom surface.....	112
Figure 3.15: Comparison of top surface fluxes obtained from different models.....	113
Figure 3.16: Comparison of source fluxes obtained from different models.....	115
Figure 3.17: Electrical analog of heat transfer through the pipe and slab.....	122
Figure 4.1: Comparison of experimental data and model predictions for top surface temperatures in summer recharge mode.....	133
Figure 4.2: Comparison of experimental data and model predictions for exit fluid temperatures in summer recharge mode.....	134
Figure 4.3: Comparison of experimental data and model predictions for exit fluid temperatures in summer recharge mode (with modified mass flow rate).....	135

Figure 4.4: Comparison of experimental data and model predictions for top surface temperatures in summer recharge mode (with modified mass flow rate)	136
Figure 4.5: Comparison of experimental data and model predictions for heat transfer rates in summer recharge mode (with modified mass flow rate).....	137
Figure 4.6: Percentage error of the QTF predictions to experimental data on heat transfer rates in summer recharge mode (with modified mass flow rate)	138
Figure 4.7 (b): Weather information for snow event of Dec.30, 2001 (IP Units).....	140
Figure 4.8: Comparison of initial model predictions against experimental data in winter heating case (snow event of Dec.30, 2001, snow albedo=0.8)	143
Figure 4.9: Effect of the sky temperature correction on the top surface temperature predictions in winter heating mode (snow event of Dec.30, 2001, snow albedo=0.8)	146
Figure 4.10:Effect of the value of snow albedo on the top surface temperature predictions in winter heating mode (snow event of Dec.30, 2001, snow albedo=0.38, with sky temperature correction)	147
Figure 4.11: Comparison of experimental data and model predictions for slab surface temperatures in winter heating mode (snow event of Dec.30, 2001, time varying snow albedo, with sky temperature correction)	148
Figure 4.12: Comparison of experimental data and model predictions for slab surface temperatures in winter heating mode (snow event of Dec.30, 2001, estimated snow albedo = 0.8, no sky temperature correction, with consideration of saturated surface condition)	149
Figure 4.13:comparison of experimental data and model predictions in winter heating mode (snow event of Dec.30, 2001, time-varying snow albedo, with the sky temperature correction and no consideration of saturated surface condition)	151

NOMENCLATURE

α	thermal diffusivity (ft ² /h [m ² /s])
ε	effectiveness
A_i	inside pipe wall area (ft ² [m ²])
A_o	outer pipe wall area (ft ² [m ²])
A_r	free area ratio
c_p	specific heat (Btu/lb.°F)
d	inside pipe diameter (ft[m])
D	outer pipe diameter (ft[m])
f, w	transfer function coefficients for heat source calculation
F, W	transfer function coefficients for slab surface calculation
g	golden section ratio
h	heat transfer coefficient (BTU/hr-ft ² -°F [W/m ² -K])
I	solar flux (Btu/hr-ft ² [W/m ²])
k	thermal conductivity (BTU/hr-ft-°F [W/m-K])
L	length (ft [m])
LWR	long-wave radiation flux (Btu/hr-ft ² [W/m ²])
m	mass flow rate (lb/s [kg/s])
NTU	the number of transfer units
Nu	Nusselt number
Pr	Prandtl number
q	heat flux (Btu/hr-ft ² [W/m ²])
Q	heat flux (Btu/hr-ft [W/m])
R	thermal resistance (°F-ft ² -hr/BTU [K-m ² /W])
Re	Reynolds number

ρ	density (lb/ft ³ [kg/m ³])
t	time
T	temperature (°F [°C])
μ	absolute viscosity (lbm/ft-s [kg/m-s])
UA	overall heat transfer coefficient (BTU/hr-ft ² -°F [W/m ² -K])
x, y, z	transfer function coefficients for heat source calculation (BTU/hr-ft ² -°F [W/m ² -K])
X, Y, Z	transfer function coefficients for slab surface calculation (BTU/hr-ft ² -°F [W/m ² -K])

Subscripts

btm	bottom
$conv$	convective
$cond$	conductive
i	input, inlet
l	loss, low limit
o	outlet
src	heat source
$surf$	slab surface
top	top
u	upper limit

1. Introduction

1.1. Background

Hydronic and electric-cable snow-melting systems utilize heating from pipes or electrical cables embedded in the surface for pavement de-icing. Hydronic and electric-cable snow-melting systems are installed in a wide range of applications, such as sidewalks, driveways, steps, toll plazas, and bridges where icing is a serious hazard to safety. Chapman (1957) classifies snow-melting installations as three types based on the necessary of maintaining the pavement free of snow and ice. The “minimum” type is used in residential sidewalks or driveways. The “moderate” type is used in applications such as, commercial sidewalks and driveways, and hospital steps. The application in toll plazas of highways and bridges, aprons and loading area of airports, and hospital emergency entrances are classified as the “maximum” type.

As the size and the number of applications of these systems increase, economic optimization becomes increasingly important. One method to reduce the installation and operation costs is through a better design of the system. Optimization must be based on the size of the system, the frequency of operation, and the pattern of operation. Since snowfall occurs less than 10% of the time in most U.S. cities, operation of the systems is intermittent. Therefore, both transient and steady operation must be considered in the system design.

Previous research and published design guidelines for snow-melting systems (e.g. Chapman 1952a, Ramsey et al. 1999a) have generally been based on steady state conditions. Procedures for calculating the design heating requirements of snow-melting systems are given in the ASHRAE Handbook-HVAC Applications (ASHRAE 1999). In this type of calculation no account is taken of the history of the storm, and no account is taken of the dynamic response of the slab. In practical operation, the design heat transfer rate may never be provided at the surface instantaneously. Thermal mass of the heating system and the transient nature of the weather significantly affect the actual operation. A transient tool is highly recommended for a thorough understanding of the heat transfer characteristics of the systems, and is required for a better design of hydronic and electric-cable snow-melting systems.

1.2. Literature Review

Modeling of hydronic and electric cable snow-melting systems involves solving the slab heat conduction equation along with heat and mass balance equations for the surfaces. Most of the models can be broken into two categories: steady state or transient.

1.2.1. Steady State Modeling

Prior to 1952, the energy requirements considered in the design of a snow melting system were the energy required to melt the snow (heat of fusion), and the energy loss to the ground below. Heat and mass transfer requirements on the surface were ignored. In 1952, Chapman et al recognized additional complexities of the design. Between 1952 and 1957, Chapman et al. published a series of articles on design of snow melting system, in

which authors established a general equation for energy requirements on snow melting system design, and presented examples under a large range of weather conditions. All of these research papers describe one-dimensional steady state analysis.

The first article, by Chapman and Katunich (1952a), asserts that the energy losses, such as evaporation and convection, are always significant and should not be ignored. The authors stated that the complete analysis depends on five energy terms, the sum of which equals the total required heat output from the heating plant. These five terms are heat of fusion, sensible heat gain from snowfall, heat of vaporization, heat transfer by radiation and convection, and back loss to the ground. The sum of the first four terms equals the required pavement heat output at the upper surface, as shown in equation (1.1).

$$q_o = q_s + q_m + q_h + q_e \quad (1.1)$$

where,

q_o = total required heat flux off surface of slab, Btu/hr-ft² [W/m²],

q_s = sensible heat needed to raise the snow to its melting temperature, Btu/hr-ft² [W/m²],

$$= mc_i(t_f - t_a) \quad (1.1-a)$$

where

$m = 5.2s$, lb(snow)/hr-ft², (density of liquid water is 5.2 lb/ft²-in),

s = snowfall rate, inches(water equivalent)/hr [mm/hr],

c_i = specific heat of ice= 0.5 Btu/lb-°F,

t_f = water film temperature, °F [°C], 33°F has been used.

t_a = air temperature, °F [°C]. It's assumed that the temperature of the snow equals the temperature of the air.

$$\text{so, } q_s = 2.6 \cdot s \cdot (t_f - t_a) \quad (1.1-b)$$

$$\begin{aligned} q_m &= \text{heat required to melt snow (heat of fusion), Btu/hr-ft}^2 \text{ [W/m}^2\text{]}, \\ &= 143.4m = 5.2 \cdot s \cdot 143.4 = 746s \end{aligned} \quad (1.1-c)$$

$$\begin{aligned} q_h &= \text{convective and radiative heat flux, Btu/hr-ft}^2 \text{ [W/m}^2\text{]}, \\ &= f_c \cdot (t_f - t_a) \end{aligned} \quad (1.1-d)$$

where, f_c is a combined heat transfer coefficient; v is wind velocity, mph [m/s],

$$f_c = 11.4 \cdot (0.0201v + 0.055). \quad (1.1-e)$$

Constants are empirical data.

$$\begin{aligned} q_e &= \text{heat flux needed for evaporation, Btu/hr-ft}^2 \text{ [W/m}^2\text{]}, \\ &= (a \cdot v + b) \cdot (p_{wv} - p_{av}) \cdot h_{fg}. \end{aligned} \quad (1.1-f)$$

Where $a=0.0201$ and $b=0.055$ are empirical constants; p_{av} is vapor pressure of water in the air in inches of Hg; p_{wv} is vapor pressure of water at the surface in inches of Hg.

The total heating plant load q_t can be estimated by dividing the total heat output required at the surface of the slab q_o by efficiency e , as $q_t = q_o/e$, where $e=1.0-f$, f is the back loss fraction. The back loss fraction is obtained by analogy to the back loss analysis for a radiant heating slab to the ground. The author didn't give more information on how to calculate the back loss for a radiant heating slab. But he suggested that if the snow-melting system is operated intermittently, back loss may be in the neighborhood of 30 to 50%, depending on insulation; if the system is operated continuously, the instantaneous

back loss will be reduced, but would probably be as high as 30% if the slab is not insulated. It may also be noted that equation (1.1) implied that the slab surface is assumed totally snow-free.

The second article, published by Chapman (1952b), established the principle that the design energy output should be based on a frequency distribution of the loads. The article stressed that the correct procedure is to determine the actual load on an hourly basis, then make a frequency distribution analysis to set the design capacity that is adequate for a given number of hours of snowfall annually. In this article, the author introduced the concept of free area ratio, which is defined as the ratio of snow free area to total area. Selecting a proper design ratio according to the actual application requirement was recommended. With the concept of free area ratio, equation (1.1) can be updated as:

$$q_o = q_s + q_m + A_r(q_h + q_r) \quad (1.2)$$

where, A_r is snow-free area ratio, dimensionless. In this case, it is assumed that the snow-covered portion of the slab is insulated from convection, radiation and evaporation effects. When the free area ratio, A_r , is equal to zero, the slab is completely covered with snow. When the free area ratio, A_r , is equal to one, the slab is completely free of snow. This condition requires the maximum energy supply to the slab. The purpose of the slab determines the necessary performance, and thus establishes the desired free area ratio, for instance, A_r must be high for a bridge ramp, and may be low for a private driveway.

Chapman and Katunich (1956) published extended research results on heat requirements of snow melting systems. The general equation given in previous papers

was substantiated by experimental data, and the overall heat transfer coefficient, used in the calculation of heat and mass transfer to the environment, was corrected by experimental data to cover periods of no snowfall (idling periods) as well as operating period.

Two types of snow melting panels were used in the experiments. One consisted of 10 one-foot square panel made up of insulated nichrome heating elements spaced on $\frac{3}{4}$ inch centers under $\frac{1}{2}$ inch of cement mortar. The other panel was a round panel having an area of 10 ft². Its heating elements and insulations were similar to those of square panels. Power inputs to the panels were adjusted to maintain difference thickness of snow under equilibrium conditions. All measurements, such as free area ratio, mass and heat transfer, and fluid temperatures, were made when the panels were under equilibrium conditions. Experimental data were then summarized in a tabular format to allow use in design applications. The idling equation given to represent the convection and radiation transfer from a dry slab to the environment was presented as follows:

$$q_b = (0.27v + 3.3) \cdot (t_p - t_a) \quad (1.3)$$

where, q_b is heat transfer from a bare panel, Btu/hr-ft² [W/m²]. t_p is panel surface temperature, °F [°C].

Chapman (1957) presented a concluding article on the calculation of heat requirements for snow melting systems in all parts of the United States. The states were divided into eleven climatic regions. For each region, several cities were chosen as representatives. The cities chosen to represent each region have similar weather patterns.

For the Northeast region, the representative cities are Buffalo, Burlington, and Caribou. Each has the typical weather pattern of the northeastern United States, that is, the weather is varied and changeable, and the winters are prolonged and moderately cold with considerable snowfall. Punch cards and a statistical tabulating machine were used to derive the values and frequency distribution of each of the pertinent climate variables, such as humidity, wind speed, air temperature, and snowfall rate. The heat requirements for representative cities were calculated and presented for each region.

Four tables are included in the paper to allow use in design applications. The first table gives generalized information on snowfall for each representative city, such as mean number of inches per year of snowfall, and the greatest depth of snow on ground. The second table contains the operating information of a snow melting system for each representative city under the period of freezing and the period of snowfall. The “freezing period” occurs when there is no snowfall and the air temperature is 32°F or below, and the system may be “idling”. The average air temperature during freezing period is tabulated, and is used in calculating the “idling” load. The most important information represented in the second table is the frequency distribution of required heat output during the period of snowfall to maintain the free area ratio of one or zero. For example, during the period of snowfall in Chicago, to maintain a snow-free pavement, 37.4% snowfall hours require heat output in the range 50-99 Btu/ft²-hr, and 11.4 % snowfall hours require heat output in the range 100-149 Btu/ft²-hr, etc. This distribution is served as the basis for the third and the fourth tables. The third table contains the design heat requirement based on the classification of snow melting systems described in the section

1.1. Designers may adjust the idling rate according to the requirements of the application and recalculate the design heat requirement. The fourth table contains data required to estimate the operating costs of a snow melting system, such as idling/melting hours per year, and heat output per year for each class of system.

Schnurr and Rogers (1970) provided data for the heat flux and tube surface temperature requirements as functions of tube spacing, depth, diameter, and weather conditions for embedded tube snow-melting system. In this paper, a two-dimensional model was presented. As opposed to previous studies, the two-dimensional model allows the calculation of temperature distribution on the slab surface and does not assume uniform heat output at the surface. The assumptions made were that the system is in steady state operation, and the tube surface temperature is uniform. Authors stated the condition for an acceptable tube surface temperature is that the minimum pavement surface temperature is $33 \pm .5^{\circ}\text{F}$. The solution is obtained by a numerical relaxation method. A square grid with a spacing of $\frac{1}{4}$ pipe outside diameter is specified to approximate the solution domain. Equations for the temperature at each nodal point are derived by making a steady state energy balance on the nodal point and expressing terms involving temperature gradients in finite difference form. The general equation provided by Chapman (equation (1.1)) is used to establish the heat balance for each cell on the top surface. A parametric study was made with the tube diameter, tube depth, tube spacing, and weather conditions being varied. For each case, necessary heat flux and tube surface temperature to achieve a slab surface temperature of $33 \pm .5^{\circ}\text{F}$ under steady-state conditions, are found.

Kilkis (1994) published two papers on the design of embedded snow-melting systems. In the first paper, the author points out that ASHRAE guidelines seem to overestimate heat requirements due to three main factors—empirical equations that overestimate the surface heat losses, the absence of wind speed and terrain adjustment, and the way in which snowfall frequency data are interpreted. As can be seen from equation (1.1-d), the analysis doesn't recognize the split between radiant and convective losses, which are sensitive to different atmospheric factors. The empirical coefficients in equation (1.1-f) are obtained from the idling test setup, therefore, the method may overestimate the evaporation load for large surfaces, as the convection coefficient and mass transfer coefficients will be higher on smaller surfaces. Most of the wind data available are recorded at 33 ft above ground level in open fields while snow melting is usually performed at ground level, with some exceptions. Therefore, the meteorological wind data must be adjusted with respect to surrounding terrain and the height of the snow-melting surface. To avoid elaborate snowfall frequency analysis, the concept of coincident air temperature was defined to facilitate engineering calculations. Due to the small amount of humidity that cold air can hold, a heavy snowfall is usually accompanied by a rise in the air temperature, so that, the design outdoor temperature and a heavy storm do not coincide. Coincident air temperature is defined as the air temperature corresponding to the design rate of snowfall. In deriving an expression for the coincident air temperature, the typical relationships between air temperature, rate of snowfall, and snow-melting loads were considered. Comparative studies with snowfall frequency

analysis revealed a simplistic, nearly linear expression for the coincident air temperature with the design outdoor temperature.

In the other paper by Kilkis (1994b), a finite volume model is presented to model steady-state behavior while accounting for the two-dimensional geometry. The sides of the snow-melting surface are assumed to be covered with snow, with a surface temperature equal to the coincident air temperature. This surface is permitted to exchange heat by radiation with the sky. Heat transfer occurring at the snow-melting surface are as those described in equation (1.2). However, the author didn't give more information on the way to approximate the two-dimensional geometry in the numerical analysis. It states that the model achieves sufficient accuracy for engineering calculations, and comparisons indicate a close agreement with other reports, such as the report on "successfully operating" systems for 93 locations in the United States given by Potter (1967).

Ramsey (1999a) presented some results of ASHRAE research project 926, "Development of Snow Melting Load Design Algorithm and Data for Locations Around the World." In total, 46 locations in the U.S. were studied. The changes in the calculation procedure described by Chapman (1952) are primarily in the way heat losses are determined. The convective heat transfer rate is evaluated using currently accepted correlation for the turbulent convection heat transfer coefficient from a surface (Incropera and Dewitt 1996). The radiation losses are evaluated using an effective sky temperature (Ramsey et al. 1982) that is based on the dry-bulb air temperature, relative humidity, and sky cover fraction. The analogy between mass and heat transfer is used to determine the

water vapor mass transfer coefficient. The convection and evaporation losses are functions of the wind speed and the characteristic dimension of the slab. Results are presented in terms of frequency distribution that indicate the percentage of time (hours when snow is falling) that the required snow-melting load doesn't exceed the reported value. However, results also demonstrate that for a given load requirement, the distribution of the load in terms of melting, convection, radiation, and evaporation varies greatly. It points out that to accurately estimate snow-melting load, concurrent weather data are critical. A conclusion stated in the final report of RP-926 is: "Exhaustive study failed to identify an acceptable simplified approach to design snow melting systems for locations with limited meteorological data" (Ramsey et al. 1998).

In steady-state calculations, neither the history of the storm nor the dynamic response of the heated slab has been taken into account. In practical applications, the time constant of the system is on the order of hours. The design heat flux can never be achieved at the surface instantaneously. It implies that the surface may not reach the design conditions promptly as required, and to satisfy the design conditions, the actual heating element load differs from steady state load. As Chapman stated in the second paper he published in 1952, the correct procedure is to determine the actual load hourly, then make frequency analysis. A transient simulation tool is needed to calculate actual surface conditions with consideration of transient response of the system, and then further estimate the heating capacity needed to maintain a satisfactory surface condition.

Not only does the heating system have significant thermal mass but also the weather is highly transient. Ramsey's study in RP-926 shows that concurrent weather data is critical to estimate the load. A successful transient model needs to be able to simulate the transient characteristics of both snow-melting system and the weather condition. Transient models are reviewed in the next section.

1.2.2. Transient Modeling

The objective of transient modeling is to determine transient performance of hydronic and electric cable snow-melting systems under realistic transient weather conditions. The problem can be considered as two parts, one is the modeling of the two-dimensional transient heat conduction inside the slab, and the other is the modeling of heat and mass transfer between the slab surfaces and the environment.

In the following section, a brief summary of previous work on transient modeling is given. This is followed by a detailed review of a finite difference bridge deck model original developed by Chiasson, *et al* (2000), and a finite volume model for a snow-melting system developed by Rees, *et al* (2001). Last comes a brief literature review on the application of transfer function method in solving the transient heat conduction problem.

1.2.2.1 Previous Work

Besides the one dimensional steady-state approach adopted with ASHRAE, most previously published models of snow melting systems either model steady state behavior

while accounting for the two-dimensional geometry (e.g. Schnurr and Rogers 1970) or have modeled transient behavior while only accounting for one-dimensional geometry (e.g. Williamson 1967). Two exceptions are papers by Leal and Miller (1972) and Schnurr and Falk (1973).

Based on the steady state model given by Schnurr and Rogers (1970), Leal and Miller (1972) presented a transient analysis of the two-dimensional model. The transient heat conduction problem is solved by the “point-matching” technique using a digital computer. But the authors didn’t give more information on the “point-matching” technique in the paper. The general equation provided by Chapman (equation (1.1)) has been implemented for calculating the heat balance on the surface boundaries. The bottom boundary is assumed perfectly adiabatic. The results presented are not under the actual snow-melting conditions. This paper, speaking strictly, only presents an attempt to show transient conditions for snow melting system.

Schnurr and Falk (1973) presented a two-dimensional transient model for the snow-melting system. The transient problem is solved by an explicit finite difference technique. The problem had been taken as a “mixed boundary” type with one cylindrical boundary (the tube). But it’s unclear from the paper how the mixed boundary was handled. The authors stated that square grids have been used for representing the solution domain in the numerical calculation. Adiabatic assumption is used for the bottom boundary, while the general equation provided by Chapman (equation (1.1)) has been applied for the top boundary. To design for no snow accumulation at any time, it assumed

that the system is activated some length of time (lead time) before the snowfall begins. Only the convective heat transfer has been taken into account before snowfall. All terms in the general equation are used after snowfall begins. Constant weather conditions are used in the examples. Assumption that the snowfall rates are constant throughout a storm may lead to ultra conservative lead time requirements. Transient weather conditions are crucial in snow melting system simulation.

1.2.2.2 Comparison of the Finite Difference Model and the Boundary-fitted Coordinate Finite Volume Model

Two transient two-dimensional snow melting models, developed at Oklahoma State University, are discussed in this section. The finite difference model is described in detail by Chiasson, *et al.* (2000). It is used to simulate a hydronic-heated bridge. The conduction heat transfer is modeled using a finite difference algorithm. For the sake of simplicity, the finite difference model is abbreviated to FD model in this thesis.

The boundary-fitted coordinate finite volume model was developed by Rees, *et al.* (2001) for ASHRAE research project 1090. The boundary fitted coordinate technique was used to deal with the mixed geometry of the snow melting system, and the finite volume technique is applied in the numerical calculation. The work of this project was partially a continuation of RP-926. In particular, the same weather data was used in both projects and many of the heat transfer relationships used in the previous project have been utilized in RP-1090. The objectives of this project were primarily to develop a model (the boundary-fitted coordinate finite volume model) that allows transient effects

of both weather and the dynamic response of the slab system to be modeled simultaneously. This model was used to examine some general design issues such as the effects of pipe spacing, depth, and insulation placement, edge and back losses. The boundary-fitted coordinate finite volume model is abbreviated as BFC-FV model in this thesis.

In the following section, comparisons between models are given as four parts: heat conduction in the slab, grid generation, boundary conditions, and initial conditions.

- **Heat Conduction in the Slab**

Symmetry considerations reduce the problem to the determination of the temperature in the typical segment shown in Figure 1.1. This typical solution domain for the slab with tubes is from the pipe centerline to the plane of symmetry.

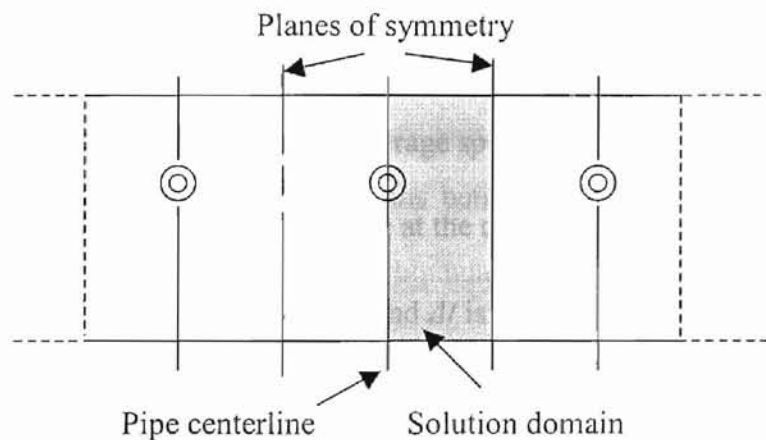


Figure 1.1: Solution domain for 2-D transient heat conduction equation.

a) FD model

Transient conduction heat transfer in the slab is represented in two-dimensional (2-D) cross-section using the Cartesian coordinate system. A fully explicit finite difference method has been used to discretize the governing equation. The transient 2-D heat conduction equation can be expressed as

$$\frac{\partial^2 T}{\partial x^2} + \frac{\partial^2 T}{\partial z^2} = \frac{1}{\alpha} \frac{\partial T}{\partial t} \quad (1.4)$$

The notation of finite difference cell is shown in Figure 1.2.

An energy balance equation is established for each node. The general form of the nodal equation from the explicit finite difference scheme is

$$\sum_{i=1}^4 q_i''(t-\Delta t) A = V \rho c_p \left(\frac{T_{(m,n)}' - T_{(m,n)}^{(t-\Delta t)}}{\Delta t} \right) \quad (1.5)$$

where $q_i''(t-\Delta t)$ is the heat flux across the cell face i at the previous time step, A is the cell face area per unit depth, V is the cell volume per unit depth, ρ is the average density of the cell material, c_p is the average specific heat capacity of the cell material, $T_{(m,n)}'$ is the nodal temperature at the current time step, $T_{(m,n)}^{(t-\Delta t)}$ is the nodal temperature at the previous time step, and Δt is the time step. The conduction heat flux q'' between neighboring nodes i and (m,n) is given by Fourier's Law as:

$$q_{i \rightarrow (m,n)}'' = k \frac{T_i - T_{(m,n)}}{l} \quad (1.6)$$

where k is the average thermal conductivity of the material between nodes i and (m,n) , and l is the distance between two nodes, equals nodal spacing.

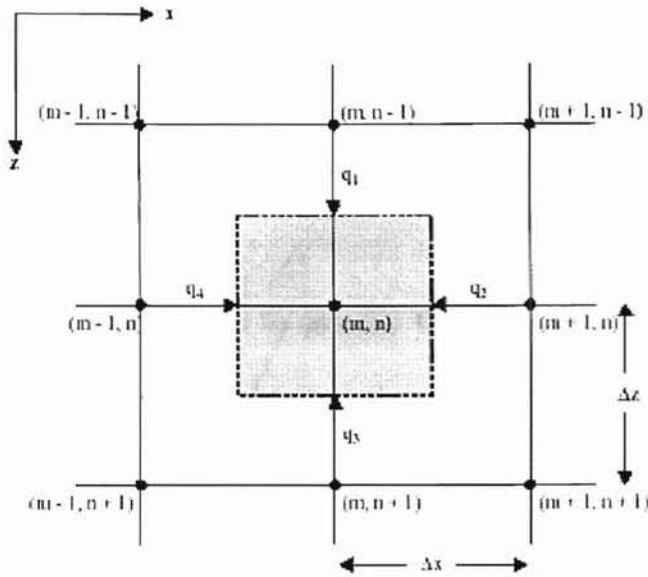


Figure 1.2: Finite difference cell geometry and notation (by Chiasson, et al. 2000).

Note that the numerical scheme used in the model is fully explicit; with a certain nodal spacing, the size of the time step is limited by the need to maintain the stability criterion for two-dimensional problems.

b) BFC-FV model

GEMS2D (General Elliptical Multi-block Solver) (Rees, *et al.* 2001), a finite volume solver, is used as the main solver in the BFC-FV model. GEMS2D is capable of solving the general convection-diffusion equation on two dimensional boundary fitted grids. The FVM (finite volume method) starts from the integral form of Fourier's equation for heat conduction.

$$\frac{\partial}{\partial t} \int_V \phi dV = \int_S \Gamma \nabla \phi \cdot \mathbf{n} dS \quad (1.7)$$

where ϕ is the temperature and Γ is the thermal diffusivity, V is the volume and S is the surface of a control volume and \mathbf{n} is a vector normal to the surface. The left-hand

term of the equation is the temporal term and the right-hand term represents the diffusion fluxes. A physical space approach for dealing with complex geometries can be derived from the vector form of the equation above.

A second order approximation is to assume that the value of the variable on a particular face is well represented by the value at the centroid of the cell face. The diffusion flux at the east face of a cell can be written as:

$$F_e^D = \int_{S_e} \Gamma \nabla \phi \cdot \mathbf{n} dS \approx (\Gamma \nabla \phi \cdot \mathbf{n})_e S_e \quad (1.8)$$

where S_e is the area of the east face.

The main difficulty is in calculating the gradient of the variable ($\nabla \phi$) at each cell face when grids are not orthogonal. The formula $F_e^D \approx \Gamma_e S_e (\partial \phi / \partial \xi)_e$ is only accurate if the grid is orthogonal. To describe the geometry more clearly, two local coordinates are defined at the cell face as shown in Figure 1.3. In the direction normal to the face at its centroid, the coordinate n is defined, and on the line between neighboring centroids, the coordinate ξ which passes through the face at point e' is defined.

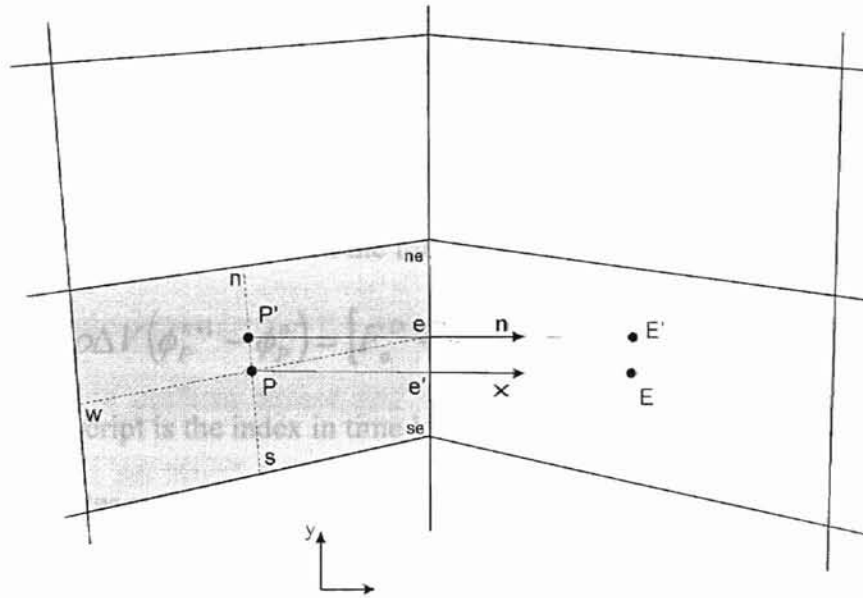


Figure 1.3: Local coordinate systems at the east face of a typical finite volume cell.

To preserve second order accuracy, the gradient needs to be calculated along the normal to the face and at the centroid of the face by using the values of the variable at points P' and E'. However, in GEMS2D, the values of the variable at the cell centroid P and E are still used to calculate the gradient of the variable, and a 'deferred correction' approach is used to calculating the flux as follows:

$$F_e^D = \Gamma_e S_e \left(\frac{\partial \phi}{\partial \xi} \right)_{e'} + \Gamma_e S_e \left[\left(\frac{\partial \phi}{\partial n} \right)_e - \left(\frac{\partial \phi}{\partial \xi} \right)_{e'} \right]^{old} \quad (1.9)$$

The gradients are calculated by central differencing. The terms labeled 'old' on the right are calculated explicitly. As the solution approaches convergence the terms $(\partial \phi / \partial \xi)_{e'}$ and $(\partial \phi / \partial \xi)_{e'}^{old}$ cancel out, leaving $(\partial \phi / \partial n)_n$. $(\partial \phi / \partial n)_n$ is calculated explicitly from the central difference $(\phi_{P'} - \phi_{E'}) / L_{PE'}$. Interpolation is required to get $\phi_{P'}$ and $\phi_{E'}$.

In FVM, the partial differential equation is integrated with respect to time. A first order backwards differencing approach is used in a fully implicit formulation. The fully implicit approach results in the following discretized equation,

$$\rho \Delta V (\phi_p^{n+1} - \phi_p^n) = [F_n^D + F_s^D + F_w^D + F_e^D]^{n+1} \Delta t \quad (1.10)$$

where superscript is the index in time level. The discretized equation can then be said to be first-order accurate in time and second-order accurate in space. This scheme is unconditionally stable. After integrating the p.d.e and applying the discretization procedures discussed, an algebraic equation is obtained for each control volume of the form,

$$a_p \phi_p = \sum a_{nb} \phi_{nb} + b \quad (1.11)$$

For a two-dimensional model this results in a penta-diagonal matrix equation that can be solved conveniently using the Strongly Implicit Method (Stone 1968).

The main advantages of GEMS2D are that the convection-diffusion problem with the complex geometry can be solved more accurately, and the numerical scheme has no limitation on the size of steps in time and space.

- **Grid Generation**

Numerical grids are used to define the geometry of the solution domain for both the FD and BFC-FV programs. The geometry of the snow-melting system, or the bridge deck, is a mixed type problem, with the circular pipes embedded in the flat slab. The

models use different coordinate systems to represent the geometry. The FD model uses a rectangular coordinate system, while the 1090 model uses a boundary fitted approach.

a) FD model

A typical grid scheme used in the finite difference model is shown in Figure 1.4. As can be seen, a uniform square grid scheme is used. The nodal spacings in both directions are set equal to the pipe radius. The orthogonal coordinates and the uniform grid size make the two-dimensional heat conduction equation relatively easy to discretize and arrange. The orthogonal grid pattern also avoids the correction that is necessary in the gradient calculation of the variable along the normal to the face in a non-orthogonal grid pattern.

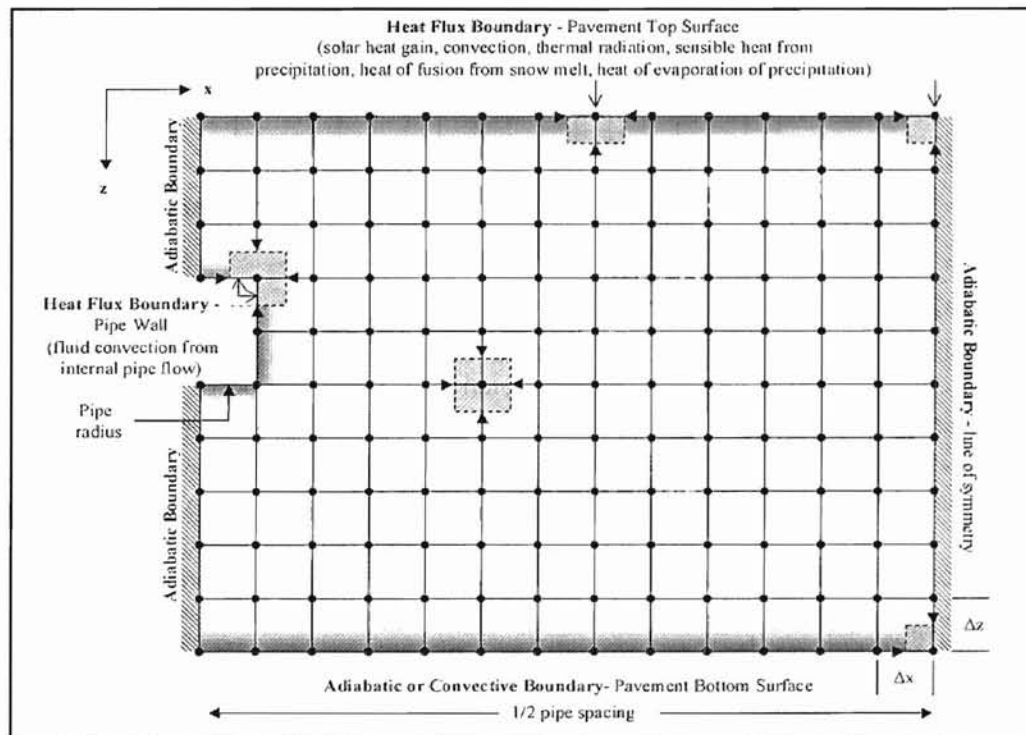


Figure 1.4: The finite-difference model grid and boundary conditions
(by Chiasson, 2000)

b) BFC-FV Model

The BFC-FV model uses boundary fitted coordinated grid system to deal with the mixed geometry problem. In this type of grid system, the cells are arranged in a structured manner but are deformed where necessary to allow the geometry of the domain boundaries to be followed very closely (Thompson *et al.* 1985). A typical boundary fitted grid sample used in 1090-RP is shown in Figure 1.5.

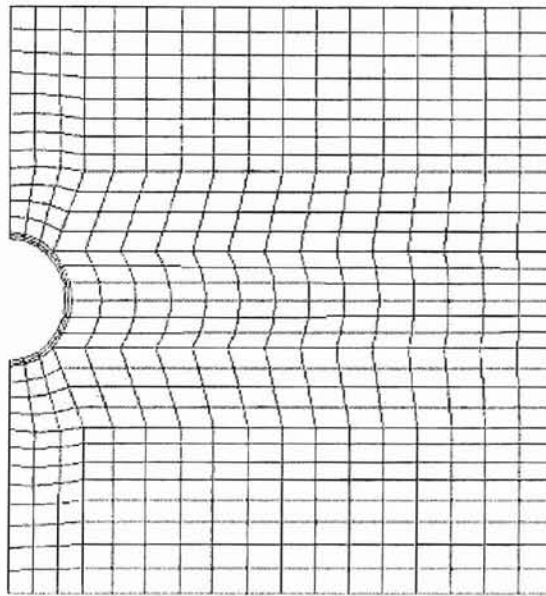


Figure 1.5: An example of a boundary fitted grid for 1090-RP

The numerical method used here is a multi-block approach. The grid outline is defined by a few design parameters provided by the user, such as pipe size, slab thickness, pipe depth and pipe spacing (RP-1090 Final Report). Then, the geometry is broken down into a number of sub-domains or blocks. Within each of these blocks, the grid cells are arranged in a regular row and column manner, and each of the blocks is effectively ‘glued’ to one or more others at the block edges. This enables more complex geometries to be defined and allows better control over the

grid cell distribution. A four-block grid definition of the slab containing a pipe is shown in Figure 1.6. Tests show that this four-block definition gives better control over grid spacing and orthogonality than the definitions with fewer blocks.

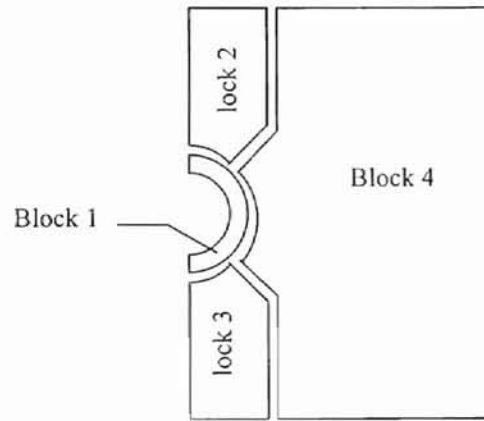


Figure 1.6: Four-block definition of the slab containing a pipe.

Grid quality is determined by smoothness, cell aspect ratio and orthogonality. A satisfactory grid quality is achieved by controlling the number of cells and the distribution of nodes along each edge. A procedure was developed for ASHRAE 1090 RP for this purpose. The main criteria are summarized as follows.

- 1) In general, 25 edges and 4 blocks are necessary to specify the grid represent the pipe and single pavement layer.
- 2) Additional pavement layers are taken as whole blocks.
- 3) It's desirable to increase cell density towards the pipe both horizontally and vertically. This is controlled by specifying different cell distribution functions at the block edges.
- 4) The cell size should change gradually.

The advantage of the boundary fitted grids is that the geometry and pipe-wall boundary condition can be represented more exactly. A simple algebraic grid generation algorithm (Gordon and Hall 1973) is applied to calculate the cell vertex positions in each block from a description of the geometry boundaries. This grid information then is supplied to the main solver of the model.

- **Boundary Conditions**

The main difficulty in boundary conditions is how to model the transient effect of weather conditions on the top surface. The following paragraphs introduce the boundary conditions applied to the FD model and BFC-FV model. Compared to the previous models that apply the relationships (equation (1.1a-1.1f)) given by Chapman (1952) at the upper boundary, the FD model is a great improvement in that it considers convective and radiant losses occurred at the upper surface separately, hence, the effect of different atmospheric factors, such as cloudiness and sky temperature, can be investigated more accurately. The BFC-FV model presents a more detailed top boundary condition model. It's capable of giving a detailed analysis of the mass transfer among snow, ice, slush, etc.

For the boundary at the pipewall, the BFC-FV model uses a boundary-fitted grid scheme to deal with the mixed geometry problem, while the FD model uses the square grid to approximate the heat transfer area of the pipewall.

a) FD model

The boundary conditions are flux-type (Neumann boundary condition). The temperature at each boundary node is given by the energy balance equation at that node.

Boundary conditions at the top and bottom surface

The bottom surface is treated either as an insulated surface or as a surface exposed to convective and radiant conditions. The top boundary condition is treated as flux-type (Neumann boundary condition). The environmental interactions on the top surface include the effects of solar radiation heat gain, long-wave radiation heat transfer, convection heat transfer to the atmosphere, sensible heat transfer to snow, heat of fusion required to melt snow, and heat of evaporation lost to evaporating rain or melted snow. In the following paragraphs, a brief introduction to the first three flux terms is given. This is followed by a more detailed introduction on the last three flux terms.

Solar radiation heat gain is the net solar radiation absorbed by the slab surface, and is decided by the absorptivity of the slab material, solar radiation incident on the slab surface and the cosine of the incident angle. The long-wave radiation heat transfer at each surface node is determined by the emissivity of the slab material, the nodal temperature, and the temperature of the surroundings. The convection heat flux at each pavement surface node is computed by the dry-bulb air temperature and the nodal temperature, and the convective heat transfer coefficient is taken as the

maximum of the free convection coefficient and the forced convection coefficient which can be found in Incropera and DeWitt (1996).

Heat flux due to the rain and snow includes both sensible and latent effects. Sensible heat flux is decided by precipitation and temperature difference between the dry-bulb air temperature and the nodal temperature. Latent heat flux is considered only if the air temperature or the slab surface temperature is above 33°F (0.55°C). There are two kinds of latent heat flux that may be considered. One is the latent heat of vaporization, and the other is the heat flux due to melting snow and ice. Both of them relate to the mass transfer occurred on the surface. One main assumption made for mass transfer is: accumulation of rain is not considered; rainfall is assumed to drain instantaneously from the pavement surface, forming a thin film from which evaporation occurs.

This model uses the j-factor analogy to compute the mass flux of evaporating water at each pavement surface node (\dot{m}_w''):

$$\dot{m}_w'' = h_d (w_{air} - w_{(m,1)}) \quad (1.12)$$

where h_d is the mass transfer coefficient, w_{air} is the humidity ratio of the ambient air, and $w_{(m,1)}$ represents the humidity ratio of saturated air at the surface node. The mass transfer coefficient (h_d) is defined using the Chilton-Colburn analogy:

$$h_d = \frac{h_c}{c_p Le^{2/3}} \quad (1.13)$$

where h_c is the convection coefficient, c_p is the specific heat capacity of the air evaluated at the pavement node - air film temperature, and Le is the Lewis number.

The heat flux due to evaporation ($q''_{evaporation}$) is then given by:

$$q''_{evaporation} = h_{fg} \dot{m}''_w \quad (1.14)$$

where h_{fg} is the latent heat of vaporization.

The heat flux due to melting snow and ice is determined using a mass balance on freezing precipitation that has accumulated at the pavement surface. The sum of the rainfall rate and the snowfall rate are taken as the accumulation of the ice when the air temperature or the slab surface temperature is below 33°F. The mass flux of water due to melting ice ($\dot{m}''_{icemelted}$) at the pavement surface is then given by:

$$\dot{m}''_{icemelted} = \frac{q''_{solar} + q''_{thermal} + q''_{convection} + q''_{rain,snow_sensible} + q''_{evaporation} + q''_{conduction,ice}}{h_{if}} \quad (1.15)$$

where $q''_{conduction,ice}$ is the conduction heat flux from the pavement surface into the ice layer and h_{if} is the latent heat of fusion of water. The other heat flux terms are solar radiation heat gain q''_{solar} , long-wave radiation heat transfer $q''_{thermal}$, convection heat transfer $q''_{convection}$ to the atmosphere, sensible heat transfer $q''_{rain,snow_sensible}$ to snow, and heat of evaporation $q''_{evaporation}$ lost to evaporating rain or melted snow. The numerator in equation (1.16) is the heat flux into each pavement surface node ($q''_{(m,1)}$):

$$q''_{(m,1)} = -q''_{solar} + q''_{thermal} + q''_{convection} + q''_{rain,snow_sensible} + q''_{evaporation} + q''_{conduction,ice} \quad (1.16)$$

The thickness of the ice layer at the end of the time step ($l_{ice,new}$) is given by:

$$l_{ice,new} = l_{ice,old} - \left(\frac{\dot{m}_w'' + \dot{m}_{icemelted}''}{\rho_{ice}} \right) \Delta t. \quad (1.17)$$

Boundary conditions at the pipe wall

The boundaries of the left and right hand of the solution domain are adiabatic, except the boundaries of the pipe surface nodes. Heat fluxes at these nodes are determined by the heat transfer due to heat exchange fluid as equation (1.18).

$$q''_{fluid} = U_{pipe} (T_{fluid} - T_{(m,n)}) \quad (1.18)$$

where the average fluid temperature T_{fluid} is used to characterize the fluid. U_{pipe} is the overall heat transfer coefficient for the pipe and expressed as:

$$U_{pipe} = \frac{1}{\frac{1}{h_{pipe}} + \frac{l}{k_{pipe}}} \quad (1.19)$$

where h_{pipe} is the convection coefficient due to fluid flow through the pipe, k_{pipe} is the thermal conductivity of the pipe material, and l is the wall thickness of the pipe.

Since the outlet temperature at any current time step is not known, the outlet fluid temperature is solved in an iterative manner. The iteration is considered converged when the heat flux calculated by the resistance method is consistent with that resulted from the overall energy balance calculation.

Boundary conditions implemented in the FD model have two main shortcomings.

The model can't give the mass distribution of each phase on the surface nodes. In

this model, although snow is a porous medium, it is treated as an equivalent ice layer, and it hasn't considered the interactions among snow, slush, and ice. Thus, the heat and mass transfer calculation for the surface is relatively rough. Approximating the round geometry at the source location by square grids enlarges the actual heat transfer area, and the model tends to over-predict the heat transfer rate occurring at the boundary. As can be seen from Figure 1.4, the nodes labeled as pipe wall do not represent the pipe geometry well. They are actually nodes in the concrete that have direct contact with the outer pipe wall. The square grid scheme used in the FD model doesn't include the pipe in the solution domain. In addition to causing steady state error, it may cause error early on in the transient response.

b) BFC-FV Model

Boundary conditions at the pipe wall

The boundary condition at the pipe wall is specified in a relatively simple form in the BFC-FV model. Users can specify either the constant heat flux at the pipe wall as the boundary condition, or the average fluid temperature and Reynolds number.

Boundary conditions at the bottom surface

The bottom surface is treated either as a surface exposed to convective and radiant conditions, or as a surface in contact with the ground. In modeling an exposed condition where the slab is not ground coupled, such as in a bridge or ramp, a simple boundary condition is applied. In this case the surface is assumed dry and exposed to

the wind, but not exposed to the sky. Convective and long-wave radiant heat transfer to surroundings is considered.

In the case that soil is considered beneath the slab, users can decide whether to include an insulation layer at the slab bottom, and set the ground temperature of the very lower surface of the ground if necessary. Otherwise, the BFC-FV model would specify a ground temperature as the bottom boundary condition for the model. A one-dimensional analytical solution developed by Kusuda and Achenbach (1965) is applied to calculate the annual temperature cycle at the surface of the earth. It makes use of a simple harmonic function based on simplified conduction theory, where it is assumed that earth is a semi-infinite homogeneous heat-conducting medium, with constant thermal diffusivity. The harmonic function provided in the paper is expressed as:

$$t = A - BOe^{-\left(\sqrt{\frac{\pi}{DT}}\right)x} \cos\left(\frac{2\pi\theta}{T} - \left(\sqrt{\frac{\pi}{DT}}\right)x - PO\right) \quad (1.20)$$

where,

x = downward distance from the earth's surface, ft [m],

t = earth temperature, °F [°C],

θ = time coordinate which is taken as zero on January 1st,

T = period of the temperature cycle (8766 hour),

A = annual average earth temperature °F [°C],

BO = earth surface temperature amplitude, radians,

PO = earth surface temperature phase angle, radians,

D = thermal diffusivity of the earth ft²/hr [m²/hr].

The paper provides information regarding A , BO , PO , and D for many locations around U.S. However, for locations for which the values of A , BO , PO , and D are not available, the values corresponding to the nearest location available in Kusuda and Anchebach (1965) have been used.

Boundary conditions at the top surface

The BFC-FV model includes a boundary condition model to present more detailed temperature and mass distributions on the slab upper surface. The boundary condition model is a collection of heat and mass sub models for each type of surface condition that may occur. The approach to this aspect of the modeling task has been to treat the snow layer as quasi one-dimensional. Each surface node on the two-dimensional slab is coupled to an instance of the surface boundary condition model. The function of the boundary condition model is to identify a number of possible surface conditions and apply the sub models to calculate the temperature and mass distribution at local nodes. Which model is applied to calculate the surface condition at the end of current time step of the simulation is decided based on the conditions at the end of the last time step, the current type of precipitation, and the current surface temperature.

There are a variety of surface conditions that may occur. The slab may be dry, covered in "slush", or solid ice. The slab may be wet not only because of rain but also at the final stages of melting. The surface condition is determined from the surface temperature and the mass of ice and water on each cell. A summary of the

possible current conditions, and the possible conditions at the end of the time step, are given in Table 1.1. The surface conditions that have been considered are defined as follows:

Dry: The surface is free of liquid and ice. The surface temperature may be above or below freezing.

Wet: The surface is above freezing and has some liquid retained on it, but no ice.

Dry Snow: The snow has freshly fallen snow on it but no liquid. The snow can be regarded as a porous matrix of ice. The surface temperature is below freezing so that snow is not currently being melted.

Slush: The surface contains ice in the form of snow crystals that are fully saturated with water. Water penetrates the ice matrix to the upper surface. The surface temperature is at the freezing point.

Snow and Slush: The surface contains snow that is partly melted. The lower part of the snow is saturated with water and the upper is as dry snow. This is the general melting snow condition and the surface temperature is at freezing point.

Solid Ice: The ice on the surface is in solid form rather than porous like snow. The surface temperature must be below freezing.

Solid Ice and water: The surface consists of solid ice and water. This can occur when rain falls on solid ice or when the solid ice is being melted. Melting can be from below or above. The surface temperature is at freezing.

Table 1.1

Possible Slab Surface Conditions vs. Different Initial Conditions

Note: unlikely conditions are indicated in parenthesis.

Initial Surface Condition	Precipitation Condition		
	None	Rain	Snow
1. Dry	1	2,6	1, 3, 4, 5, (2)
2. Wet	1, 2, 6	2, 6, (1)	2, 4, 6
3. Dry snow layer	3, 4, 5, (2)	4, 5	3, 4, 5, (2)
4. Slush layer	2, 4, 6, (1)	2, 4, 6, (1)	2, 4, 5, (7)
5. Snow & Slush	4, 5, (6, 7)	4, 5, (6, 7)	4, 5, (6, 7)
6. Solid ice layer	2, 4, 6	2, 4, 6	5, 7, (4)
7. Solid ice & water	7, 6, 2, 1, (4)	7, 2, 6	5, 7, (2, 4)

The calculation of surface conditions requires simultaneous consideration of both heat and mass transfer, and keeping track of the mass of both ice and liquid on each cell at each step. For example, the mass of dry snow is calculated through the calculation of the height of the saturated layer in the snow; the mass of the solid ice is calculated if the situation arises. Keeping track of the masses of each phase and type of solid requires the integration of the melting rate, evaporation rate, and the rate of liquid runoff. The rules used to define the surface condition by mass and temperature information are as follows:

The surface is assumed **dry** unless;

If the mass of liquid is greater than zero and the mass of ice is zero the condition is **wet**;

If the mass of liquid is greater than zero and the mass of ice is greater than zero and the mass of snow is greater than zero, it is assumed to be **snow and slush**;

If the mass of liquid is greater than zero and the mass of ice is greater than zero, but the mass of snow is zero, it is assumed **slush**;

If the mass of liquid is zero and the mass of ice is greater than zero and the mass of snow is greater than zero, it is assumed to be **dry snow**;

If the mass of liquid is zero and the mass of solid ice is greater than zero, but the mass of snow is zero, it is assumed to be **solid ice**;

If the mass of liquid is greater than zero and the mass of solid ice is greater than zero, but the mass of snow is zero, it is assumed to be **solid ice and water**.

The boundary conditions of the finite volume solver can be specified as fixed temperature, fixed flux, or a linear mixed condition. The boundary conditions are highly non-linear as phase change occurs at the boundary. It is necessary to have a much more complicated model for the calculation of the slab surface temperature that is more loosely coupled to the finite volume solver.

The finite volume solver (GEMS2D) is coupled to the boundary condition model by passing surface temperature information and heat flux information between the two models. Because the temperature becomes fixed at the point of melting, it is necessary that the finite volume solver pass the surface flux it has calculated to the boundary condition model. The boundary condition model then calculates the surface temperature and the mass condition under this surface flux input. The new surface temperature is, in turn, passed back to the finite volume solver. This iterative process is considered converged when the heat flux calculated by the finite volume solver becomes consistent with the surface temperature calculated by the boundary condition model.

There are seven pairs of sub models corresponding to seven types of surface conditions that may occur as tabulated in Table 1.1. For brevity, only the melting snow model is discussed in detail.

The melting snow model

First, conceptually the snow during the melting process is considered as a layer of “dry” snow (ice crystals with no liquid water), and a layer of saturated snow (slush) adjacent to the slab surface. Both the snow layer and the saturated layer may be considered as porous media. The dry snow layer has air in the void space between the snow crystals, and the saturated layer has water in the void space between the snow crystals.

The mass transfers of interest to or from the snow layer are shown in Figure 1.7. The snowfall rate is determined from weather data. Snowmelt rates are determined based on an energy balance, to be discussed below. Sublimation isn't included in the model, as it seemed an insignificant effect. It is also assumed that as melting occurs the slush-snow line will move so that previously dry snow will become saturated slush. Mass transfers to and from the saturated (slush) layer are shown in Figure 1.8.

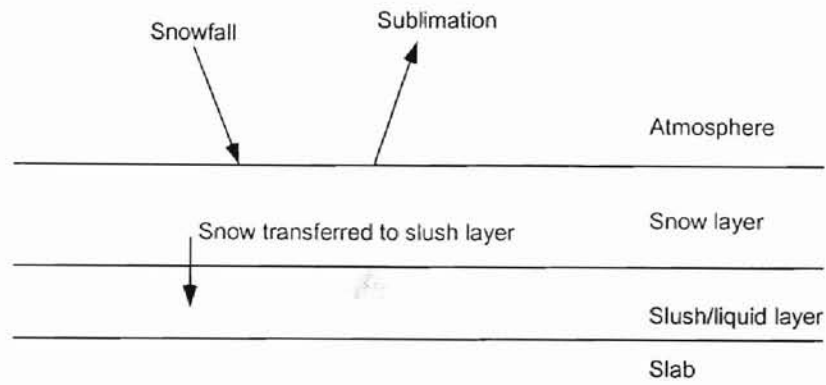


Figure 1.7: Mass transfer to/from the snow layer.

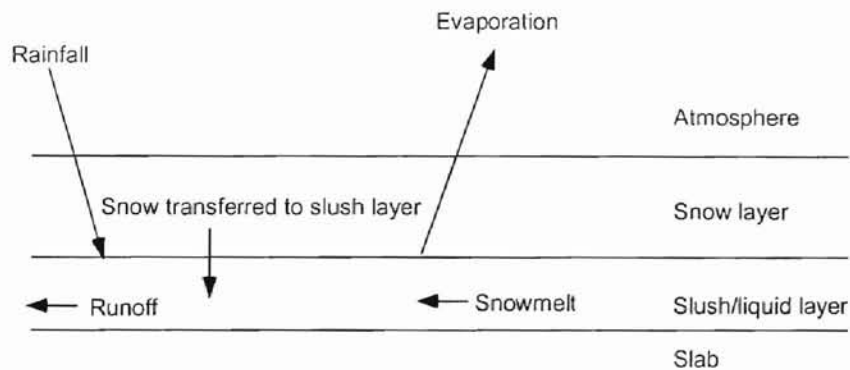


Figure 1.8: Mass transfer to/from the slush layer

All of the mass transfer processes described above have some corresponding heat transfer. In addition, convection and radiation from the top surface of the snow layer and conduction heat transfer to and through the snow and slush layers are important. The approach adopted in the model employs three nodes – one at the upper surface of the snow layer, one in the center of the snow layer and one at the saturated (slush) layer. This model is represented schematically in Figure. 1.9.

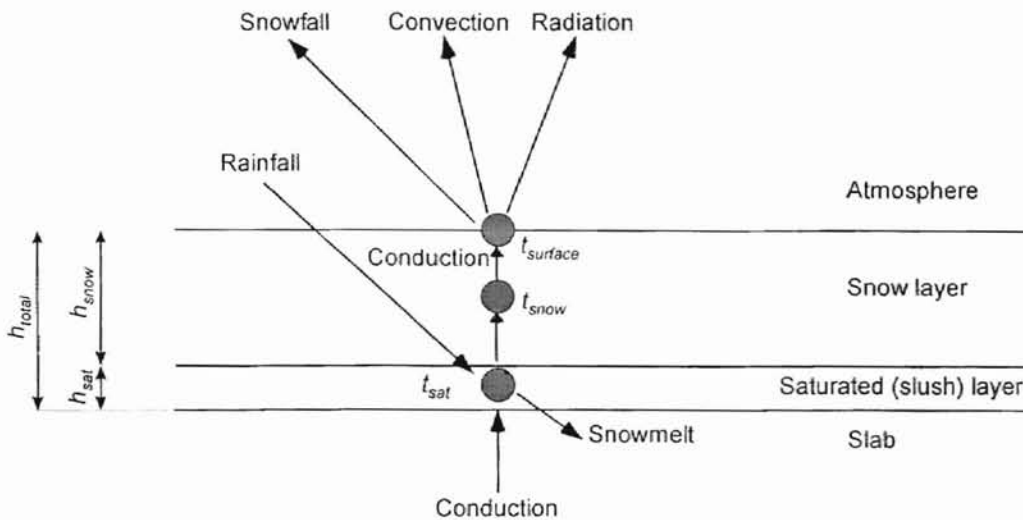


Figure 1.9: Schematic representation of heat transfer in the snowmelt model

A number of assumptions are made with this model. These include:

- Uniform temperature in the slush/liquid layer.
- Melting of snow occurs at the lower node only, either at the interface between the snow and slush layers, or in the slush layer.
- Transfer of solid snow from the snow layer to the slush layer is explicitly accounted for in the mass balance. However, from a heat transfer standpoint, it may be neglected. Because the lower node covers both the slush layer and the bottom of the snow layer, it makes no difference whether the snow melts at the interface or in the slush layer. Therefore, no heat transfer path accounting for the transfer of solid snow from the snow layer to the slush layer is shown in Figure 1.9.
- While convection from the upper surface of the snow is accounted for, convection due to airflow through the porous snow layer is neglected. The model does not necessitate neglecting this convection, so it may be included if further research indicates that it is important.

- Likewise, convection and evaporation from the slush layer are neglected (when covered with a layer of dry snow).
- Rainfall occurring after a snow layer has formed is accounted for directly only at the saturated layer.
- The snow melting process is treated as a quasi-one-dimensional process.

The model is formed by five primary equations – a mass balance for the solid ice, a mass balance for liquid water, and a heat balance on each node. The mass balance on the ice is given by:

$$\frac{dm_{ice}}{d\theta} = \dot{m}''_{snowfall} - \dot{m}''_{melt} \quad (1.21)$$

where,

m_{ice} = the mass of snow per unit area in the snow layer, lbm/ft² [kg/m²],

θ = the time, hr or s

$\dot{m}''_{snowfall}$ = the snowfall rate in mass per unit area, lbm/(hr-ft²) [kg/s-m²],

\dot{m}''_{melt} = mass rate of snow that is transferred to the slush in solid form, lbm/(hr-ft²) or [kg/s-m²].

The mass balance on the liquid is given by:

$$\frac{dm_l}{d\theta} = \dot{m}''_{melt} + \dot{m}''_{rain} - \dot{m}''_{runoff} \quad (1.22)$$

m_l = the mass of liquid water per unit area in the slush layer, lbm/ft² [kg/m²],

\dot{m}''_{rain} = the rainfall rate in mass per unit area, lbm/(hr-ft²) [kg/s-m²],

\dot{m}_{melt}'' = the snowmelt rate in mass per unit area, lbm/(hr-ft²) [kg/s-m²],

\dot{m}_{runoff}'' = the rate of runoff in mass per unit area, lbm/(hr-ft²) [kg/s-m²].

A simple heuristic approach has been taken to estimate the amount of runoff. In order to approximate the effect of water being retained in the snow due to capillary action, the runoff is limited to 10% of the melt rate until the saturated layer is 2 inches thick. The runoff rate is increased to the melt rate after this point in order to prevent more water being retained.

In order to calculate the heat balances on the snow and saturated layers it is necessary to work out the total mass of these two layers. This can be done by assuming an effective porosity (or relative density) and calculating the thickness of these layers. The total height of the snow and slush layers can be found from the mass of ice by:

$$h_{total} = \frac{m_{ice}}{\rho_{ice}(1 - n_{eff})} \quad (1.23)$$

where

h_{total} = the total thickness of the snow and saturated layers, ft [m],

n_{eff} = the effective porosity of the ice matrix (applies to both layers), dimensionless,

ρ_{ice} = the density of ice, lbm/ft³ [kg/m³].

The height of the saturated layer can be calculated from the mass of liquid,

$$h_{sat} = \frac{m_l}{\rho_l n_{eff}} \quad (1.24)$$

The height of the snow layer can be found by subtracting, $h_{snow} = h_{total} - h_{sat}$. Having worked out the height of the respective layers their mass of the dry snow layer can be found:

$$m_{snow} = \rho_{ice} h_{snow} (1 - n_{eff}) \quad (1.25)$$

The mass balance equations are coupled to the energy balance equations by the melt rate. The energy balance on the snow layer is given conceptually as:

$$m_{snow} c_p \frac{dt_{snow}}{d\theta} = q_{conduction,snow}'' - q_{snowfall}'' - q_{convection}'' - q_{radiation}'' \quad (1.26)$$

However, each of the various terms must be defined in additional detail. The conduction heat flux from the slush layer to the snow layer is given by:

$$q_{conduction,snow}'' = \frac{k_{snow}}{0.5h_{snow}} (t_{slush} - t_{snow}) \quad (1.27)$$

where

k_{snow} = the thermal conductivity of the snow. Btu/(hr-ft-F) [W/m-K],

t_{sat} = the temperature of the slush layer, °F [°C],

t_{snow} = the temperature of the snow node, °F [°C],

The heat flux due to snowfall is given as:

$$q_{snowfall}'' = \dot{m}_{snowfall}'' c_{p,ice} (t_{snow} - t_a) \quad (1.28)$$

The convective heat flux is given by:

$$q''_{convection} = h_c(t_{surface} - t_a) \quad (1.29)$$

The radiative heat flux is given by:

$$q''_{radiation} = \sigma \epsilon_s (T_{surface}^4 - T_{MR}^4) \quad (1.30)$$

$T_{surface}$ is the absolute temperature of the slab surface, and T_{MR} is the absolute mean radiant temperature of surroundings. Under snowfall condition, surroundings are approximately at the ambient air temperature. When there is no snow precipitation, the mean radiant temperature is approximated by the following equation:

$$T_{MR} = [T_{cloud}^4 F_{sc} + T_{sky\ clear}^4 (1 - F_{sc})]^{1/4} \quad (1.30-a)$$

where, F_{sc} is the fraction of the radiation exchange that takes between slab and clouds, T_{cloud} is the absolute temperature of clouds, and $T_{sky\ clear}$ is the absolute temperature of clear sky.

The snow surface temperature is found from a heat balance on the surface node:

$$t_{surface} = t_{snow} - \frac{k_{snow}}{0.5h_{snow}} (q''_{convection} + q''_{radiation}) \quad (1.31)$$

The surface temperature has to be determined iteratively for the radiation and heat balance calculation at each node. The slush layer is presumed in thermodynamic equilibrium so that the temperature of the slush is uniform at melting point. Then, the energy balance is given by:

$$\dot{m}''_{melt} h_{if} = q''_{conduction,slab} + q''_{rainfall} - q''_{conduction,snow} \quad (1.32)$$

Assuming rainwater will be at the air temperature, the heat flux due to rainfall is given by:

$$q''_{rainfall} = \dot{m}''_{rainfall} c_{p,water} (t_a - t_{slush}) \quad (1.33)$$

The mean radiant temperature and convection coefficient are calculated in the same manner as in Ramsey *et al.* (1999a).

The boundary condition model of the BFC-FV model also has disadvantages. The heat flux from solar radiation is not considered. This may be acceptable under design snowfall weather conditions. But to determine actual system performance, solar radiation needs to be considered. The price for the detailed treatment of the mass and temperature distribution on the surface is the computing time. Much time has been spent on the iteration between the main solver and the boundary condition model.

As noted in the section of grid generation, the pipe is included in the solution domain. The boundary conditions at the pipe nodes can be specified as usual types, fixed temperature, fixed flux, or a linear mixed condition. Temperatures at these nodes are solved by the main solver with the other nodal temperatures inside the domain.

- **Initial Conditions**

In a transient calculation, the initial conditions applied to the calculation can be just as significant as the boundary conditions. For the FD model, the initialization is

relatively simple- all the nodal temperatures are set to the dry bulb air temperature at the simulation starting time, and as described in the previous section, the bottom is set adiabatic. In the BFC-FV model, the initial slab and the ground temperatures have been initialized according to location and weather conditions.

In order to take account of ground heat transfer, it is necessary not only to specify the temperature at the bottom boundary (the lower surface of the ground), but also to calculate the temperature profile through the calculation domain. This temperature profile is driven by the ground temperature and the weather prior to the storm event. Therefore, the BFC-FV model extends the period of simulation to include many more hours before the start of the storm. The approach taken involves using a one-dimensional model of slab and ground. The ground temperature is specified at the lower boundary, and a two-week period is simulated. To initialize the two-dimensional model, the final temperature profile calculated using the one-dimensional model is taken and used to define the initial temperatures (according to cell depth) over the 2D grid. For each storm, the two-dimensional calculation is made of six hours of weather data before the start of any snow precipitation.

1.2.2.3 Transfer Function Method

Transient heat transfer in the two-dimensional slab can be solved numerically in a variety of ways. The models mentioned above use numerical methods- finite difference and finite volume. However, these methods have drawbacks in computational efficiency because a large number of cells have been used to ensure accuracy. Another possible

modeling method is a time series method. Generally, this method requires less time in computing. Several of the detailed building energy analysis programs such as EnergyPlus use a time series solution to transient heat conduction in building wall. The most basic time series solution is the response factor equation, which relates the flux at one surface of an element to an infinite series of temperature histories on both sides. The conduction transfer formulation replaces the infinite series of temperatures with a finite number of temperature and flux history terms.

The basic form of a conduction heat transfer function (CTF) solution without a heat source or sink, giving heat flux at the inside surface, is shown as follows:

$$q_{i,t}'' = \sum_{m=1}^M X_m T_{i,t-m+1} - \sum_{m=1}^M Y_m T_{o,t-m+1} + \sum_{m=1}^k F_m q_{i,t-m}'' \quad (1.34)$$

Where k is the order of the conduction transfer functions, M is a finite number defined by the order of the conduction transfer functions, and X , Y , and F are the conduction function coefficients. The equation relates the current heat flux at the interior surface via a linear, algebraic equation to temperature and heat flux histories.

Strand (1995, 1997) developed and verified heat source transfer functions (QTFs) for transient heat conduction with a source or sink. As with the CTFs, the QTFs can be derived by a Laplace transform or a state space method while the heat source transmitted to the slab is treated as a definable, variable input. The QTFs are in a similar form to the CTFs as:

$$q_{i,t}'' = \sum_{m=1}^M X_{k,m} T_{i,t-m+1} - \sum_{m=1}^M Y_{k,m} T_{o,t-m+1} + \sum_{m=1}^k F_m q_{i,t-m}'' + \sum_{m=1}^M W_m q_{source,t-m+1} \quad (1.35)$$

Where, X , Y , Z , F and W are the heat source transfer function coefficients. The heat source history is taken into the consideration. The QTF method is described in more detail in Chapter 3.

1.3. Thesis Objective and Scope

This study aims at modeling transient performance of the hydronic heating/cooling system. The study is intended to achieve a better understanding of systems to establish better design guidelines in future. The three main objectives of this study can be summarized as follows:

- 1) Develop and implement a parametric study of snow-melting systems for ASHRAE 1090-RP. Examine general design issues such as the effects of pipe spacing, depth, insulation placement, and edge and back losses under the transient weather conditions and system operations.
- 2) Develop a new heated bridge deck model based on the time series method (QTFs).
- 3) Use the model to analyze the performance and behavior of actual bridge deck heating systems.

Chapter 2 of this thesis addresses the first objective. The snow-melting model developed for ASHRAE 1090-RP is used to simulate the transient response of the slab during the storm event. A center zone is evaluated for 360 cases of various configurations. The minimum heat fluxes that are required to achieve the specified free area ratio are found for these cases. The back losses are examined. An edge zone is

studied with 180 cases of various configurations. The minimum fluxes found in the center zone study are applied in the edge zone cases. The surface conditions achieved in the edge zone are checked. The edge losses are examined.

Chapter 3 of this thesis addresses the second objective. The development and validation of a bridge deck model based on the time series method is presented. The simulation results are compared with the analytical solution and results from other software.

Chapter 4 of this thesis addresses the third objective. The model based on the time series method is applied to predict the performance of a hydronic bridge deck system under real weather conditions. The heating mode and the recharge mode are examined. Results are compared to experimental measurements.

Finally, Chapter 5 of this thesis summarizes the conclusions of the individual studies.

2. Parametric Study of Snow-Melting System

2.1. Introduction

The transient behavior of snow-melting systems is caused by dynamic weather conditions and intermittent system operation. The thermal mass in the system is quite significant and introduces significant time lag into the system. The thermal history of the system and the transient nature of the weather have been taken into account in this chapter.

The work of this chapter has been performed as a part of the ASHRAE 1090-RP (research project). The numerical method is based on the earlier contributions of the project. This project is aimed at studying the significance of transient effects on the snow-melting system performance. This chapter describes an investigation of the effects of two phenomena on the transient snow-melting system behavior. One is back and edge losses, and the other is transient design conditions and operation of the snow-melting system. Two parametric studies are described. The studied parameters include pipe spacing, pipe depth, pipe diameter, insulation level, soil conductivity, location, and storm. The minimum pipe fluxes have been found to maintain either:

- A free area ratio of one, for all hours of the storm, except a number of hours equivalent to the number of hours for which the steady-state 99% non-exceedance conditions were exceeded (the concept of the steady-state 99% non-exceedance condition is introduced below).

- Or, for the free area ratio of zero case, the minimum pipe flux was found that only allowed the snow height to increase for a number of hours equivalent to the number of hours for which the steady-state 99% non-exceedance conditions were exceeded.

If input pipe flux is less than the minimum, the surface can't achieve or maintain the specified free area ratio. Some terminology is defined as follows.

- A certain percentile steady-state load and non-exceedance conditions

The steady-state loads (according to the ASHRAE 926-RP calculation procedure) for each location were calculated for 12 years of available data for a free area ratio of 1.0 or 0.0. Sorting of all the hours of data according to the size of load allows different percentile loads to be found. For a given storm, the number of hours the steady-state loads are above a particular percentile can be counted. There are four percentiles conventionally considered, namely the 99, 95, 90, and 75 percentile.

The number of hours in the storm above the percentile of interest is probably a good indication of the severity of the storm. The steady-state percentile non-exceedance condition is that the steady-state loads of a given storm are below the specified percentile.

- Heat fluxes

Heat flux supplied to the pipe is called input heat flux or input flux. When specifying the boundary condition at the pipe wall, input flux is in units of BTU/(hr per ft of pipe). Heat flux at the upper surface of the slab is called surface flux. Heat flux at the bottom surface of the slab is called back loss, and edge loss is the heat transfer

through the slab edges. In the original outputs of the simulation, the units of these heat fluxes are BTU/(hr per ft of pipe). But heat fluxes are presented as BTU/(hr-ft²) in the analysis by dividing the original output by the pipe spacing.

- Percentage loss (per)

$$per = \frac{Q_e}{Q_i} * 100\% \quad (2.1)$$

where, Q_e is the summation of energy loss at each cell through the back/edge of the slab, BTU/(hr per ft of pipe) [W/m], Q_i is the total energy input to the slab, BTU/(hr per ft of pipe) [W/m].

- Center zone and edge zone

Two representative zones of the heated slab are shown in Figure 2.1. Center zone is the domain far away from slab edges. Thus, effects of slab sides are negligible. To simplify the simulation, center zone is from the pipe centerline to the plane of symmetry. The edge zone is the domain near the slab edge, and is used to analyze the heat losses from the edge to ground. As shown in Spitler, *et al.* (2001), two pipes should be sufficient to allow edge losses to be estimated.

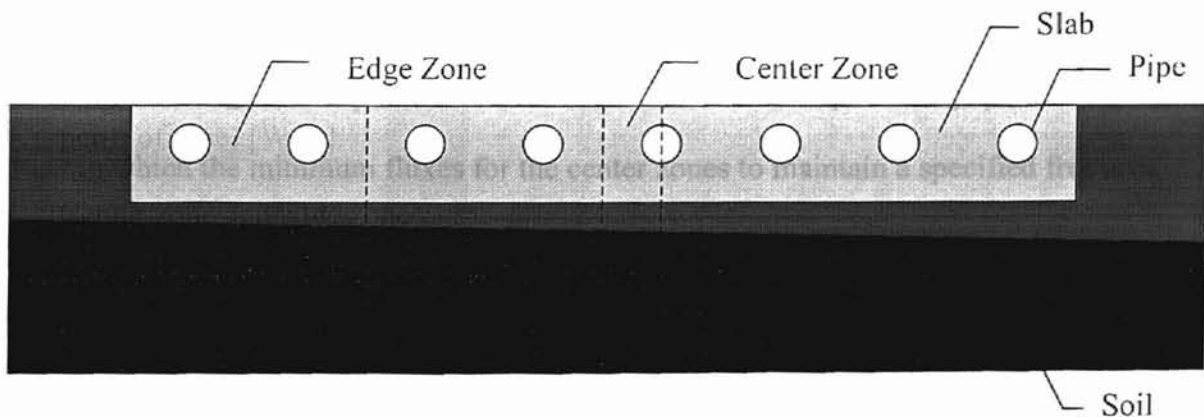


Figure 2.1: Representation of soil and slab for edge and center zone

- System operation

Based on the recommendations of the ASHRAE Project Monitoring Subcommittee, idling isn't considered in the study, as it is never or almost never utilized today.

- Number of hours excluded

The number of hours where the performance is allowed to fall below the design criterion is called the number of hours excluded in the parametric study.

2.2. Methodology of Parametric Study

The snow-melting model used in ASHRAE 1090-RP is the highly detailed two-dimensional transient model (the BFC-FV model) described in Chapter 1. The model can provide the temperature distribution of the slab and surroundings for the whole length of the storm.

2.2.1. Organization and Methodology of Parametric Study

Current snow-melting system design procedures are based on conditions typical of the center slab zone. Some snow coverage at the edge of the slab is likely to be tolerated. Accordingly, edge losses and snow-melting performance at the edge of the slab are based on design heat inputs found for center. So the first step is a large parametric study in which the minimum fluxes for the center zones to maintain a specified free area ratio are determined. The results enable us to determine the transient effect of the design conditions/operations and back losses on the design loads. Then the same input heat fluxes are supplied to the edge zone. This enables us to find the edge losses under these conditions and the corresponding minimum free area ratio achieved.

The parametric study for the center zone is summarized in Table 2.1. The tube spacing, tube depth, insulation, soil conductivity, location, and storm type are the parameters varied. The soil conductivity is varied when the insulation level at the slab bottom is 2”(50mm). Totally, there are 360 different cases, and a substantially large number of simulations are required to find the correct minimum flux.

Table 2.1
Center Zone Parametric Study

Number	Parameter Levels
3	Spacing (6,8,12 inches)
2	Depths (2,4 inches)
2	Insulation levels at the slab bottom (none, 2” expanded polystyrene)
1.5	Soil conductivities (for non-insulated case, 2 values corresponding to saturated clay and dry light soil; for insulated case just use saturated clay)
10	Locations (Spokane, Reno, SLC, Colorado Springs, Chicago, OKC, Minneapolis, Buffalo, Boston and Philadelphia)
2	Storms (1 99% storm each for free area ratio one or zero)
?	Simulations is required find either the minimum flux for $A_f=1$ or $A_f=0$.

The parametric study for the edge zone is summarized in Table 2.2. In many cases, it’s not practical to keep the surface snow free for the edge zone. It often requires unreasonable high flux input to the pipe. Therefore, the study in edge zone focuses on the edge losses and the corresponding minimum free area ratio achieved for the design flux found for the center zone.

Table 2.2

Edge Zone Parametric Study

Number	Parameter Levels
3	Spacing (6,8,12 inches)
2	Depths (2,4 inches)
2	Insulation levels at the slab bottom (none, 2" expanded polystyrene)
1.5	Soil conductivities (for non-insulated case, 2 values corresponding to saturated clay and dry light soil; for insulated case just use saturated clay)
10	Locations (Spokane, Reno, SLC, Colorado Springs, Chicago, OKC, Minneapolis, Buffalo, Boston and Philadelphia)
2	Storms (1 99% storm each for free area ratio one or zero)
1	Heat flux (the same as the minimum flux found by center zone study).

2.2.2. Methodology of Center Zone Parametric Study

The center zone parametric study investigates the effect of the transient design condition/operation and back losses on the design loads and compare these transient design loads. As shown in Table 2.1, there are 360 cases to study and a large number of simulations are needed for finding the minimum flux. The methodology for the center zone study may be described in three parts,

- development of minimum flux search algorithm,
- batch processing,
- post-processing of data.

Search Algorithm for Minimum Flux

The search algorithm automatically and iteratively runs the simulation to find the minimum flux within some tolerance. A flow chart for the search algorithm is shown in Figure 2.2.

To save computational time, the simulation has been modified internally to check whether or not the specified conditions have been exceeded, and if so, to stop prematurely. For example, if searching for free area ratio $A_r=1$, at a certain flux the number of hours where there is some snow on the slab may exceed the allowable number of hours. Once this happens, there is no need to continue the simulation. Therefore, it is stopped; that flux is now known to be too low, and the search continues.

In addition to the inputs for the two dimensional snow-melting model, the other inputs needed for the flux search are kept in a file named INPUT.dat. The information includes the upper limit flux, the free area ratio expected, the number of hours excluded and the search tolerance. The initial lower limit flux is assumed zero. Hourly free area ratio and the search results are written to the OUTPUT.dat.

The search scheme may be described as root finding over an interval that is bounded by the lower and upper limit input fluxes. The interval is shortened step-by-step in the searching process. A new evaluation point (the new input heat flux) is selected by applying golden section over the interval. The selection can be described as follows,

$$q_i = q_l + g(q_u - q_l) \quad (2.2)$$

where

g = golden section ratio, 0.618

q_i = the new input flux for the next time step, BTU/(ft-hr) [W/m],

q_l = the lower limit flux for the search, BTU/(ft-hr) [W/m],

q_u = the upper limit flux for the search, BTU/(ft-hr) [W/m].

At any step in the search, a lower limit flux and upper limit flux will have already been determined. If the simulation using the input flux at the evaluation point allows the required conditions to be met, this input flux becomes the new upper limit. Otherwise, it becomes the new lower limit.

For the cases that the expected free area ratio is nonzero, if current flux input is lower than required, the program looks for the last hour index where the free area ratio is less than the requirement. For the cases that the expected free area ratio equals to zero, the program searches the last hour index that the snow height increases. The value of this hour number is set as the length for the next simulation.

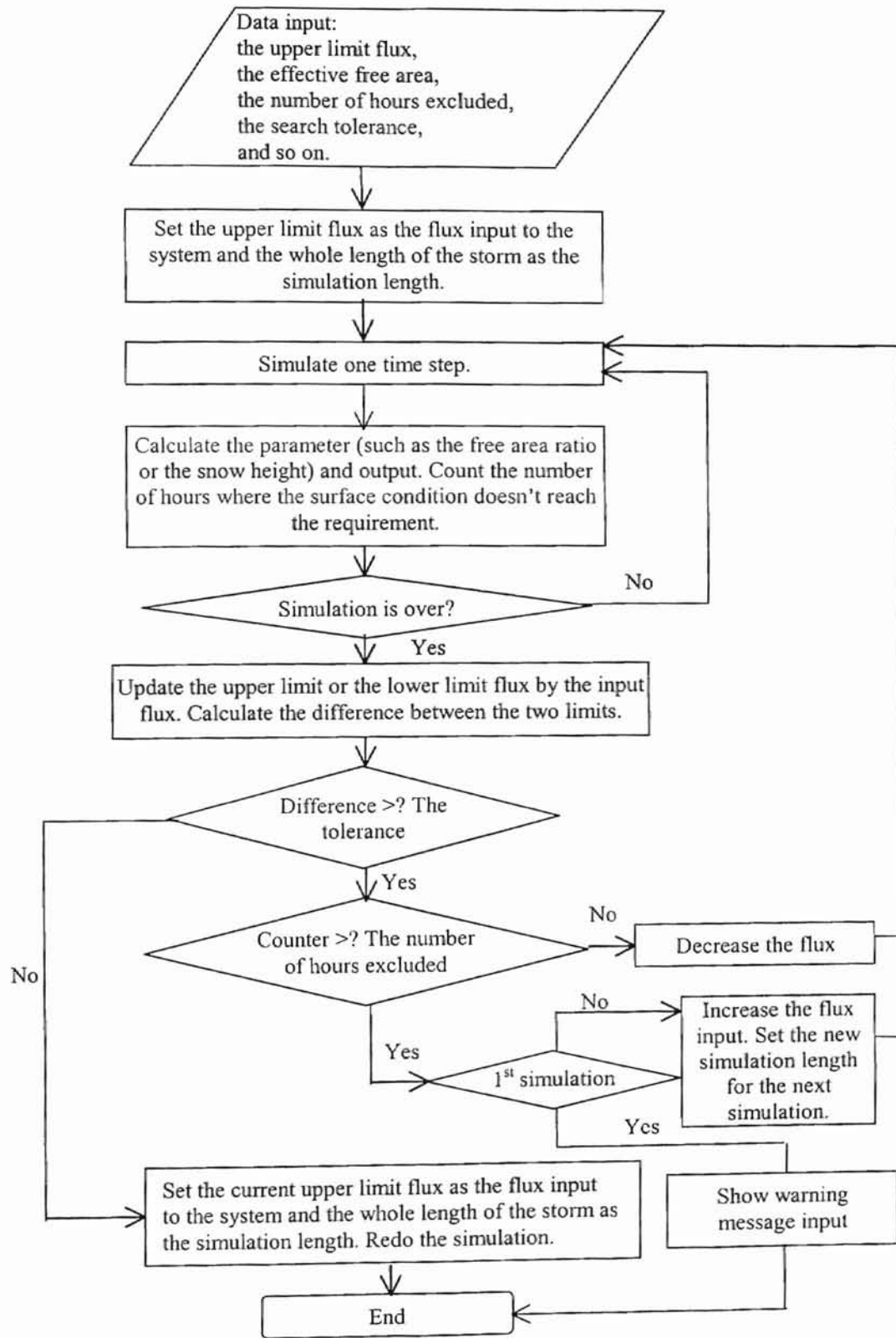


Figure 2.2: The Flow Chart for the Minimum Flux Search

In order to keep the simulation time reasonable, the flux is only found within a certain tolerance. Once the uncertainty of the flux is within this tolerance, the program stops. As described above, the program updates the upper limit and lower limit of the flux after every simulation and calculates the difference. The upper limit flux satisfies the surface requirement and the lower limit flux does not. The exact value of the minimum flux must be in the interval of the two limits. Because the simulation program internally uses heat input per unit length of pipe, and the tolerance was specified as 5.0 BTU/(hr per ft pipe), the final uncertainty in input heat flux with unit BTU/(hr-ft²) presented in the analysis varies depending on the tube spacing, for instance, if the minimum input flux found by program is X BTU/(hr per ft pipe), the exact value of the minimum flux is in the interval of $(X-5.0, X)$ BTU/(hr per ft pipe), that is, for cases that pipe spacing is 6", the uncertainty of the exact value of the minimum flux is 10 BTU/(hr-ft²), while for cases that pipe spacing is 12", the uncertainty of the exact value of the minimum flux is 5 BTU/(hr-ft²). The tolerance is summarized in Table 2.3.

Table 2.3
Tolerance of Minimum Fluxes

	Flux found by program (BTU/(ft ² -hr))	The value of minimum flux (BTU/(ft ² -hr))
Spacing = 6"	Y	(Y-10.0)~Y
Spacing = 8"	Y	(Y-7.5)~Y
Spacing = 12"	Y	(Y-5.0)~Y

Batch Processing

A parametric study of center and edge geometries is made using the following parameter variations.

- 10 locations (Spokane, Reno, SLC, Springs in Colorado, Chicago, OKC, Minneapolis, Buffalo, Boston, Philadelphia)
- 2 storms at each location (99%-tile $A_r=1$, 99%-tile $A_r=0$)
- Insulated and un-insulated slabs
- 3 pipe spacing
- 2 pipe depth
- 2 soil conductivities

It represents 360 combinations of location, storm and configuration. A batch command file is used to deal with the cases automatically. Through batch processing, groups of simulations could be run on different computers at different time. Batch command files are generated using a program created in Visual Basic.

2.2.3. Methodology of Edge Zone Parametric Study

Because the edge zone parametric study doesn't require searching for the minimum flux, a similar but simpler approach than that used for the center zone parametric study is utilized. The batch processing is similar.

2.3. Results and Discussion

2.3.1. Center Zone Parametric Study

2.3.1.1. Case $A_r=1$

Table 2.4 and Table 2.5 show the results for the center zone parametric studies with expected free area ratio 1. The minimum fluxes for each combination of the

parameters are tabulated in Table 2.4. The fluxes maintain a free area ratio of 1 for the entire storm, except the number of hours where the steady-state design load exceeded the 99% non-exceedance level. The 99% non-exceedance loads can be found from the ASHRAE handbook.

By normalizing the minimum fluxes against the 99% non-exceedance loads, it shows more clearly in Table 2.5 the relationship between the steady-state design loads without back losses and the actual transient load with back losses. Looking at Table 2.5, the following observation may be made:

- Several searches are stopped due to the flux requirement exceeded the upper limit (900 Btu/h-ft²). The very high flux requirements indicate it's impractical to achieve the design goal that maintains the surface free of snow when the system is operated without idling. The high flux requirements generally occur when storms start with relatively high calculated steady-state loads. Without idling, very high fluxes are required to raise the slab temperature sufficiently at the start of the storm.
- The results are most sensitive to the storm itself. This will be discussed in more detail below. Briefly, it has been noted that storms that start off with relatively low loads, perhaps even ceasing to snow for a few hours, then increasing in intensity, will have much lower ratios than storms that start off with high load.
- After the storm itself, the results are most sensitive to the spacing. The farther apart the tubes, the more difficult it is to maintain a completely snow-free surface. Also, as the tubes are placed deeper, the effect of spacing is less important.

- The results are somewhat less sensitive to the depth of the tubing. Generally, the depth is more important for the storms that are intense early on. With storms that are less intense in the early hours, the depth make relatively little difference. Furthermore, there are a significant number of scenarios where increasing the depth decreases the flux requirement.
- The results are almost completely insensitive to the soil conductivity and whether or not insulation has been installed.

Also, unless further research proves otherwise, we would not assume that the storms are typical of the location. Currently, we would not draw the conclusion by locations. A better way to draw conclusions is to categorize the results by storms.

Sensitivity to Storm

As stated above, the most important factor for the load is the storm itself. To illustrate the sensitivity to the storm, we might first consider storms where the ratios of the minimum required heat flux to the 99% steady-state load are fairly high, in Spokane and Oklahoma City. Weather data for these storms are plotted in Figures 2.3 and 2.4. The top plot of each figure shows the weather conditions; the bottom plot shows the steady-state design loads calculated for each hour.

Table 2.4

Minimum Required Heat Flux (BTU/hr-ft²) for Transient Conditions with Back Losses (Free Area Ratio = 1.0)

				Spokane	Reno	SLC	Springs	Chicago	OKC	Minneapolis	Buffalo	Boston	Philadelphia
99% steady load (Btu/(h-ft ²))				159	137	120	219	235	260	254	330	229	246
no insulation layer	K _{soil} =0.5 Btu/(h-ft ² -F)	Depth=2"	Spacing=6"	367	227	146	364	342	420	344	438	334	301
			Spacing=8"	437	258	157	432	398	510	385	495	376	342
			Spacing=12"	738	372	191	704	616	850	533	692	509	462
		Depth=4"	Spacing=6"	523	295	167	567	530	620	444	515	374	337
			Spacing=8"	599	301	167	614	563	668	460	531	386	379
			Spacing=12"	854	353	184	831	757	>900	564	623	451	448
	K _{soil} =1.4 Btu/(h-ft ² -F)	Depth=2"	Spacing=6"	367	223	146	350	319	404	335	430	334	308
			Spacing=8"	432	250	161	420	356	487	379	489	380	348
			Spacing=12"	792	367	195	685	559	816	530	692	520	475
		Depth=4"	Spacing=6"	535	295	175	554	482	594	444	520	390	349
			Spacing=8"	596	304	173	595	510	644	453	541	396	362
			Spacing=12"	854	361	195	812	689	>900	568	649	472	469
with 2" insulation layer	K _{soil} =0.5 Btu/(h-ft ² -F)	Depth=2"	Spacing=6"	367	212	133	372	356	434	345	412	292	271
			Spacing=8"	429	242	135	429	410	518	375	458	328	298
			Spacing=12"	687	317	161	642	631	854	513	581	420	418
		Depth=4"	Spacing=6"	494	240	138	511	523	601	404	417	300	301
			Spacing=8"	532	242	135	544	551	649	419	425	302	303
			Spacing=12"	717	281	146	704	726	885	502	481	343	343

* 1 BTU/hr-ft² = 3.155 W/m².

Table 2.5

Normalized Minimum Required Heat Flux for Transient Conditions with Back Losses (Free Area Ratio = 1.0)

				Spokane	Reno	SLC	Springs	Chicago	OKC	Minneapolis	Buffalo	Boston	Philadelphia	
99% steady load (Btu/(h-ft ²))				159	137	120	219	235	260	254	330	229	246	
no insulation layer	K _{soil} =0.5 Btu/(h-ft ² -F)	Depth=2"	Spacing=6"	2.3	1.7	1.2	1.7	1.5	1.6	1.4	1.3	1.5	1.2	
			Spacing=8"	2.7	1.9	1.3	2.0	1.7	2.0	1.5	1.5	1.6	1.4	
			Spacing=12"	4.6	2.7	1.6	3.2	2.6	3.3	2.1	2.1	2.2	1.9	
		Depth=4"	Spacing=6"	3.3	2.2	1.4	2.6	2.3	2.4	1.7	1.6	1.6	1.6	1.4
			Spacing=8"	3.8	2.2	1.4	2.8	2.4	2.6	1.8	1.6	1.7	1.7	1.5
			Spacing=12"	5.4	2.6	1.5	3.8	3.2	-	2.2	1.9	2.0	2.0	1.8
	K _{soil} =1.4 Btu/(h-ft ² -F)	Depth=2"	Spacing=6"	2.3	1.6	1.2	1.6	1.4	1.6	1.3	1.3	1.3	1.5	1.3
			Spacing=8"	2.7	1.8	1.3	1.9	1.5	1.9	1.5	1.5	1.5	1.7	1.4
			Spacing=12"	5.0	2.7	1.6	3.1	2.4	3.1	2.1	2.1	2.1	2.3	1.9
		Depth=4"	Spacing=6"	3.4	2.2	1.5	2.5	2.1	2.3	1.7	1.6	1.6	1.7	1.4
			Spacing=8"	3.7	2.2	1.4	2.7	2.2	2.5	1.8	1.6	1.6	1.7	1.5
			Spacing=12"	5.4	2.6	1.6	3.7	2.9	-	2.2	2.0	2.1	2.1	1.9
with 2" insulation layer	K _{soil} =0.5 Btu/(h-ft ² -F)	Depth=2"	Spacing=6"	2.3	1.6	1.1	1.7	1.5	1.7	1.4	1.2	1.3	1.1	
			Spacing=8"	2.7	1.8	1.1	2.0	1.7	2.0	1.5	1.4	1.4	1.4	1.2
			Spacing=12"	4.3	2.3	1.3	2.9	2.7	3.3	2.0	1.8	1.8	1.8	1.7
		Depth=4"	Spacing=6"	3.1	1.8	1.1	2.3	2.2	2.3	1.6	1.3	1.3	1.3	1.2
			Spacing=8"	3.3	1.8	1.1	2.5	2.3	2.5	1.6	1.3	1.3	1.3	1.2
			Spacing=12"	4.5	2.1	1.2	3.2	3.1	3.4	2.0	1.5	1.5	1.5	1.4

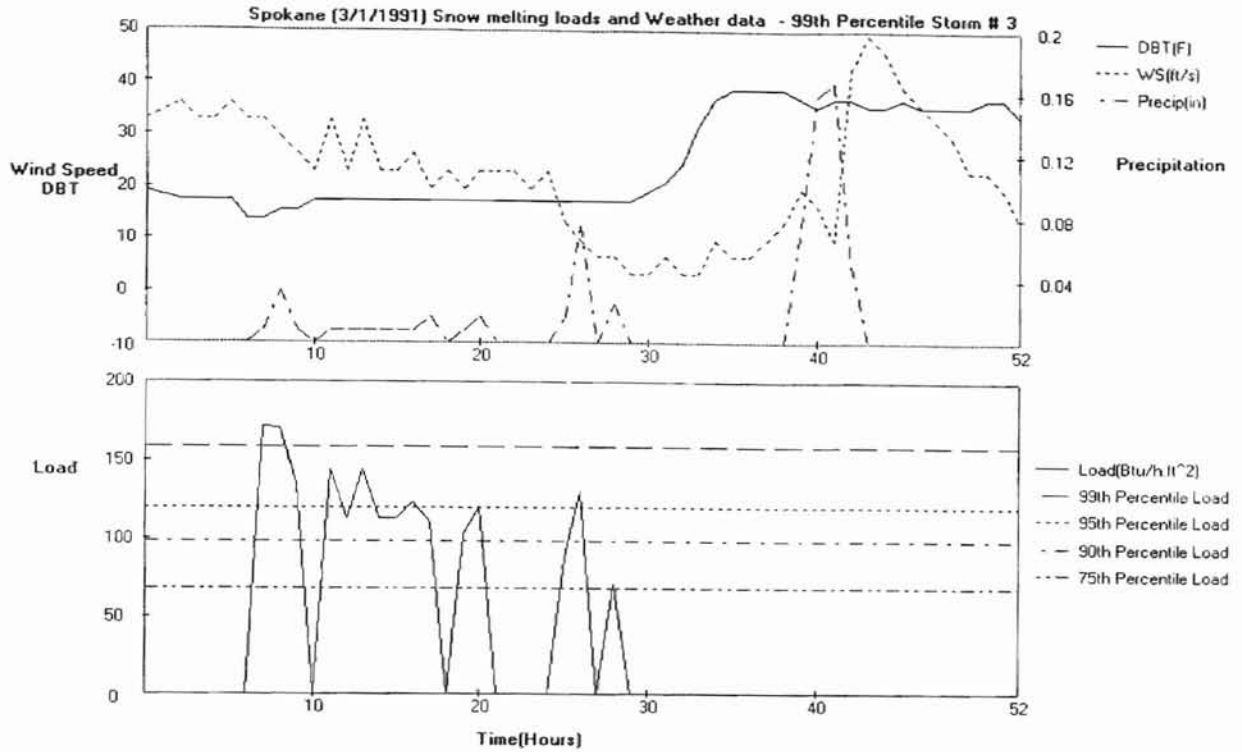


Figure 2.3: Weather conditions and loads for Spokane, $A_r=1$

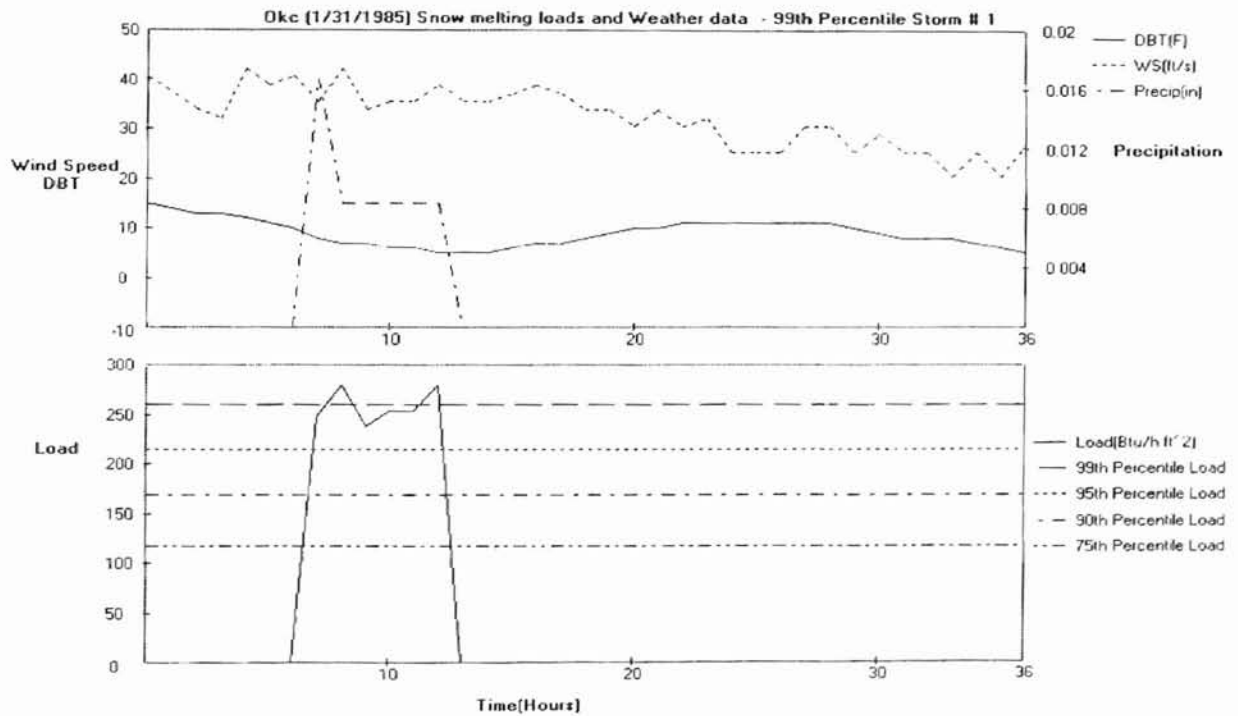


Figure 2.4: Weather conditions and loads for OKC, $A_r=1$

For both of these storms, in the first couple hours, the storm intensity is high. Heat supplied to the slab not only raises the slab temperature above the freezing point but also clears the high load in time. Another point worth noting is that for both of these storms, the number of hours that exceed the 99%-tile steady state load is small, only two hours. That means only two hours are allowed when the free area ratio is less than one. In other words, the supplied heat flux must be high enough to raise the surface temperature and clear the snow in the beginning one or two hours.

To summarize, there are three factors significantly affecting the ratio of transient, with back loss required heat flux to steady state required heat flux: the storm, the initial slab temperature and the number of hours excluded.

As an alternative, consider Salt Lake City, which has relatively low ratios between the transient requirement and the 99%-tile steady state load. Weather conditions and loads for the Salt Lake City storm are shown in Figure 2.5.

For this storm, the high intensity occurs late. But the system will turn on very early because there is 75% load occurring at the beginning of the storm. Before the rest of the storm hits, the system has enough time to warm the slab, so a relatively lower flux is required. This is analogous to idling the system. It's effective in lowering the flux requirement. To further demonstrate the phenomenon, the storm is artificially modified by moving the second batch of precipitation forward in time. The artificially modified storm is shown in Figure 2.6.

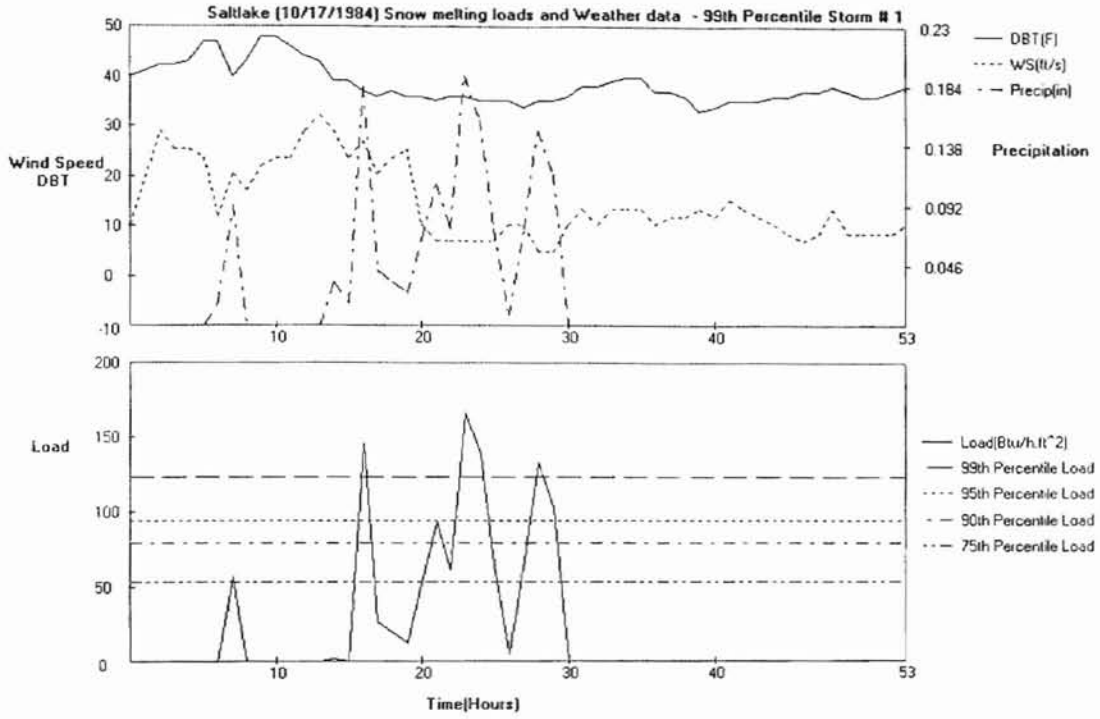


Figure 2.5: Weather Conditions and Loads for Salt Lack City, $A_r=1$

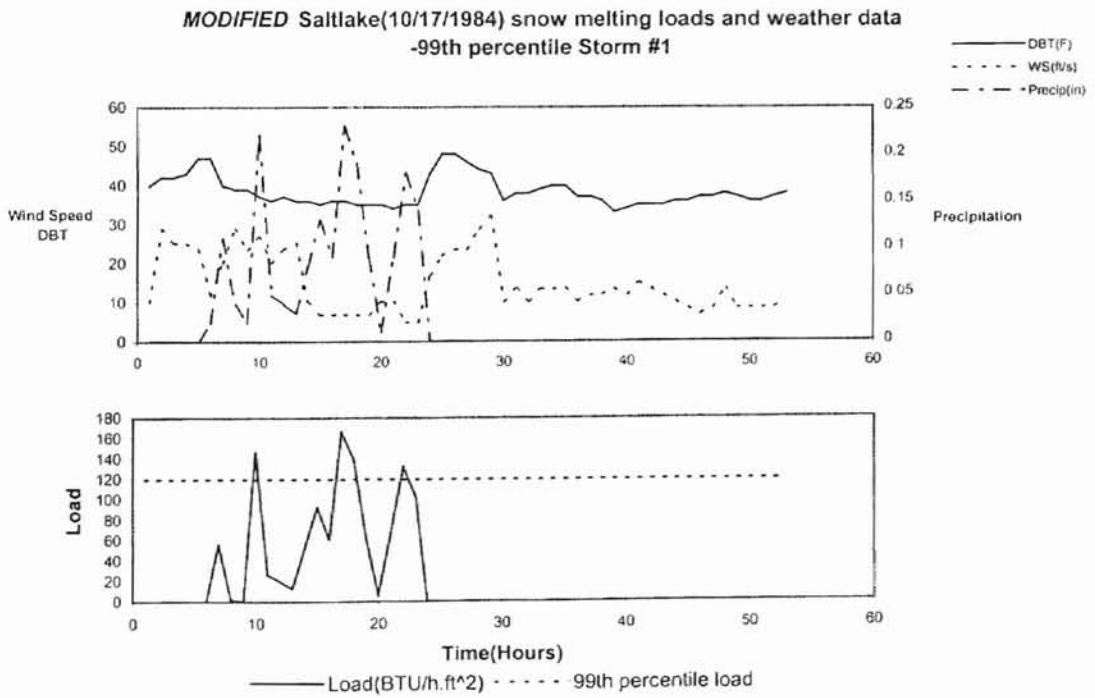


Figure 2.6: Artificially Modified Storm in Salt Lake City, $A_r=1$

For the case with no insulation, soil conductivity of $0.5 \text{ Btu}/(\text{h}\cdot\text{ft}^2\cdot\text{F})$, spacing 12", the minimum heat flux required with the original storm is $191 \text{ Btu}/(\text{h}\cdot\text{ft}^2)$. While with the artificial modified storm, it increases to $229 \text{ Btu}/(\text{h}\cdot\text{ft}^2)$. This represents an increase in the ratio from 1.6 to 1.9.

More examples are available to demonstrate the importance of the actual snowfall pattern on the ratio required heat flux for transient conditions. If a free area ratio of one is absolutely required, idling at some level will probably be necessary. On the other hand, if some time lag in clearing off the snow is allowable, then the steady state heat fluxes or moderately increased heat fluxes might be acceptable.

Effect of Depth on the Minimum Flux Requirement

It might be expected that the deeper tubing would increase the heat flux requirement due to the slower response of the surface flux to the source. However, there are a large number of cases where increasing the depth either decreases the heat flux requirement or has a negligible influence. The cases generally occur in the storms for which the high intensity hours come late and the normalized flux requirement ratios are relatively low. For this type of storm, the latter hours of the storm are more important to maintain the expected requirement. It makes the additional time delay caused by the deeper tubing not significant. Conversely, for storms with relatively high ratios, the deeper the tubing, the more likely it is that the flux requirement increases. For this type of storms, the high intensity hours occur early. The response speed of the slab in the first

several hours has the most significant effect on the surface conditions that may be achieved.

Within any given storm, the wider the spacing, the more likely it is that increasing the depth of the tubing will decrease the minimum heat flux requirement. The more uniform heat flux yielded by the deeper tubing allows more uniform melting.

To demonstrate the point above, the concept of the controlling hour is introduced. It's very obvious that for any given storm, in the flux searching process, there is one or two hours that tend to control the required heat flux. For example, decreasing the heat flux slightly will cause the free area ratio to drop below one for that hour. For the Buffalo storm, we have studied the surface heat flux and surface conditions for a heat flux of $622.7 \text{ BTU/hr-ft}^2$, 12" spacing, and 2" and 4" depths, at the controlling hour, in Figures 2.7 and 2.8. In these plots, the distance "0.0" represents the location above the tube; and the distance "0.5" would be midway between the tubes. For this hour, the more uniform heat flux of the deeper pipe allows $622.7 \text{ BTU/hr-ft}^2$ to be sufficient for the 4" deep tubing, but not for 2" deep tubing.

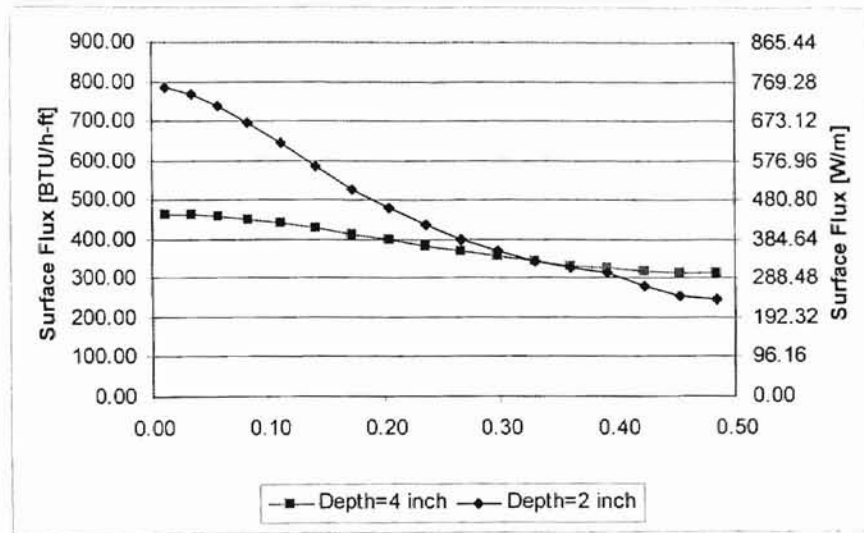


Figure 2.7: Distribution of the surface heat flux (Buffalo, 12'' spacing)

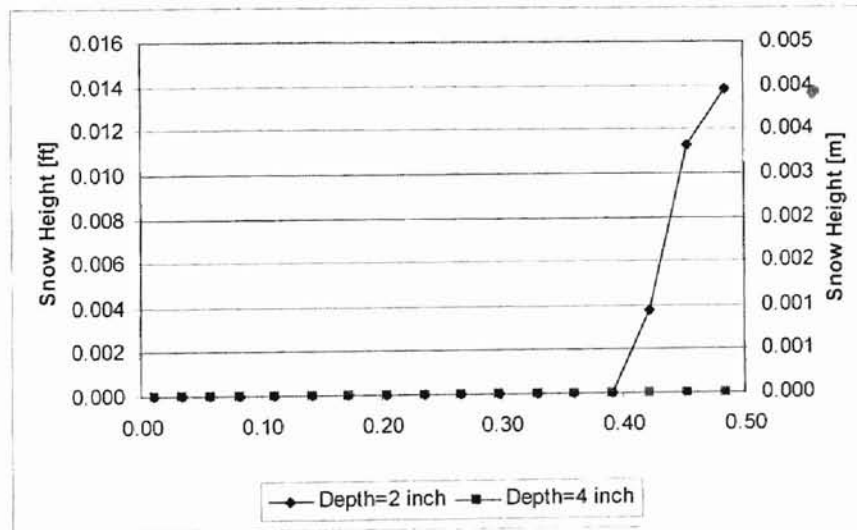


Figure 2.8: Surface conditions at the controlling hour (Buffalo, 12'' spacing)

2.3.1.2 Case $A_r=0$

Table 2.6 and Table 2.7 show the results for the center zone parametric studies with expected free area ratio equals to 0. As the results for $A_r=1$, the minimum flux requirement is more sensitive to the storm itself than any other factors. After that, the spacing is most important. The effect of the tubing depth is less important, and highly storm-dependent. Again, the soil conductivity and insulation have little, if any, effect.

Table 2.6

Minimum Required Heat Flux (BTU/hr-ft²) for Transient Conditions with Back Losses (Free Area Ratio = 0.0)

				Spokane	Reno	SLC	Springs	Chicago	OKC	Minneapolis	Buffalo	Boston	Philadelphia
99% steady load (Btu/(h-ft ²))				67	113	104	112	83	113	113	112	172	150
no insulation layer	K _{soil} =0.5 Btu/(h-ft ² -F)	Depth=2"	Spacing=6"	161	146	127	83	185	185	267	168	267	404
			Spacing=8"	193	157	146	75	208	239	301	192	296	482
			Spacing=12"	319	219	201	89	283	487	406	364	395	804
		Depth=4"	Spacing=6"	316	210	172	140	233	366	333	256	344	643
			Spacing=8"	312	213	180	139	242	420	329	290	342	694
			Spacing=12"	319	260	261	139	289	587	381	372	386	>900
	K _{soil} =1.4 Btu/(h-ft ² -F)	Depth=2"	Spacing=6"	151	146	134	83	185	150	261	168	267	386
			Spacing=8"	162	167	146	72	208	201	296	185	296	468
			Spacing=12"	273	236	211	81	287	399	397	328	399	788
		Depth=4"	Spacing=6"	271	188	178	134	240	299	323	220	350	631
			Spacing=8"	267	199	188	134	247	344	322	252	345	685
			Spacing=12"	278	240	273	130	295	564	376	376	399	>900
with 2" insulation layer	K _{soil} =0.5 Btu/(h-ft ² -F)	Depth=2"	Spacing=6"	178	146	123	79	172	220	250	175	252	404
			Spacing=8"	204	157	134	72	193	280	280	240	275	482
			Spacing=12"	347	208	178	84	237	500	376	361	368	792
		Depth=4"	Spacing=6"	333	188	151	123	199	400	289	269	319	620
			Spacing=8"	334	193	154	121	204	422	288	279	309	654
			Spacing=12"	342	229	211	122	256	559	300	328	328	>900

* 1 BTU/hr-ft² = 3.155 W/m².

Table 2.7

Normalized Minimum Required Heat Flux for Transient Conditions with Back Losses (Free Area Ratio = 0.0)

			Spokane	Reno	SLC	Springs	Chicago	OKC	Minneapolis	Buffalo	Boston	Philadelphia	
99% steady load (Btu/(h-ft ²))			67	113	104	112	83	113	113	112	172	150	
no insulation layer	K _{soil} =0.5 Btu/(h-ft ² -F)	Depth=2"	Spacing=6"	2.4	1.3	1.2	0.7	2.2	1.6	2.4	1.5	1.6	2.7
			Spacing=8"	2.9	1.4	1.4	0.7	2.5	2.1	2.7	1.7	1.7	3.2
			Spacing=12"	4.8	1.9	1.9	0.8	3.4	4.3	3.6	3.2	2.3	5.4
		Depth=4"	Spacing=6"	4.7	1.9	1.7	1.3	2.8	3.2	2.9	2.3	2.0	4.3
			Spacing=8"	4.7	1.9	1.7	1.2	2.9	3.7	2.9	2.6	2.0	4.6
			Spacing=12"	4.8	2.3	2.5	1.2	3.5	5.2	3.4	3.3	2.2	-
	K _{soil} =1.4 Btu/(h-ft ² -F)	Depth=2"	Spacing=6"	2.2	1.3	1.3	0.7	2.2	1.3	2.3	1.5	1.6	2.6
			Spacing=8"	2.4	1.5	1.4	0.6	2.5	1.8	2.6	1.7	1.7	3.1
			Spacing=12"	4.1	2.1	2.0	0.7	3.5	3.5	3.5	2.9	2.3	5.3
		Depth=4"	Spacing=6"	4.1	1.7	1.7	1.2	2.9	2.6	2.9	2.0	2.0	4.2
			Spacing=8"	4.0	1.8	1.8	1.2	3.0	3.0	2.8	2.3	2.0	4.6
			Spacing=12"	4.1	2.1	2.6	1.2	3.6	5.0	3.3	3.4	2.3	-
with 2" insulation layer	K _{soil} =0.5 Btu/(h-ft ² -F)	Depth=2"	Spacing=6"	2.7	1.3	1.2	0.7	2.1	1.9	2.2	1.6	1.5	2.7
			Spacing=8"	3.0	1.4	1.3	0.6	2.3	2.5	2.5	2.1	1.6	3.2
			Spacing=12"	5.2	1.8	1.7	0.7	2.9	4.4	3.3	3.2	2.1	5.3
		Depth=4"	Spacing=6"	5.0	1.7	1.4	1.1	2.4	3.5	2.6	2.4	1.9	4.1
			Spacing=8"	5.0	1.7	1.5	1.1	2.5	3.7	2.5	2.5	1.8	4.4
			Spacing=12"	5.1	2.0	2.0	1.1	3.1	4.9	2.7	2.9	1.9	-

Transient Effect on the Load

It might be noted that for some combinations of parameters, the transient load required by the Colorado Springs storm is less than the steady state load. This may be explained by the actual weather condition before the storm hits. For Colorado Springs, the storm starts from the 18th hour. The air temperature is quite warm prior to the storm. It is expected that the slab temperature will be above freezing at the start of snow precipitation, and will melt some of snow using the thermal energy stored in the slab. Therefore, in this case, the transient effects help rather than hinder the performance.

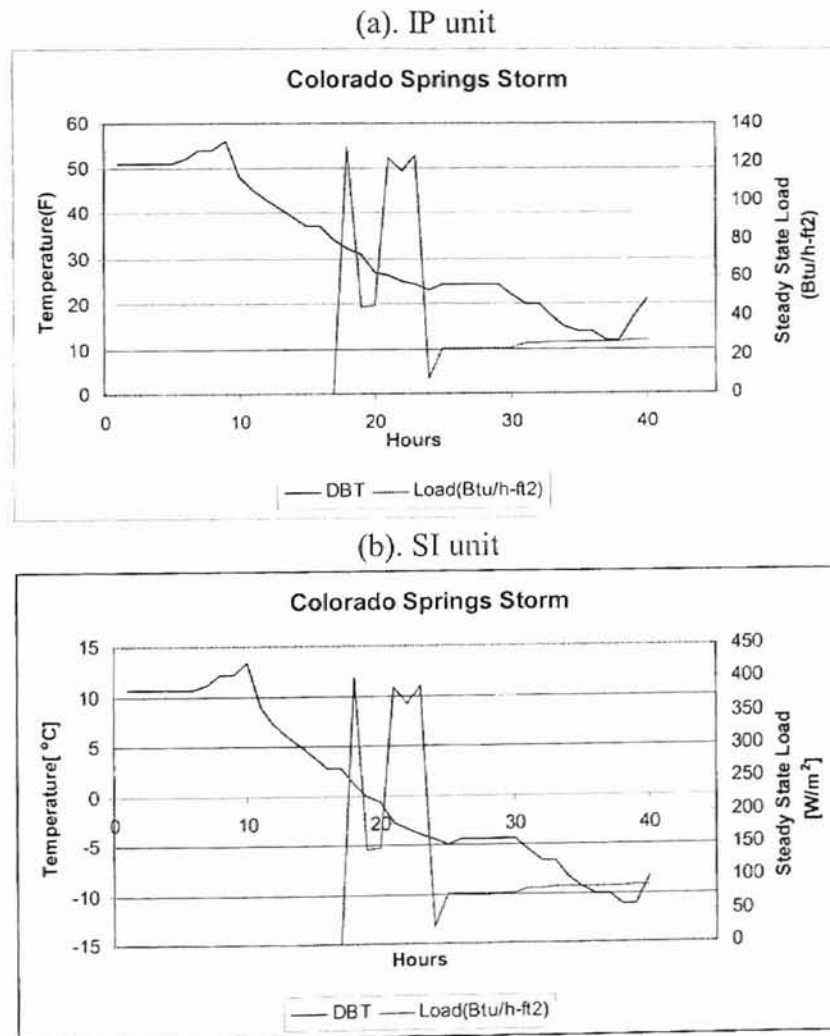


Figure 2.9: Colorado Springs Storm with Warm Conditions prior to Snowfall

2.3.1.3 Back Losses

Designers are interested not only in the minimum flux requirement of the system but also in the actual back losses. Table 2.8 and Table 2.9 show the results of maximum percentage back loss for free area ratio of 1 and 0 respectively. Because the back loss varies every hour, what's tabulated is the maximum percentage back loss.

The following trends may be observed:

- Insulation is quite effective in reducing the back loss.
- Soil conductivity has significant impact on the back losses.
- The depth is relatively important – the deeper tubing has, as expected, higher back losses. Naturally, this is more significant for uninsulated slabs and higher conductivity soil.
- Pipe spacing has less impact on the back losses.

Table 2.8

Maximum Percentage Back Loss (BTU/hr-ft²) for Transient Conditions (Free Area Ratio = 1.0)

			Spokane	Reno	SLC	Springs	Chicago	OKC	Minneapolis	Buffalo	Boston	Philadelphia	
no insulation layer	Ksoil=0.5 Btu/(h-ft ² -F)	Depth=2"	Spacing=6"	16.4	18.1	16.6	12.89	17.5	11.1	12.2	12.1	13.3	13.5
			Spacing=8"	17.1	18.7	16.8	13.86	18.0	12.2	13.1	12.6	13.7	14.1
			Spacing=12"	16.6	19.0	16.7	15.32	18.1	13.5	14.3	13.3	18.6	14.5
		Depth=4"	Spacing=6"	22.5	23.9	24.3	21.82	25.2	20.6	20.7	20.9	22.0	21.8
			Spacing=8"	21.6	24.4	24.6	22.50	25.6	21.3	21.3	21.3	22.4	22.4
			Spacing=12"	21.0	24.6	24.6	23.22	25.7	-	21.9	21.6	22.4	22.6
	Ksoil=1.4 Btu/(h-ft ² -F)	Depth=2"	Spacing=6"	17.3	20.3	19.1	14.15	18.0	11.6	13.5	13.9	15.0	15.0
			Spacing=8"	18.4	21.2	19.4	15.56	18.7	13.1	14.7	14.3	15.5	15.7
			Spacing=12"	16.9	22.0	19.4	17.37	19.8	15.2	16.4	14.9	22.1	16.5
		Depth=4"	Spacing=6"	24.5	27.8	28.4	24.76	27.7	23.2	23.8	23.5	24.8	24.8
			Spacing=8"	24.1	28.4	28.8	25.58	28.3	24.0	24.4	24.1	25.3	25.4
			Spacing=12"	23.6	28.8	28.7	26.74	28.8	-	25.5	24.6	25.5	26.0
with 2" insulation layer	Ksoil=0.5 Btu/(h-ft ² -F)	Depth=2"	Spacing=6"	2.3	2.4	2.2	1.97	1.5	1.0	1.6	2.7	2.1	1.5
			Spacing=8"	2.5	2.4	2.2	2.13	1.7	1.1	1.7	2.6	2.5	1.6
			Spacing=12"	2.5	2.4	2.4	2.29	1.9	1.3	2.0	1.9	2.0	1.8
		Depth=4"	Spacing=6"	3.6	3.3	3.2	3.23	2.8	2.2	2.8	1.9	3.0	2.7
			Spacing=8"	3.5	3.3	3.3	3.34	2.9	2.2	3.0	2.0	3.5	2.7
			Spacing=12"	3.6	3.5	3.4	3.42	3.0	2.3	3.1	3.0	3.1	3

Table 2.9

Maximum Percentage Back Loss for Transient Conditions (Free Area Ratio = 0.0)

				Spokane	Reno	SLC	Springs	Chicago	OKC	Minneapolis	Buffalo	Boston	Philadelphia
no insulation layer	Ksoil=0.5 Btu/(h-ft ² -F)	Depth=2"	Spacing=6"	18.1	15.1	16.7	9.7	14.0	14.4	15.0	11.4	15.0	19.0
			Spacing=8"	19.0	15.6	18.3	8.1	14.5	15.9	15.4	12.4	15.3	19.7
			Spacing=12"	19.9	16.2	20.3	9.6	15.0	17.6	15.5	14.6	15.4	19.2
		Depth=4"	Spacing=6"	25.3	23.1	24.2	16.5	22.3	23.8	22.2	19.8	21.9	26.1
			Spacing=8"	25.7	23.5	25.0	16.8	22.7	24.6	22.6	20.7	22.3	26.1
			Spacing=12"	25.8	23.8	26.3	19.5	22.9	25.1	22.7	21.4	22.3	-
	Ksoil=1.4 Btu/(h-ft ² -F)	Depth=2"	Spacing=6"	18.9	15.3	20.1	9.6	15.7	13.7	15.5	12.9	17.5	21.9
			Spacing=8"	19.7	16.4	21.5	7.6	16.4	16.4	16.3	14.0	17.9	22.5
			Spacing=12"	21.9	17.7	24.0	8.1	17.1	21.4	16.9	16.7	18.1	22.1
		Depth=4"	Spacing=6"	28.3	24.8	28.6	17.6	25.6	26.2	24.6	22.3	25.9	30.2
			Spacing=8"	28.8	25.6	29.5	18.2	26.0	27.4	25.0	23.6	26.3	30.6
			Spacing=12"	28.9	26.2	31.0	21.7	26.4	28.9	25.5	25.2	26.4	-
with 2" insulation layer	Ksoil=0.5 Btu/(h-ft ² -F)	Depth=2"	Spacing=6"	2.1	1.5	2.4	0.6	1.8	1.4	1.6	1.2	1.9	2.0
			Spacing=8"	2.3	1.6	2.5	0.4	1.9	1.6	1.8	1.5	1.8	1.9
			Spacing=12"	2.7	1.8	2.8	0.9	2.3	1.8	1.9	1.8	2.0	1.9
		Depth=4"	Spacing=6"	3.7	2.7	3.6	2.1	3.0	2.7	2.8	2.6	2.8	2.6
			Spacing=8"	3.7	2.7	3.7	2.2	3.0	2.6	2.9	2.7	3.0	2.6
			Spacing=12"	3.7	2.9	3.8	2.5	2.9	2.7	2.9	2.9	3.0	-

2.3.2. Edge Zone Parametric Study

The minimum heat fluxes determined by the center zone study are used as heat flux input in the edge zone simulations. The numerical domain is shown in Figure 2.10. To display properly, the plot is truncated- the soil domain width and depth extend well beyond what is shown. The left hand side, the right hand side and the bottom of the domain are assumed adiabatic. The bold lines separate the slab from the soil. For purposes of calculating the free area ratio or average snow height of the edge zone, the surface of the edge zone is considered to be that part labeled Patch 1 and Patch 2.

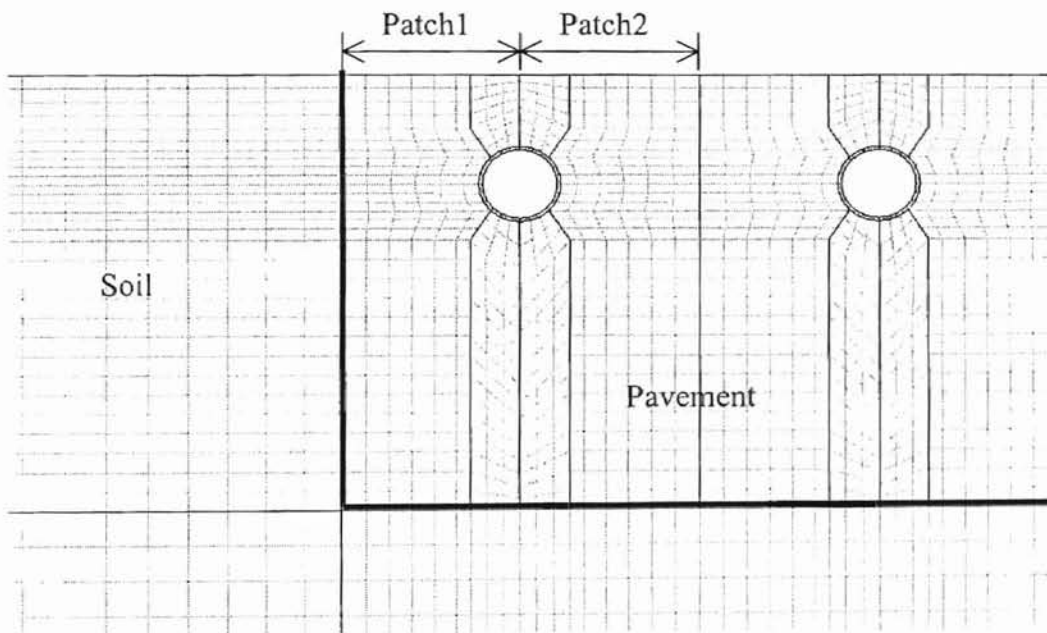


Figure 2.10: Grid Sample for Edge Zone Simulation

The minimum free area ratios achieved are tabulated in Table 2.10 for the $A_r=1$ storms. The number of hours that the steady-state design load exceeds 99% design load has been excluded from the analysis. In the table, a value of 1 would indicate that the edge zone performed similarly to the center zone. For all cases where the edge was

insulated with 2”(50mm) of insulation, the edge zone performed similar to the center zone as expected. That is, the edge zone was completely snow free by the time the center zone was completely snow free.

For cases that the edge zone was not insulated, it can be observed that the performance has been degraded. The heat flux supplied to the pipe is the minimum flux for the center zone that maintains the free area ratio of 1. For edge zone cases without the insulation, this heat flux can't maintain the expected free area ratio. The ratio is still very close to one, indicating that only at the very edge was the performance degradation significant.

As expected, higher soil conductivity and deeper tube depth cause more degradation in performance. Higher tube spacing generally appears to have better performance. This may be specious, as the analysis area (Patch 1 and Patch 2) increase with higher tube spacing. Presumably, smaller tube spacing should give better performance near the edge.

Vertical text on the right margin, possibly a page number or reference, oriented vertically.

Table 2.11
Maximum Percentage Edge Losses for Transient Conditions (Free Area Ratio = 1.0)

				Spokane	Reno	SLC	Springs	Chicago	OKC	Minneapolis	Buffalo	Boston	Philadelphia
no insulation layer	K _{soil} =0.5 Btu/(h-ft ² -F)	Depth=2"	Spacing=6"	23.7	27.2	26.8	20.8	21.6	17.3	18.7	20.4	20.9	19.6
			Spacing=8"	23.1	26.4	25.6	20.2	20.7	16.4	17.8	19.4	19.6	18.0
			Spacing=12"	19.6	22.7	22.8	17.7	17.2	13.8	15.6	16.4	16.4	14.8
		Depth=4"	Spacing=6"	27.2	29.4	20.2	25.8	24.2	22.3	23.1	24.7	25.3	23.8
			Spacing=8"	24.9	28.7	29.3	24.5	22.9	21.1	22.2	23.6	24.2	22.9
			Spacing=12"	21.8	26.1	26.6	21.9	19.8	-	20.0	20.8	21.2	19.7
	K _{soil} =1.4 Btu/(h-ft ² -F)	Depth=2"	Spacing=6"	27.3	33.0	34.3	27.6	28.1	23.4	24.3	26.3	27.0	25.1
			Spacing=8"	26.9	31.9	32.7	26.8	26.2	21.9	22.8	24.9	25.0	22.9
			Spacing=12"	20.9	28.1	28.4	23.1	23.1	17.9	19.2	20.9	20.4	18.7
		Depth=4"	Spacing=6"	30.5	36.0	36.8	32.6	32.0	28.9	29.1	31.2	31.6	29.5
			Spacing=8"	28.5	35.0	35.7	31.3	31.0	26.7	27.6	29.9	30.0	28.0
			Spacing=12"	24.5	31.1	31.7	27.0	23.3	-	24.3	25.8	25.4	24.0
with 2" insulation layer	K _{soil} =0.5 Btu/(h-ft ² -F)	Depth=2"	Spacing=6"	4.1	4.0	4.0	3.1	2.9	2.2	3.0	3.0	2.8	2.5
			Spacing=8"	4.1	3.8	3.8	3.0	2.8	2.1	3.0	2.9	2.7	2.4
			Spacing=12"	3.6	3.6	3.6	2.9	2.5	1.8	2.7	2.6	2.4	2.1
		Depth=4"	Spacing=6"	5.0	4.8	4.8	4.1	3.8	2.9	4.0	3.8	3.7	3.3
			Spacing=8"	4.8	4.6	4.7	4.0	3.6	2.8	3.9	3.7	3.6	3.2
			Spacing=12"	4.3	4.4	4.4	3.7	3.3	2.5	3.6	3.4	3.3	2.9

2.4. Conclusion of Parametric Study

The parametric study of snow-melting systems investigates the effects of transient conditions, back losses, tube spacing, tube depth, insulation, and soil conductivity on system performance. Key findings for cases with free area ratio of one include:

- The 99% steady-state non-exceedance loads are not closely correlated to the performance of the system under transient conditions with back losses. The heat flux required to maintain the pavement snow-free for the number of hours with steady-state loads less than the 99% non-exceedance loads, may be from 1 to 5 times as high as the 99% non-exceedance load.
- For some cases, the flux requirement exceeds the level that is feasible to obtain in practice. It indicates that in many situations, it's impractical to meet the design goal of maintaining a free area ratio of one. In these cases, idling is suggested.
- More than any other factor, the results are most sensitive to the storm itself. Storms that start off with relatively low loads, perhaps even ceasing to snow for a few hours, then increasing in intensity, will have much lower ratios of heat flux requirement than the storms that start off with high loads.
- After the storm, the results are most sensitive to pipe spacing. The farther apart the tubes, the more difficult it is to maintain free area ratio of one. As the tubes are placed deeper, the effect of spacing is less important.
- The flux requirements are almost insensitive to the soil conductivity and the insulation level. Insulation is useful for reducing back losses, particularly as the snow event increases in time.

For a free area ratio of zero, the results are much more difficult to interpret. With respect to the importance of the storm, the tube spacing, and the tube depth, the results are similar to those for a free area ratio of one. However, with respect to the ratio between the heat flux required under the transient conditions to the 99% non-exceedance load, the results of a free area ratio of zero depend highly on how the concept of a free area ratio of zero is mapped to transient conditions. In the parametric study, free area ratio of zero is interpreted as the equivalent dynamic condition that the snow height does not increase for any more hours beyond the number that exceed the 99% non-exceedance load. This has resulted in some cases for which there is very little snow on the slab edges, and a higher flux was required to decrease the snow height near the edges while at the other area of the surface, the snow height has already stopped increasing. An alternative (untried) would be to interpret free area ratio of zero as the condition where the slab may be entirely covered during all hours of storm.

3. Modeling the Bridge Deck by Transfer Function Method

3.1. Introduction

The BFC-FV model described in Chapter 2 uses a finite volume solver to calculate the temperature distribution of the slab and surroundings. This method requires a large amount of program storage space and must go through the time consuming procedure of calculating temperatures, such as nodal temperatures inside the slab, which are not needed in the analysis of the surface conditions. An alternative is to replace the finite volume solver with a time series technique that improves both the speed and storage requirements.

One type of time series solution is the transfer function method, which relates the current flux via a linear, algebraic equation to flux and temperature histories. For the flux at one surface of an element, because it only relates to the series of temperature and flux histories at the both surfaces, and the history of heat sources or sinks inside the element, there is no need to calculate the other inside nodal temperatures, thus, the transfer function method becomes much more computationally efficient.

This chapter aims at developing a bridge deck model by heat source transfer function method (Strand, 1995, 1997). This new model, abbreviated to QTF model, is expected to be used as a design and simulation tool for modeling the performance of hydronic and electric-cable heating system. The QTF model can calculate one-dimensional or two-dimensional heat transfer depending on the transfer function

coefficients supplied to the model. The model is tested by comparing simulation results to analytical solutions and the results from other simulation programs.

3.2. Modeling by Transfer Function Method

3.2.1. Heat Transfer in Bridge Decks

Conduction through the deck material and convection due to the flow of the heat transfer fluid are the two heat transfer mechanisms within the bridge deck. The heat transfer due to the hot fluid is taken as an internal source of the bridge deck.

Without heating, the conduction heat transfer within the bridge deck can be solved by the conduction transfer functions (CTFs) as a common slab. Strand (1995) has developed and verified heat source transfer functions (QTFs) that are similar in form to the standard CTFs for the low temperature radiant heating systems. The QTFs may be derived from either a Laplace transform or a state space method, and the heat source transmitted to the slab is treated as a definable, variable input.

The QTF model in this thesis solves the heat transfer within the bridge deck by heat source transfer functions. A program that generates transfer functions, the “QTF calculator”, developed by Strand (1995), has been used to provide the transfer function coefficients to the model prior to the simulation. Figure 3.1 shows a typical arrangement of bridge heating pipe loop. In the one-dimensional heat transfer problem, the heat source described is planar and evenly distributed along the X direction. In the two-dimensional

problem, the heat source is distributed at discrete intervals as shown in Figure 3.1. Heat transfer in Y-direction is calculated by the CTFs and QTFs.

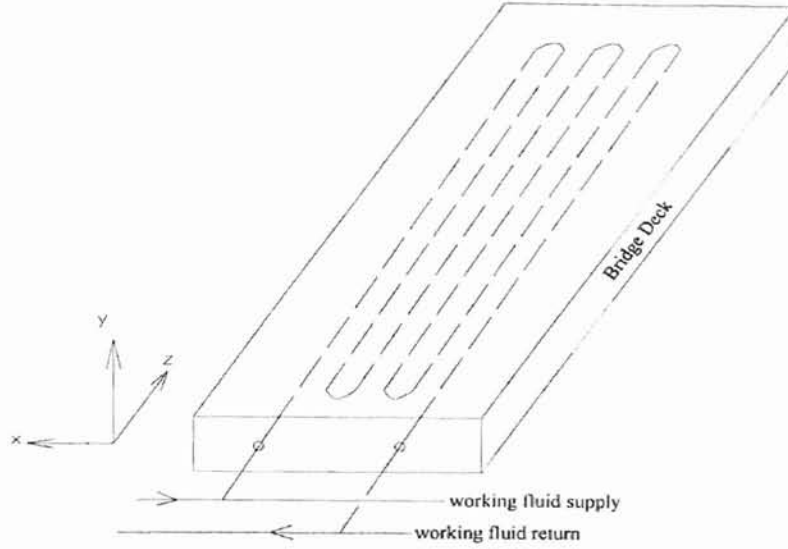


Figure 3.1: Typical arrangement of bridge deck heating pipe loop.

The combined CTF-QTF solution takes the form for the surface fluxes:

$$q''_{btm,t} = \sum_{m=1}^M X_{k,m} T_{btm,t-m+1} - \sum_{m=1}^M Y_{k,m} T_{top,t-m+1} + \sum_{m=1}^k F_m q''_{btm,t-m} + \sum_{m=1}^M W_m q_{source,t-m+1} \quad (3.1)$$

$$q''_{top,t} = \sum_{m=1}^M Z_{k,m} T_{top,t-m+1} + \sum_{m=1}^M Y_{k,m} T_{btm,t-m+1} + \sum_{m=1}^k F_m q''_{top,t-m} + \sum_{m=1}^M W_m q_{source,t-m+1} \quad (3.2)$$

where, X , Y , Z , F and W are the transfer function coefficients, X , Y , and Z are in unit W/m^2-K , and F and W are dimensionless. Subscript *source* refers to the inside heat sources or sinks, and subscripts *btm* and *top* refer to the bottom and the top surface of the bridge deck respectively.

The relations shown in equation (3.1) and (3.2) are identical to the traditional CTFs except for the presence of the QTF series which take the internal heat source or

sink into account. Histories of surface temperatures, surface heat flux and heat source are required. Note that the current heat flux of the internal source is an input to the surface fluxes calculation. This flux may be determined by the heat balance between the bridge deck and the working fluid. Current surface temperatures are also required. In most situations, these temperatures are unknown and need to be determined through a heat balance at the surface.

As stated in the previous section, the QTF model can calculate one-dimensional or two-dimensional heat transfer depending on the transfer function coefficients supplied to the model. However, the two-dimensional transfer functions do not give a two-dimensional answer. Actually, when generating two-dimensional transfer functions, surface fluxes do vary along the surface, but the summation of those terms happens before it calculates the transfer functions. Thus, results for the two-dimensional problem might be described as “mean” value, such as “mean temperature”, “mean flux”, and so on. Equation (3.1) and equation (3.2) are still applied to two-dimensional problems, with transfer functions that are formulated as one-dimensional in the Y-direction as shown in Figure 3.1. This limitation of the heat source transfer functions generated by the “QTF calculator” makes it impossible to calculation flux and temperature distribution along the surface.

There are two more assumptions made in the program generating transfer functions for two-dimensional cases. It assumes uniform surface temperature, and

homogeneous slab. These may not be true, for in many applications, slabs are multiplayer, and surface temperatures vary with location in two-dimensional cases.

3.2.2. Boundary Conditions

Surface conditions are significantly affected by weather conditions. Boundary models should be able to reflect the various and transient effects of weather conditions. Both the top and bottom boundary condition are mixed type with convection and radiation occurring at the surfaces. However, the bottom of the slab is approximated as adiabatic if insulated.

In the following section, radiation and convection heat flux calculation are discussed separately, and it's followed by an introduction of the boundary model for the top surface.

3.2.2.1. Radiation occurring at the boundary

Solar Radiation Heat Gain

Solar radiation occurs at both the top and the bottom surface. Solar radiation heat gain (q_{solar}) is the net solar radiation absorbed by the slab. It is decided based on the surface absorptance α and the solar flux incident on the surface. The solar radiation term should be included in the heat balance calculation. It is significant both in the summer when the bridge deck may be used to recharge the ground (the fluid circulating in the system is supposed to absorb heat from the bridge deck, and release heat to the ground), and in the winter when solar radiation may reduce the heat flux required from the system.

www.researchgate.net/publication/310111111

The total short-wave solar radiation flux incident on an exterior surface can be expressed as

$$I_t = I_D + I_d \quad (3.3)$$

where

I_t = total short-wave solar radiation flux incident on the surface (W/m²)

I_D = direct solar radiation flux on the surface (W/m²)

I_d = diffuse radiation flux incident on the surface (W/m²)

Then,

$$q_{solar} = \alpha \cdot I_t \quad (3.4)$$

The solar radiation absorbed by the snow/slush surface is estimated by the formula given by Kondo and Yamazaki (1990).

$$G_t = (1 - \alpha)G_{th} \quad (3.5)$$

where,

α = Snow albedo = Snow reflectance

$G_{th} = I_t$ = Total horizontal solar radiation (direct and diffuse) (W/m²).

G_{th} can be obtained from Mesonet, and the value of α is estimated by the following equations given by Tarboton and Luce (1996).

$$\alpha_v = (1 - C_v F_{age}) \alpha_{v,o} \quad (3.5-a)$$

$$F_{age} = \frac{\tau}{1 + \tau} \quad (3.5-b)$$

$$\Delta \tau = \frac{r_1 + r_2 + r_3}{\tau_0} \Delta t \quad (3.5-c)$$

where,

α_v = Snow albedo in the visible range;

$\alpha_{v,o}$ = Fresh snow albedo: $\alpha_{v,o} = 0.85$;

C_v = Sensitivity parameter to snow aging: $C_v = 0.2$;

F_{age} = Function to account for aging of the snow surface,

$$= \frac{\tau}{1 + \tau};$$

τ = Non-dimensional snow surface age, $\tau = \tau_{old} + \Delta \tau$;

$\tau_0 = 10^6$ seconds;

Δt = time step, seconds;

r_1 = Parameter dependent on snow surface temperature T ($^{\circ}\text{K}$)

$$= e^{5000 \cdot \left(\frac{1}{273.15} - \frac{1}{T} \right)}$$

r_2 = Additional effect near and at freezing point due to melt and refreeze

$$= \text{minimum} (r_1^{10}, 1);$$

r_3 = Effect of dirt and soot (= 0.03)

One difficulty is how to set the start of snow surface age τ . The most complex situation is that large precipitation would restore the surface to new condition. As recommended by Tarboton and Luce (1996), 0.01 m of snowfall is assumed to restore the snow surface to new conditions ($\tau = 0$) in the QTF model.

Currently, the QTF model has two ways to set the value of snow albedo. One is the calculation according to the equation (3.5a-c), and the other requires the estimation of snow albedo α as an input. With new snow surface, the estimated value of snow albedo is 0.8 recommended for the QTF model, which means about 20% solar radiation is considered absorbed by the snow surface. A lower estimated value of snow albedo can be used when snow surface is not new.

The only short-wave solar radiation flux incident on the bottom is the diffuse solar radiation flux from the ground. This term is assumed to be negligible, and hasn't been considered in the heat balance at the bottom boundary.

Solar radiation data are available from a variety of sources. For purposes of validating against local experimental data, solar radiation (I_t) incident on the horizontal surface can be found in the data set provided by the Oklahoma Mesonet, which is a network of environmental monitoring stations. At each site, the environment is measured by a set of instruments located on or near a 10-meter-tall tower. The measurements are packaged into "observations" every 5 minutes, then the observations are transmitted to a central facility every 15 minutes, 24 hours per day year-round. The Stillwater Mesonet Station is about 1 mile (1.6 km) from the medium-scale heated bridge deck.

Thermal Radiation Heat Transfer

With the assumption that the bridge deck is horizontal, the formula of the long-wave radiation heat flux can be simplified. For the top surface of the bridge deck, the

view factor of surface to the sky is one, and the long-wave radiation heat flux can be determined by:

$$q_{LWR} = \varepsilon\sigma(T_{sky}^4 - T_{surf}^4) \quad (3.6)$$

For the bottom surface of the horizontal bridge deck, the view factor of surface to the ground is nearly one, and the long-wave radiation heat flux is calculated by:

$$q_{LWR} = \varepsilon\sigma(T_g^4 - T_{surf}^4) \quad (3.7)$$

where, ε is the emissivity coefficient of the slab surface, σ is the Stefan-Boltzmann constant, T_{surf} is the surface temperature in absolute units, and T_{sky} is the effective sky temperature in absolute units. The ground temperature T_g is assumed to equal the air temperature, though, it may need further research.

Among the numerous models available for estimating the effective sky temperature, the Brown sky model (Brown 1996) demonstrates the best agreement with more sophisticated models (ASHRAE 2001). The Brown sky model has been selected to predict the sky temperature in the QTF model, and it solves for an effective sky emissivity, which directly relates outdoor dry bulb temperature to the effective sky temperature as:

$$T_{sky} = \sqrt[4]{\varepsilon_s} \cdot T_{air} \quad (3.8)$$

where ε_s is the sky emissivity.

$$\varepsilon_s = 0.65 + 0.41p_{vap}^{0.9} \cdot \exp(-0.01033T_r - 6.060 \times 10^{-4}T_r^2 + 6.121 \times 10^{-6}T_r^3) \quad (3.8-a)$$

where p_{vap} is water vapor pressure (kPa), and T_r is the reference temperature(K).

$$T_r = T_{air} - 240.0 \quad (3.8-b)$$

3.2.2.2. Convection Occurring at the Boundaries

Convection coefficient is calculated by the BLAST detailed convection model (Walton 1981). Convection is split into forced and natural components. The total convection coefficient is taken as the sum of these two components.

$$h_c = h_f + h_n \quad (3.9)$$

The forced convection component is based on a correlation given by Sparrow, Ramsey, and Mass (1979):

$$h_f = 2.537 \cdot W_f R_f \sqrt{\frac{P V_{az}}{A}} \quad (3.9-a)$$

where, h_f is the forced convection coefficient (W/m^2-K), W_f is the wind direction modifier, R_f is the surface roughness multiplier, P is the perimeter of surface(m), V_{az} is wind speed, modified for height above ground (m/s), and A is the area of the surface (m^2). The surface roughness multiplier R_f is based on the ASHRAE graph of surface conductance and the value is 1.52 with the roughness index 3 for the concrete.

The wind speed is modified from the wind speed at standard conditions by the equation

$$V_{az} = V_o \cdot (z/9.14)^{1/\alpha} \quad (3.9-b)$$

where α is defined according to the terrain type of the building's surroundings –7.0 for flat, open country, 3.5 for rough wooded country, and 2.5 for towns and cities (Walton 1981) – and z is the bridge deck height (m) above ground.

For the top surface, the natural convection component in W/m^2 is taken as

$$h_n = 9.482 \cdot \frac{\sqrt[3]{|T_{surf} - T_{air}|}}{7.238 - |\cos \phi|} \quad (3.9-c)$$

when the heat flow is up (the surface temperature is higher than the air temperature), and

$$h_n = 1.810 \cdot \frac{\sqrt[3]{|T_{surf} - T_{air}|}}{1.382 + |\cos \phi|} \quad (3.9-d)$$

when the heat flow is down (the surface temperature is lower than the air temperature).

For the bottom surface, conversely, equation (3.9-c) is for the case that the heat flow is down, and equation (3.9-d) is for the case of upward heat flow. ϕ in equation (3.9-c and d) is surface tilt angle. Under the assumption of horizontal bridge deck, the tilt angle is zero for the top slab surface, and 180 degree for the bottom.

3.2.2.3. Boundary Model at the Top Surface

For a hydronic and electric-cable heating system, heat transfer due to the environmental interactions at the top surface of the bridge include the effects of solar radiation heat gain, convection heat transfer to the atmosphere, thermal radiation heat transfer, sensible heat transfer to snow, heat of fusion required to melt snow, and heat of evaporation lost to evaporating rain or melted snow. A detailed boundary model is added to the QTF model to deal with the complex top surface condition. This boundary model was originally developed in the ASHRAE 1090-RP (Spitler *et al.* 2001) and coupled with the BFC-FV model. It was adapted for use with the QTF method. One of the modifications is that the original formula of calculating convective heat transfer coefficient used in the ASHRAE 1090-RP, which is for turbulent flow, is replaced by the

method described in the previous section. Please refer to Chapter 1 for the details of the ASHRAE 1090-RP boundary model for the top surface. In addition, solar radiation heat gain has been added, and the long-wave radiation model has been modified as discussed in the section 3.2.2.1.

The transfer function model is coupled to the boundary condition model by passing surface temperature information and heat flux information between the two models. Surface temperatures are required as inputs for the transfer function method. The current time step's temperatures are unknown – for each time step, a guess must be made initially, then iterated on. The transfer function model passes the surface flux it has calculated to the top and the bottom boundary condition models. The boundary condition models then calculate the surface temperatures and the mass condition under these surface flux inputs. The new surface temperatures are, in turn, passed back to the transfer function model. This iterative process is considered converged when the surface temperatures calculated by the boundary model become consistent with those used in the transfer function model.

3.2.3. Heat Transfer at the Source Location

For slabs with the internal heat source, $q_{source, t}$, heat flux at the source location at the current time t , is an input to calculate the current surface fluxes as Equation (3.1) and (3.2). Different system control schemes start with different known conditions. In flux control, the heat source is defined and the temperatures of the working fluid need to be calculated. However, in temperature control, the control profile defines the inlet fluid

temperature. The heat flux at the source location needs to be calculated to satisfy the heat balance between the heat loss of the fluid and the heat gain of the bridge material. That is,

$$q_{fluid,t} = q_{source,t} \quad (3.10)$$

It should be made clear that the source location refers to the outside tube wall that directly has contact with concrete. Then, it assumes that the tube quickly reaches the heat balance with the working fluid.

The transfer function for the calculation of $T_{src,t}$, the temperature at the source location at time t , is in the form:

$$T_{src,t} = \sum_{m=1}^M x_{k,m} T_{i,t-m+1} - \sum_{m=1}^M y_{k,m} T_{o,t-m+1} + \sum_{m=1}^k f_m T_{src,t-m} + \sum_{m=1}^M w_m q_{source,t-m+1} \quad (3.11)$$

This equation can be arranged to show the current source flux as a function of current temperatures, past temperature and past source heat fluxes.

$$q_{source,t} = \frac{\sum_{m=1}^M x_{k,m} T_{i,t-m+1} - \sum_{m=1}^M y_{k,m} T_{o,t-m+1} + \sum_{m=1}^k f_m T_{src,t-m} + \sum_{m=2}^M w_m q_{source,t-m+1} - T_{src,t}}{-w_1} \quad (3.12)$$

That is, once the source temperature is known, the source flux can be determined by the transfer function. The source flux then can be used to calculation the heat flows occurred at the surfaces. Thus, the problem of calculating $q_{source,t}$ in the temperature control reduces to how to calculate the temperature at the source location ($T_{src,t}$).

To calculate the temperature at the outer pipe wall, which is also the temperature at the source location for the QTF equations, the overall bridge deck system can be thought of as a heat exchanger. Concrete can be taken as a stationary fluid with heat

exchange with the working fluid inside of the tube. (This is an approximation, but it seems to be the best we can do.) Generally, there are two alternative heat exchanger methodologies. It's more convenient to use the effectiveness-NTU method in this case.

NTU algorithm for the calculation of the temperature at the source location

The effectiveness ε is defined as:

$$\varepsilon \equiv \frac{q}{q_{\max}} \quad (3.13)$$

The actual heat transfer rate q can be obtained through the effectiveness and the maximum possible heat transfer rate.

It's assumed that the temperature along the outside tube wall in the calculation domain is uniform. This assumption was made in the transfer functions calculation (Strand 1995). The maximum heat transfer rate can be obtained if one of the fluids were to undergo a temperature change equal to the maximum temperature difference present in the exchange, which is the difference in the entering temperatures of the hot and cold fluids. In this case, because the source is characterized by a single temperature, the maximum temperature difference is the difference in the entering temperature of the hot fluid and the source temperature. It limits the source temperature to be lower than the outlet fluid temperature, which may not be true in actuality.

In the following section, the calculations of the effectiveness and the convective heat transfer coefficient are explained. It's followed by an explanation of the relation

between the source temperature and the fluid inlet and outlet temperatures. This is summarized in the flow chart shown in Figure 3.2.

- **Effectiveness calculation**

The effectiveness is related to the NTU (the number of transfer units) and capacity ratio C , which can be found in any introductory heat transfer book.

$$NTU = \frac{UA}{C_{\min}} \quad (3.14)$$

$$C = \frac{C_{\min}}{C_{\max}} \quad (3.15)$$

Where $C_{\min} = \min\left((\dot{m}c_p)_{\text{fluid}}, (\dot{m}c_p)_{\text{concrete}}\right)$, $C_{\max} = \max\left((\dot{m}c_p)_{\text{fluid}}, (\dot{m}c_p)_{\text{concrete}}\right)$.

The assumption of uniform temperature at the source location implies that “the stationary fluid” undergoes a very small temperature difference. To satisfy the energy balance between fluids, it infers that heat capacity of the concrete deck is much larger than that for working fluid, which results in the capacity ratio C going to zero. In the case that $C \rightarrow 0$, the heat-exchanger effectiveness relation approaches a simple formula,

$$\varepsilon = 1 - e^{-NTU} \quad (3.16)$$

$$NTU = \frac{UA}{(\dot{m}c_p)_{\text{fluid}}} \quad (3.16\text{-a})$$

where UA is the overall heat transfer coefficient between the fluid and the outer pipe wall. With the consideration of the effect caused by the tubes, convection resistance R_{conv}

and the conductive resistance R_{cond} caused by pipe wall are presented in the overall heat transfer coefficient, and UA is in term of the outer pipe area A_o .

$$UA = \frac{1}{R_{conv} + R_{cond}} A_o \quad (3.16-b)$$

$$R_{conv} = \frac{1}{h} \frac{A_o}{A_i} = \frac{1}{h} \frac{D}{d} \quad (3.16-c)$$

$$R_{cond} = \frac{A_o \ln\left(\frac{D}{d}\right)}{2\pi k_{pipe} L} = \frac{D \ln\left(\frac{D}{d}\right)}{2k_{pipe}} \quad (3.16-d)$$

where h is the convection coefficient, A_i is the inside pipe area, k_{pipe} is the conductivity of tube, D is the tube outer diameter, d is the interior tube diameter and L is the tube length.

- **Convection heat transfer coefficient**

As shown in equation (3.15-c), the convective heat transfer coefficient h is required for NTU and effectiveness ε calculation. The convective heat transfer coefficient can be obtained from internal flow correlations.

$$Nu_D = \frac{h \cdot d}{k} \quad (3.17)$$

where k is the thermal conductivity of the working fluid.

For laminar flow in a tube of constant surface temperature, the Nusselt number is defined as a constant, 4.36. For the turbulent internal flow, the correlation given by Gnielinski (1976) is used to determine the Nusselt number:

$$Nu_D = \frac{(f/2)(Re_D - 1000)Pr}{1 + 12.7(f/2)^{1/2}(Pr^{2/3} - 1.0)} \quad (3.18)$$

where Pr is the Prandtl number of the working fluid, f is the friction factor given by the Eq(3.18-a), and Re_D is the Reynolds number which is defines by equation (3.18-b).

$$f = \frac{1}{(1.58(\ln Re_D) - 3.28)^2} \quad (3.18-a)$$

$$Re_D = \frac{4\dot{m}}{\pi \cdot \mu \cdot d} \quad (3.18-b)$$

where μ is the absolute viscosity of the working fluid. If the Reynolds number is greater than 2300, the flow is taken as turbulent.

- **Relation between the source temperature and the fluid temperature**

Through the definition of the effectiveness, a relation between the temperature at the source location and fluid temperature can be established. First, the formula for the heat balance on the fluid side is

$$q = (\dot{m}c_p)_{fluid} (T_i - T_o) \quad (3.19)$$

where q is the heat transfer rate, and equals the heat transfer rate between the tube and the concrete, \dot{m} is the mass flow rate of the working fluid, c_p is the specific heat of the working fluid, T_i is the inlet fluid temperature and T_o is the outlet fluid temperature. The maximum amount of heat transfer that can occur is

$$q_{max} = (\dot{m}c_p)_{fluid} (T_i - T_{src}) \quad (3.20)$$

where T_{src} is the current temperature at the source location. Substituting equation (3.19) and equation (3.20) into the definition of the effectiveness, a relation between the source temperature and the fluid temperature is established.

$$T_{src} = T_i - \frac{T_i - T_o}{\epsilon} \quad (3.21)$$

Note that there is a heat balance restriction that T_{src} and T_o need to obey. The heat flux q due to the heat exchange fluid should be consistent with the source flux given by equation (3.10). Together with equation (3.21), two equations for two unknowns, then, T_{src} and T_o , can be solved.

- **Flow chart for NTU method**

The flow chart below describes the calculation for the temperature control system.

For the flux control system, a minor modification needs to be made to the algorithm.

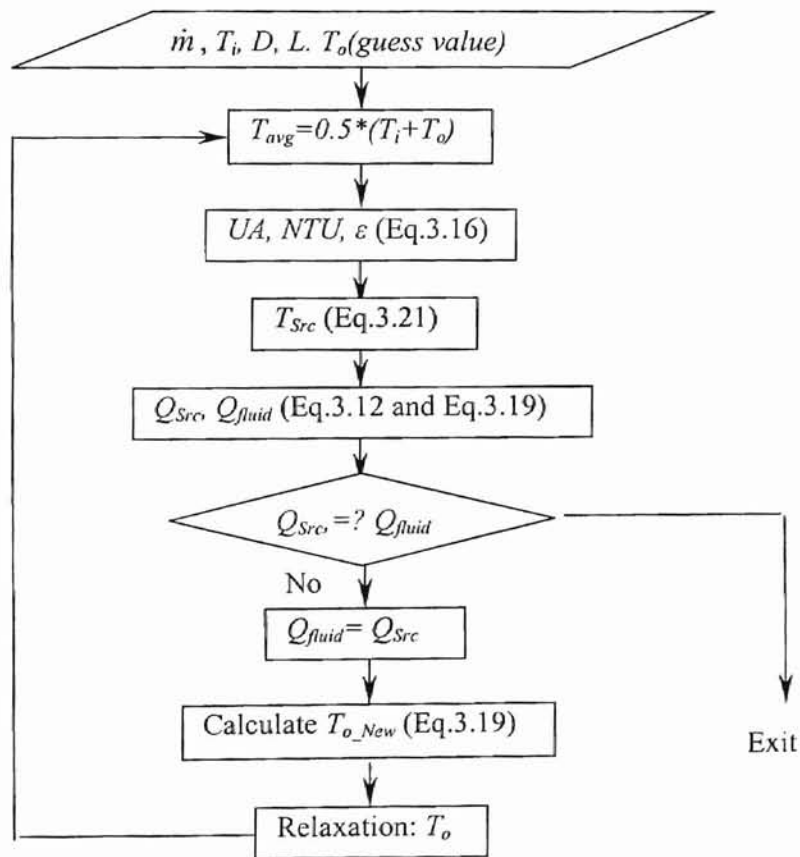


Figure 3.2: Flow chart for the NTU method

3.3. Implementing in HVACSIM+ Environment

The following changes are made to make the transfer function model compatible to HVACSIM+ environment (Clark, 1985):

- Change the subroutine calling arguments of the models.
- Assign the input variables and parameters, the values contained in XIN and PAR arrays.
- Save the variables required for the next time step.
- Assign the output array, OUT to the output variables.

Once the necessary changes have been made to the model to make it compatible with HVACSIM+, the next step is to install the model as a component model in the component library. A description of the model must be added to the file TYPAR.DAT, which is read by HVACGEN for creating the simulation work file.

The first line in TYPAR.DAT starts with an asterisk to indicate the beginning of a new TYPE description. The second line contains the TYPE number, followed by a brief description of the component. The third line contains information on the number of SAVED variables, differential equations, inputs, outputs, and parameters respectively. Next comes a set of lines describing the inputs, outputs and parameters.

Once the description has been added to the TYPAR.DAT listing, the model TYPE routine is added to the “types.for” file of MODSIM and a CALL statement for the subroutine is added to the subroutine SELECT. Now, the component model is ready to be

used for simulation. The TYPAR.DAT listing for the bridge deck model is included in Appendix.

3.4. Results and Discussion

As stated in the previous section, the QTF model can calculate one-dimensional or two-dimensional heat transfer depending on the transfer functions supplied to the model. For one-dimensional problems, the model is tested by comparing simulation results to analytical solutions. For two-dimensional problems, results are compared with those from other simulation programs.

3.4.1. One Dimensional Comparative Studies

3.4.1.1. Comparison of Numerical and Analytical Solutions under No Heating Conditions

Two tests, step change test and sinusoidal change test, have been conducted for the surface response to changes in the air temperature under no flow conditions. The numerical solution obtained using the QTF model in the HVACSim+ environment and the analytical solutions obtained using the ASHRAE Analytical Test Suite (Spitler *et al*, 2001), have been compared. Both the numerical and analytical tests are carried out using the same set of parameters described in the following sections. The thermo-physical properties for material used in the tests have been tabulated below in Table 3.1.

Table 3.1

Parameters Used for One-dimensional Analytical and Numerical Testing

Material	Sublayer	l [m]	k [W/m-k]	c_p [kJ/kg-K]	ρ [kg/m ³]
Lightweight Concrete Block	Lightweight Concrete Block	0.203	0.5711	0.8373	680.7
Bridge Deck	Asphalt	0.0254	0.74	0.920	2100.0
	Concrete	0.0508	0.93	0.653	2300.0
	Concrete	0.127	0.93	0.653	2300.0

TC2: Transient conduction-Step response

The TC2 test in the ASHRAE Analytical Test Suite is applicable to a homogeneous slab. The material tested is lightweight concrete block. In this case, the boundary is convective on either side of the slab. The TC2 test finds the response to step changes in top dry bulb temperature when the bottom air temperature is held constant. Before the step change, the air temperatures are held at constant 20°C (68°F). The amplitude of the step change is +10°C (18°F) while the bottom air temperature is unchanged as shown in Figure 3.3. A constant convection coefficient of 17 W/m² K (3 BTU/h-ft²-°F) for both surfaces is assumed for both numerical and analytical cases.

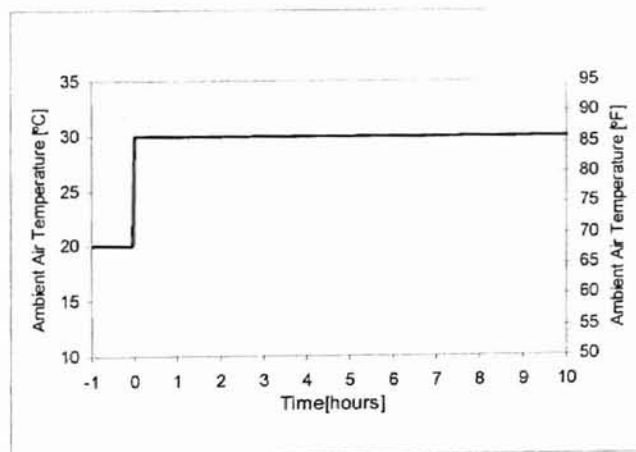
**Figure 3.3:** Profile of the ambient air temperature

Figure 3.4 shows the comparison results for the test TC2 for the bridge deck top and bottom surface temperatures against the numerical results. The numerical solution obtained from the QTF model is in perfect agreement with the analytical solution.

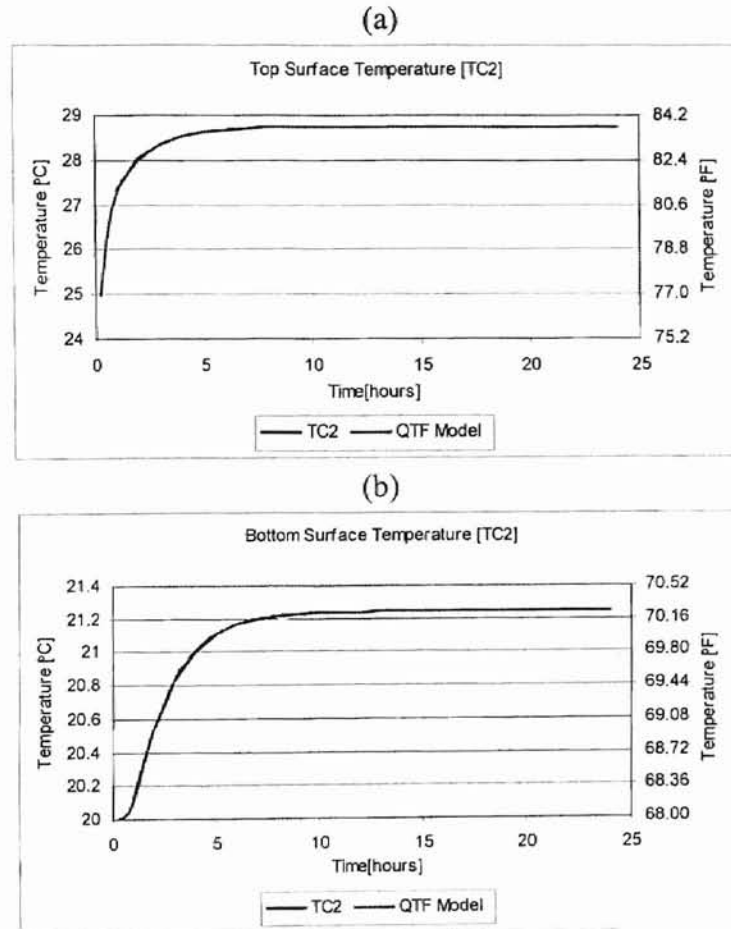


Figure 3.4: Comparison of numerical and analytical solutions for top and bottom surface temperatures (Test TC2)

TC3: Transient conduction- sinusoidal response

The TC3 test in the ASHRAE Analytical Test Suite is applicable to a multi-layer slab. The material tested is “bridge deck” as shown in Table 3.1. Test TC3 finds the response to sinusoidal top dry bulb temperature when the bottom dry bulb temperature is held constant at the mean temperature. Before the sinusoidal top temperature starts, air

temperatures are kept constant at the mean temperature 20°C (68°F). The amplitude of change in top dry bulb temperature is 5°C (9°F), with a period of 24 hours. A constant convection coefficient of 18 W/m² K (3.17 BTU/h-ft²-°F) for both surfaces is assumed for both numerical and analytical cases. The sinusoidal top dry bulb temperature is shown in Figure 3.5.

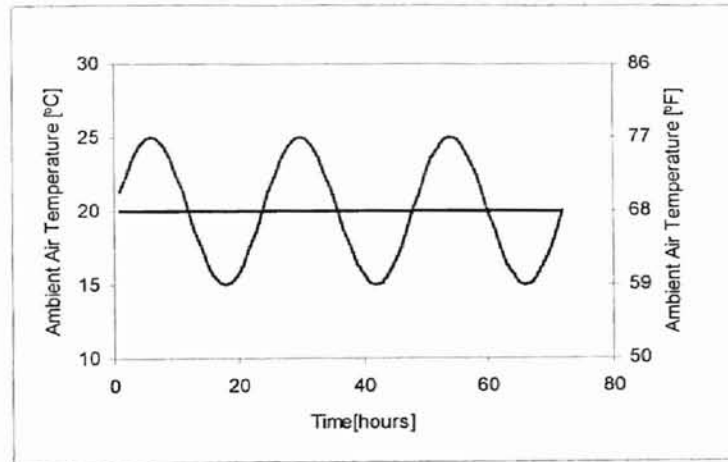


Figure 3.5: Profile of the top ambient air temperature

Figure 3.6 shows the comparison results of the top and bottom surface temperatures. The numerical solution is in good agreement with the analytical solution.

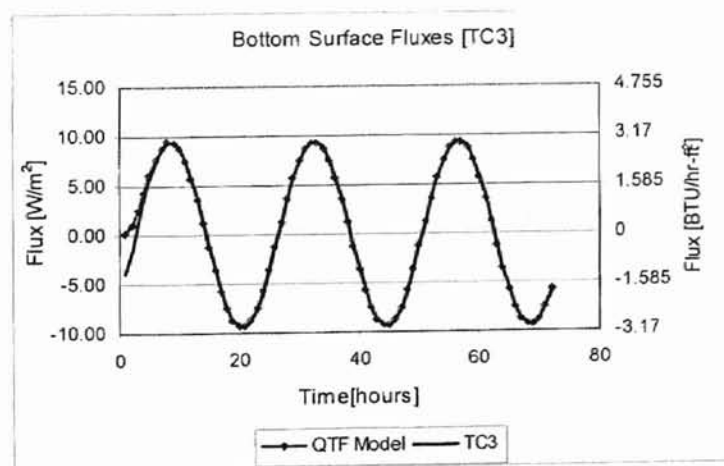


Figure 3.6: Comparison of numerical and analytical solutions for bottom surface fluxes (Test TC3)

3.4.1.2 Response to Changes in Source Fluxes

The tests discussed in section 3.4.1.1 validate the responses of the top and bottom surface temperatures or fluxes computed numerically by the transfer function model against their respective analytical solutions. But, the heat transfer to/from the source embedded in the slab has not been examined in those validations. This section examines the response of slab to changes in source flux.

There are three tests in this section. The numerical calculation results obtained using the one-dimensional QTF model are compared with the analytical results presented by Luikov (1968) and summarized by VanSant (1983) for one dimensional heat transfer in a single layer slab with constant physical properties. For this solution, both the initial temperature of the slab and the boundary conditions at each surface of the slab are taken to be the same constant temperature T_0 . At time = 0, an instantaneous pulse of strength Q (J/m) occurs at the location $x = x_1$ ($0 < x_1 < l$). The temperature distribution within the slab at any location x and time t is reported as:

$$T(x, t) = T_0 + \frac{2Q\alpha}{kl} \sum_{n=1}^{\infty} \sin\left(n\pi \frac{x_1}{l}\right) \sin\left(n\pi \frac{x}{l}\right) e^{\left[-n^2\pi^2 \frac{\alpha t}{l^2}\right]} \quad (3.22)$$

The solution is integrated over time (Strand 1995) to account for a time varying heat input $Q(t)$ (W/m) to the slab as follows:

$$T(x, t) = T_0 + \frac{2\alpha}{kl} \int_0^t \left\{ Q(t') \sum_{n=1}^{\infty} \sin\left(n\pi \frac{x_1}{l}\right) \sin\left(n\pi \frac{x}{l}\right) e^{\left[-n^2\pi^2 \frac{\alpha(t-t')}{l^2}\right]} \right\} dt' \quad (3.22-a)$$

The heat flux at any location x and time t ($q''(x,t)$ (W/m²)) is obtained through differentiation as:

$$q''(x,t) = -\frac{2\pi\alpha}{l^2} \int_0^t \left\{ Q(t') \sum_{n=1}^{\infty} n \sin\left(n\pi \frac{x_1}{l}\right) \cos\left(n\pi \frac{x}{l}\right) e^{\left[-n^2\pi^2 \frac{\alpha(t-t')}{l^2}\right]} \right\} dt' \quad (3.23).$$

In the following tests, the slab is homogeneous with the convective boundary conditions on either side of the slab. Convective heat transfer coefficients are set to constants. The top and bottom surface temperature are held at 10°C (50°F). Test 1 is to find the response to step changes in internal source flux. In Test 2, the instantaneous pulse of strength q occurring at the source location is periodic. In Test 3, the instantaneous pulse of strength q is periodic with a higher frequency, 3hours. The slab material is lightweight concrete. The heat source is located at $x_1/l=1/3$.

Response to step change in internal source flux

The heat source input function is governed by equation (3.24) when time $t > 0$.

$$q'' = 1.0 \text{ (W / m}^2\text{)}. \quad (3.24)$$

The analytical solutions are obtained through equation (3.22) and equation (3.23).

As can be observed from Figure 3.7 and 3.8, transfer function method gives accurate results in the surface fluxes and source temperature calculations. The analytical and numerical results agree perfectly in Figure 3.7. The maximum difference in Figure 3.8 is 0.001°C.

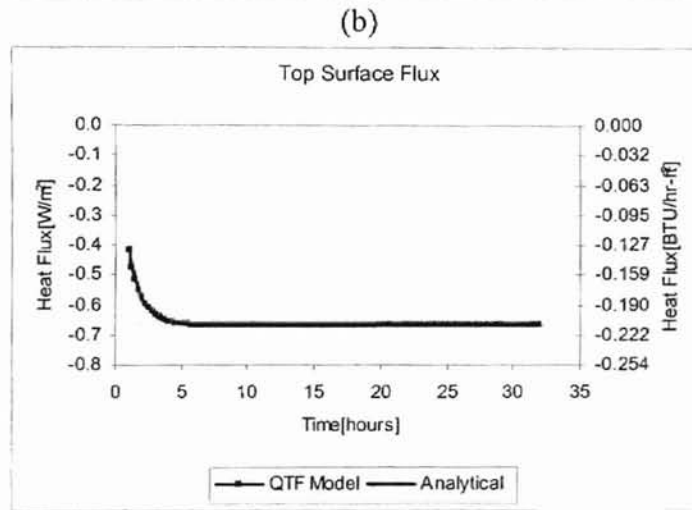
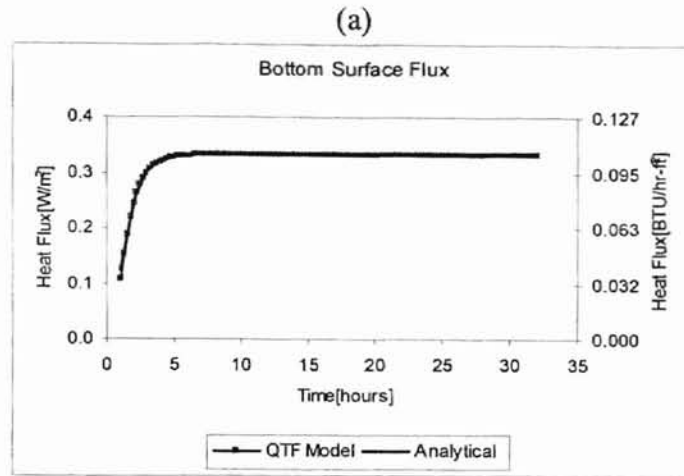


Figure 3.7: Comparison of numerical and analytical solutions for top and bottom surface fluxes (step change in the input function)

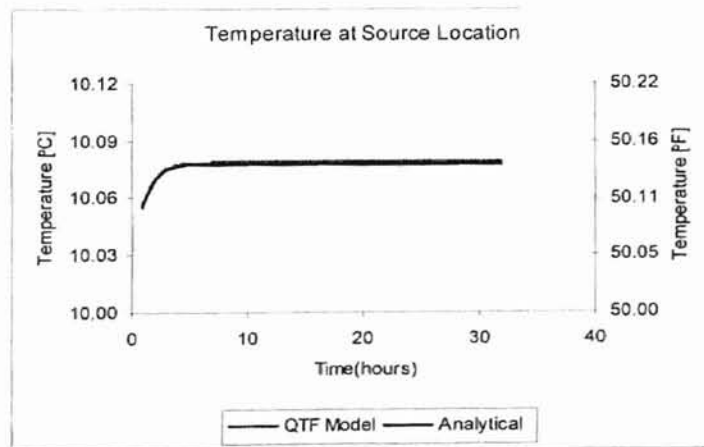


Figure 3.8: Comparison of numerical and analytical solutions for temperature at source location (step change in the input function)

Response to sinusoidal change in internal source flux

The heat source input function is governed by

$$q''(t) = 1.0 + 1.0 \sin\left(\frac{2\pi t}{24}\right) \text{ (W / m}^2\text{)} \quad (3.25)$$

where t is the hour in the simulation. The analytical solutions are obtained through equation (3.22) and equation (3.23).

As can be seen from Figure 3.9, the transfer function method give accurate results in surface flux calculation. In fact, the analytical and numerical results are indistinguishable in Figure 3.9. The same indistinguishable trend can be observed from the source temperature calculation as shown in Figure 3.10.

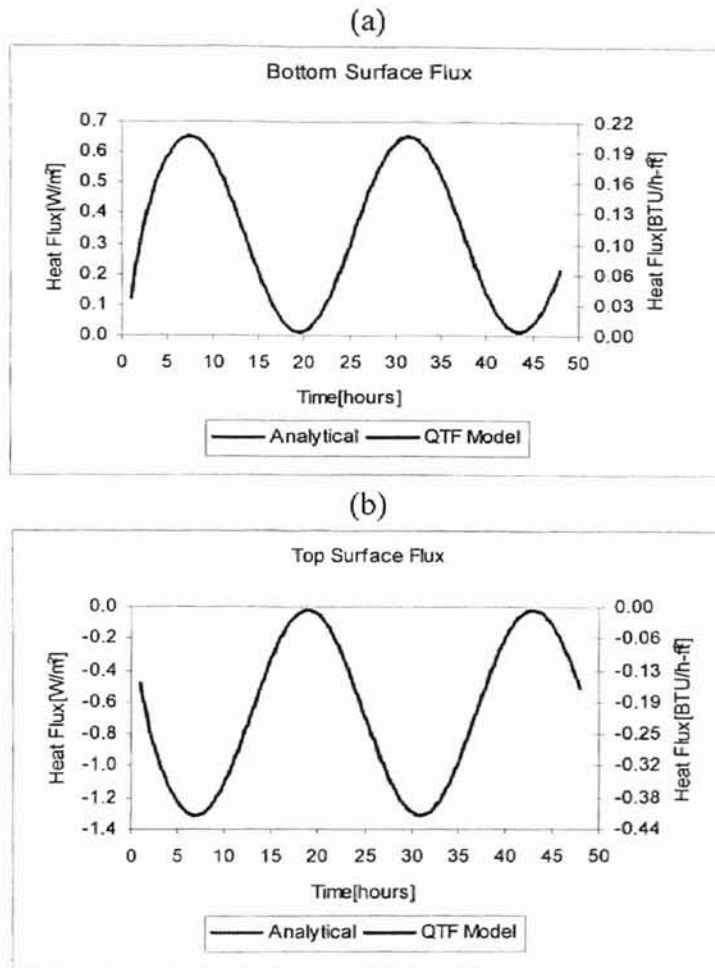


Figure 3.9: Comparison of numerical and analytical solutions for top and bottom surface fluxes (input function period of 24 hours)

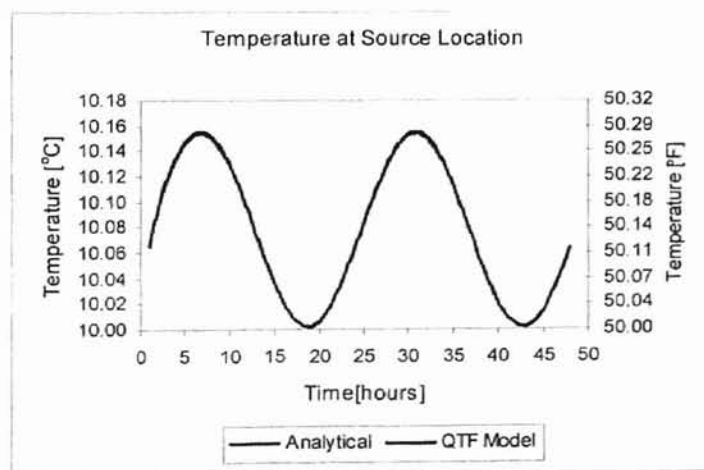


Figure 3.10: Comparison of numerical and analytical solutions for temperature at source location (input function period of 24 hours)

Response to high frequency sinusoidal change in internal source flux

The heat source input function is governed by

$$q''(t) = 1.0 + 1.0 \sin\left(\frac{2\pi t}{3}\right) \quad (\text{W} / \text{m}^2) \quad (3.26)$$

where t is the hour in the simulation. The analytical solutions are obtained through equation (3.22) and equation (3.23). Time step used in the QTF model is 0.25 h/step. Too short time step may cause the instability in the transfer functions generation.

As can be seen from Figure 3.11 and 3.12, under the high frequency heat input function, the numerical results deviate from the analytical solutions. The maximum percentage errors shown in Figure 3.11 are 42% and 56%, respectively. The difference is caused by the linearization of the heat input function in the numerical solutions (Strand 1995).

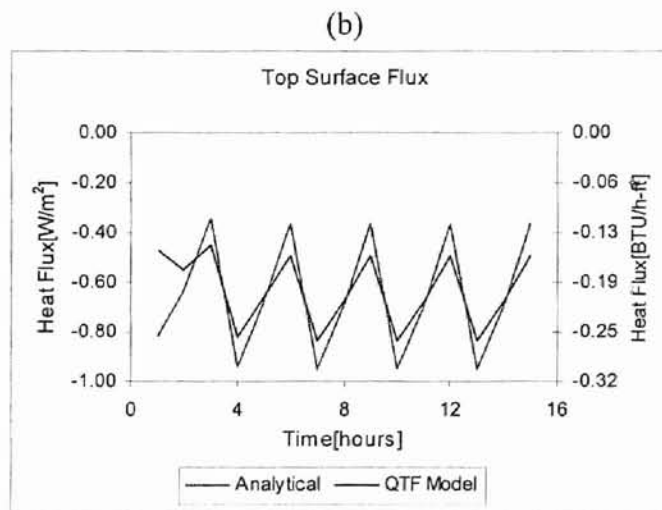
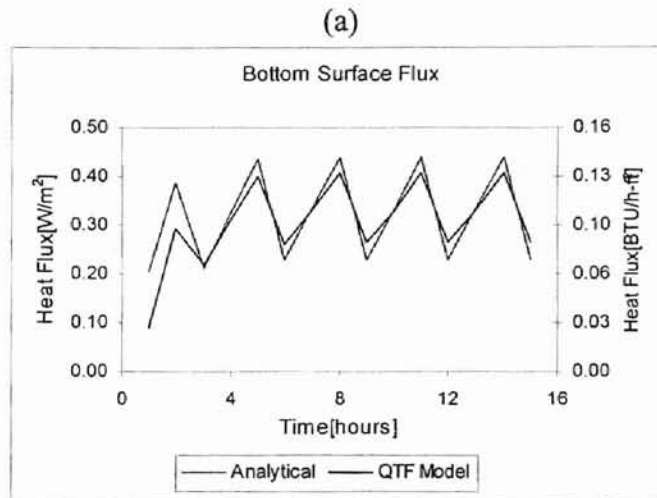


Figure 3.11: Comparison of numerical and analytical solutions for top and bottom surface fluxes (input function period of 3 hours)

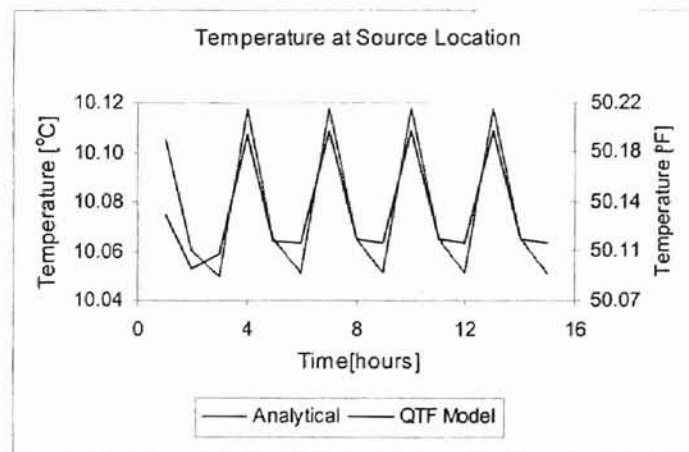


Figure 3.12: Comparison of numerical and analytical solutions for temperature at source location (input function period of 3 hours)

3.4.1.3 Response to Step Change in Fluid Temperature

This section examines the response of the slab to a step change in the temperature of the heat exchanger fluid that is circulated inside the slab. The TC2 test in the ASHRAE Analytical Test Suite serves as the analytical solution. As described before, the TC2 test examines the response to the step change in the outside dry bulb temperature. In the following test, the interior source is centered in the slab as a uniform plane. The step change in the temperature of the heat exchange fluid is analogous to the step change in the outside dry bulb temperature. To match the surface convective heat transfer coefficients used in the TC2 test, the convective heat transfer coefficient specified at the source location in the QTF model is the double surface convective heat transfer coefficient used in the TC2 Test. The heat transfer coefficient at the bottom surface in the TC2 test may be applied directly to the top and bottom surfaces in the QTF model.

The material tested is lightweight concrete block listed in Table 3.1. Before the step change, the air temperatures are held at constant 10°C (50°F). The amplitude of the step change is +30°C (54°F). The bottom air temperature in the TC2 test (or, the air temperature at either surface in the QTF model) is unchanged. A constant convection coefficient of 17 W/m²-K (3 BTU/h-ft²-°F) is assumed for all surfaces, except that a constant convection coefficient of 34 W/m²-K (6 BTU/h-ft²-°F) is assumed for the source location in the QTF model.

Figure 3.13 and 3.14 show the comparison results. The results from the QTF model agree well with those from the TC2 test. Because of symmetry in the geometry and boundary conditions supplied to the QTF model, the temperature distribution obtained from the QTF model is symmetric, and the same surface temperatures are obtained for both surfaces.

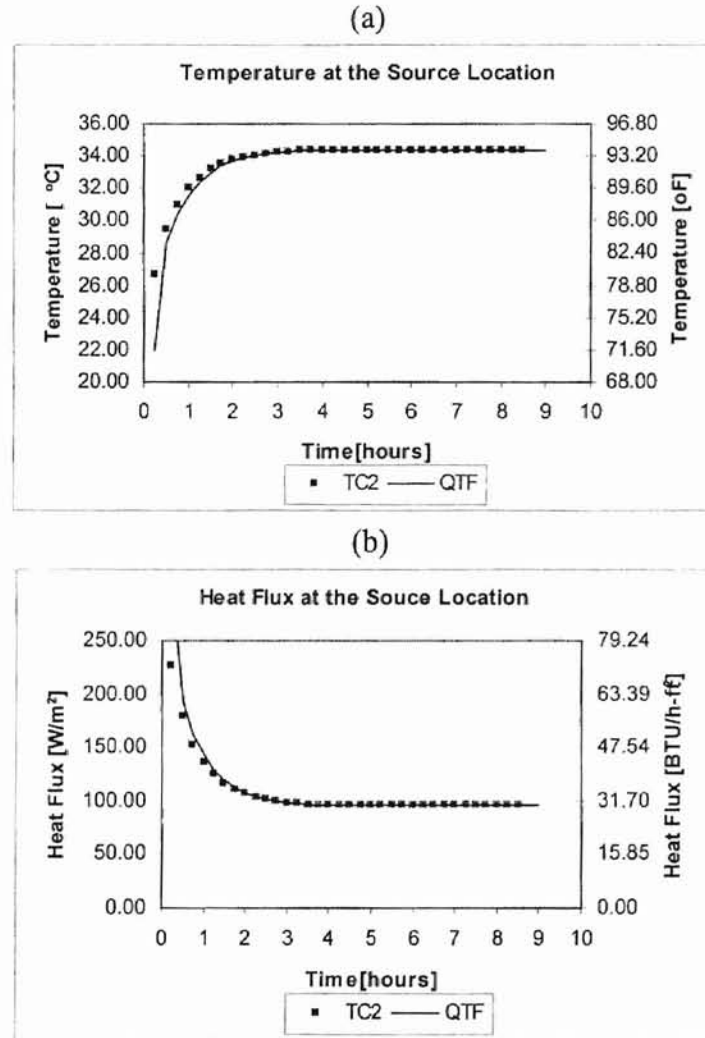


Figure 3.13: Comparison of numerical and analytical solutions for the temperature and the heat flux at the source location

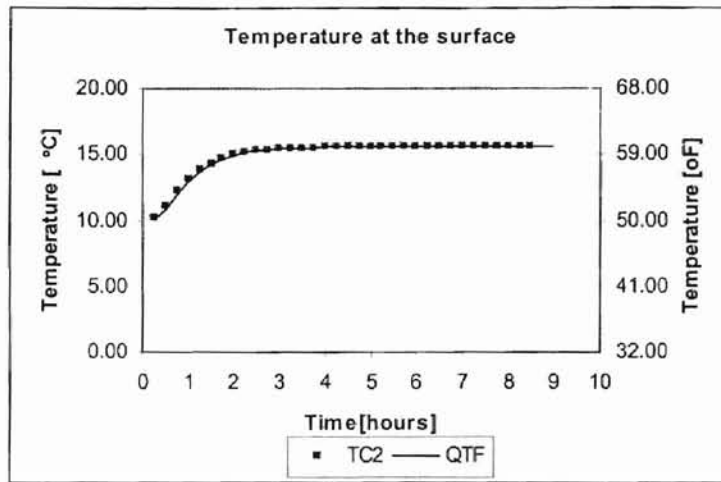


Figure 3.14: Comparison for the temperature at the bottom surface

3.4.2. Two Dimensional Comparative Studies

In this section, studies focus on two-dimensional problems in which the internal heat source is distributed as shown in Figure 3.1. Results from the QTF model are compared against results from the FD model and the BFC-FV model. To simplify the test, a homogeneous slab with an embedded cylinder on the centerline is used. The thermal properties and geometry are tabulated in Table 3.2.

Table 3.2
Parameters Used for Two-dimensional Study

	Material	k [W/m-k]	c_p [kJ/kg-k]	ρ [kg/m ³]
Slab	Concrete	0.57	0.84	608.7
	Material	k [W/m-k]	Outer diameter [mm]	Wall Thickness [mm]
Pipe	E-PexB	0.57 ⁺	22.2	1.6
	Pipe Spacing [m]	Pipe Depth [m]	Pipe Length L [m /circuit]	Slab Thickness [m]
	0.225	0.113	60.0	0.225

⁺: For E-PexB pipe, thermal conductivity is 0.45 W/m-K. To simplify the test, this property is modified to be consistent with the thermal conductivity of slab.

3.4.2.1. Response to Step Change in Source Flux

An instantaneous unit pulse of strength occurs at the source location at time zero. The pulse flux is in unit $W/(slab\ surface\ area, m^2)$. To simplify the test, the top and bottom surfaces of the slab are hold in a constant temperature, $10^{\circ}C$ ($50^{\circ}F$). Because of the symmetric geometry and boundary conditions applied, the temperature and flux distributions are symmetric to the centerline of the slab. Only the comparison of the sums of cell fluxes at the top surface is shown in Figure 3.15.

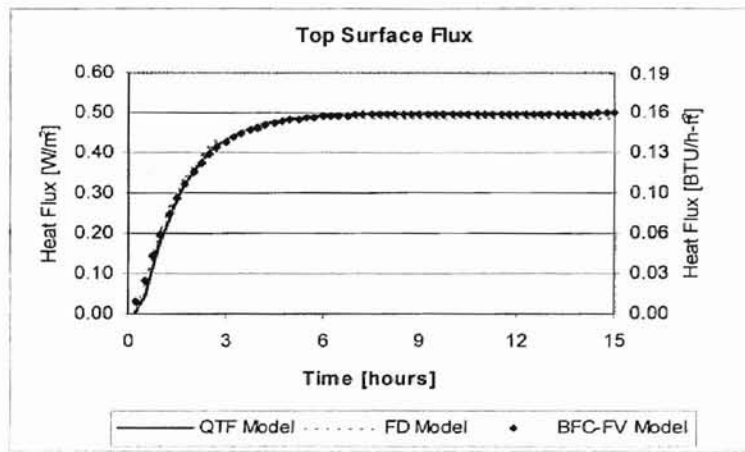


Figure 3.15: Comparison of top surface fluxes obtained from different models

As can be observed from Figure 3.15, results from three models agree well, except that the steady state flux obtained from the FD model shows a little bit lower than the other two. It may be caused by the coarse grid pattern used in the FD model. The flux calculated here is based on the difference between the surface temperature and the average temperature of two neighboring nodes located one level lower than the surface nodes. If the surface flux is calculated through the difference between the surface temperature and the nodal temperature, the sum is higher than $0.5 W/m^2$ ($1.673 BTU/ft^2$). It implies that the calculation of cell fluxes is affected by how temperatures between

neighboring nodes are linearized. If finer grids were used, the temperature distribution would be smoother from node to node, and the error would be diminished.

3.4.2.2. Response to Step Change in Fluid Temperature

The validation in section 3.4.2.1 may be applied to electrical heating systems with cables embedded. In this section, hydronic heating systems are considered. Heat exchange fluid circulates in the hydronic pipes embedded in the slab, and the heat exchange to/from the fluid is the internal source/sink of the system.

The thermal properties of the material and the geometry of the slab can be found in Table 3.2. To eliminate the effect of complex boundary conditions that may occur, temperatures at the top and bottom surface are maintained at 10°C (50°F). The system turns on from the first hour with the inlet fluid temperature 40°C (104°F). The flux and temperature at the source location are calculated according to the NTU method described in the section 3.2.3. The comparison of source fluxes is shown in Figure 3.16.

As can be observed from Figure 3.16, the results from the BFC-FV model and the FD model agree well except the first hour that the system turns active. The QTF model gives a quite different response to the step change. At the first time step that system is active, the QTF solution gives a good approach to the FD solution. The difference in heat flux is 10.4 W/m² (3.296 BTU/ft²) at the first time step. As can be seen from Figure 3.16, the QTF model generally gives a lower source flux than the other two models. The

difference in heat flux when it approaches the steady state is about 24.1 W/m^2 (7.639 BTU/ft^2), and the relative error is 14.8%. This error is examined in the next section.

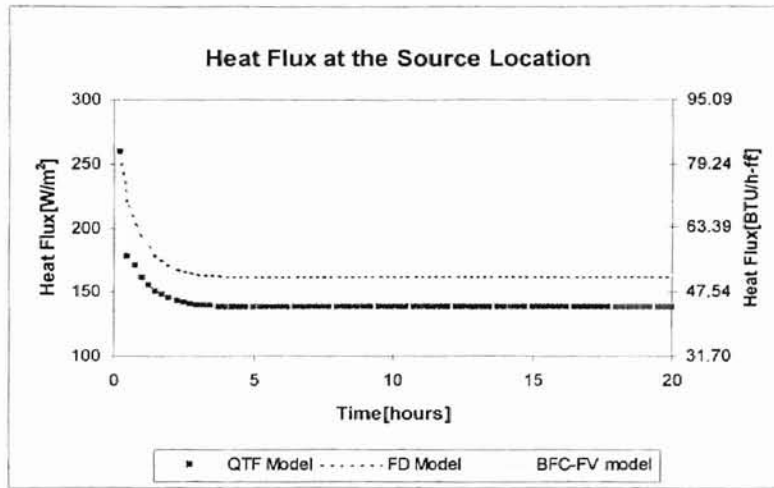


Figure 3.16: Comparison of source fluxes obtained from different models

3.4.3. Error Analysis

In general, results from the QTF model matches well with analytical solutions, or those from other models, except for the hydronic heating cases. This section describes further analyses of the discrepancy in the hydronic heating cases. Various test conditions are examined. The BFC-FV model is selected as the comparison model for its more accurate representation of geometry and boundary conditions compared to the FD model.

Tests are summarized in Table 3.3. All tests have a step change in the average fluid temperature, or the inlet fluid temperature. The average fluid temperature, if specified, is used directly as the fluid temperature. If the inlet fluid temperature is specified, the NTU method described in the section 3.2.3 is used to obtain the outlet fluid temperature and the heat transfer rate. Tests are divided into five categories. The second column in Table 3.3 is the case number in its category, and it is followed by the

description of test conditions. In the column “Results”, steady state results of heat flux and temperature are listed. The last column reports the relative error of the steady state flux at the outer pipe wall.

For cases in category I, slab surfaces are exposed to ambient air with fixed convective heat transfer coefficients. The convective heat transfer coefficient and the fluid temperature are also fixed at the inside pipe wall. The NTU method is not needed to calculate the source temperature. The heat conduction through the pipe wall is a function of the fluid temperature, the convective and conductive resistance, and the source temperature (the temperature at the outer pipe wall). Thus, the source temperature is found, through the energy balance between the heat conduction and the heat source calculated by the transfer functions (equation (3.17)).

Cases in category II are similar to those in category I, except that the slab surface temperatures are fixed. Cases in category III examine the effect of varying the convective heat transfer coefficient at the pipe wall. For cases in the category IV, the inlet fluid temperature and the mass flow rate are specified with the convective heat transfer coefficient fixed at the fluid side. The NTU method is required to obtain the source temperature in this and following categories. For cases in category V, the heat transfer coefficient needs to be calculated by the correlations described in the previous section. Cases in category VI examine the effect of different flow rates.

Table 3.3

Tests Summary for Two Dimensional Hydronic Heating Cases

Category	Case #	Test Condition		Comparison Model	Results			Conclusion
						Comparison Model	QTF	
I.	1	Ambient Air Temperature [°C]	10.0	BFC-FV model	Steady State Flux at the Outer Pipe wall [W/m ²]	92.34	84.36	Error: 8.65%
		Fluid Temperature [°C]	40.0		Inside Pipe Wall Temperature [°C]	29.73	35.33	
		Heat Transfer Coefficient at the Surfaces [W/m ² -K]	17.0		Outer Pipe Wall Temperature [°C]	28.81	--	
		Heat Transfer Coefficient at the Inside Pipe Wall [W/m ² -K]	34.0		Source Temperature [°C]	--	29.84	
II.	1	Surface Temperature [°C]	10.0	BFC-FV model	Steady State Flux at the Outer Pipe wall [W/m ²]	101.68	91.96	Error: 9.56%
		Fluid Temperature [°C]	40.0		Inside Pipe Wall Temperature [°C]	28.7	34.91	
		Heat Transfer Coefficient at the Inside Pipe Wall [W/m ² -K]	34.0		Outer Pipe Wall Temperature [°C]	27.68	--	
					Source Temperature [°C]	--	28.92	

Table 3.3 (continued)

Tests Summary for Hydronic Heating Cases

Category	case #	Test Condition		Comparison Model	Results			Conclusion
						Comparison Model	QTF	
III.	1	Surface Temperature [°C]	10.0	BFC-FV model	Steady State Flux at the Outer Pipe wall [W/m ²]	153.78	132.44	Error: 13.88%
		Fluid Temperature [°C]	40.0		Inside Pipe Wall Temperature [°C]	38.29	39.27	
		Heat Transfer Coefficient at the Inside Pipe Wall [W/m ² -K]	340.0		Outer Pipe Wall Temperature [°C]	36.75	--	
					Source Temperature [°C]	--	37.25	
	2	Surface Temperature [°C]	10.0	BFC-FV model	Steady State Flux at the Outer Pipe wall [W/m ²]	162.1	138.54	Error: 14.54%
		Fluid Temperature [°C]	40.0		Inside Pipe Wall Temperature [°C]	39.82	39.92	
		Heat Transfer Coefficient at the Inside Pipe Wall [W/m ² -K]	3400.0		Outer Pipe Wall Temperature [°C]	38.22	--	
					Source Temperature [°C]	--	38.50	
	3	Surface Temperature [°C]	10.0	BFC-FV model	Steady State Flux at the Outer Pipe wall [W/m ²]	162.98	139.18	Error: 14.61%
		Fluid Temperature [°C]	40.0		Inside Pipe Wall Temperature [°C]	39.98	39.99	
		Heat Transfer Coefficient at the Inside Pipe Wall [W/m ² -K]	34000.0		Outer Pipe Wall Temperature [°C]	38.3	--	
					Source Temperature [°C]	--	38.64	

Table 3.3 (continued)

Tests Summary for Hydronic Heating Cases

Category	case #	Test Condition		Comparison Model	Results			Conclusion
						Comparison Model	QTF	
IV.	1	Surface Temperature [°C]	10.0	BFC-FV model	Steady State Flux at the Outer Pipe wall [W/m ²]	162.62	138.90	Error: 14.56%
		Inlet Fluid Temperature [°C]	40.0		Inside Pipe Wall Temperature [°C]	39.912	--	
		Mass Flow Rate [m ³ /s]	0.44 for 110 circuit		Outer Pipe Wall Temperature [°C]	38.28	--	
		Heat Transfer Coefficient at the Inside Pipe Wall [W/m ² -K]	34000.0		Source Temperature [°C]	--	38.58	
					Outlet Fluid Temperature [°C]	39.87	39.89	
					Mean Fluid Temperature [°C]	39.93	39.94	
V.	1	Surface Temperature [°C]	10.0	BFC-FV model	Steady State Flux at the Outer Pipe wall [W/m ²]	162.62	138.93	Error: 14.57%
		Inlet Fluid Temperature [°C]	40.0		Inside Pipe Wall Temperature [°C]	39.92	--	
		Mass Flow Rate [m ³ /s]	0.44 for 110 circuit		Outer Pipe Wall Temperature [°C]	38.28	--	
					Source Temperature [°C]	--	38.59	
					Outlet Fluid Temperature [°C]	39.87	39.89	
					Mean Fluid Temperature [°C]	39.93	39.94	

Table 3.3 (continued)

Tests Summary for Hydronic Heating Cases

Category	case #	Test Condition		Comparison Model	Results			Conclusion
						Comparison Model	QTF	
VI.	1	Surface Temperature [°C]	10.0	BFC-FV model	Steady State Flux at the Outer Pipe wall [W/m ²]	155.3	132.43	Error: 14.73%
		Inlet Fluid Temperature [°C]	40.0		Inside Pipe Wall Temperature [°C]	38.58	--	
		Mass Flow Rate [m ³ /s]	0.022 for 110 circuit		Outer Pipe Wall Temperature [°C]	37.03	--	
					Source Temperature [°C]	--	37.25	
					Outlet Fluid Temperature [°C]	37.47	37.84	
					Mean Fluid Temperature [°C]	38.73	38.92	

Table 3.4
Summary of Thermal Resistances [K-m²/W]

Category	Case #	QTF Model		BFC-FV Model	
I.	1	R _{fluid-to-Src}	0.120	R _{fluid-to-lwall}	0.111
		R _{Src-to-Slab}	--	R _{Pipe}	0.010
		R _{Src-to-Slab+Air}	0.235	R _{Slab+Air}	0.204
		Total Resistance	0.356	Total Resistance	0.325
II.	1	R _{fluid-to-Src}	0.120	R _{fluid-to-lwall}	0.111
		R _{Src-to-Slab}	0.206	R _{Pipe}	0.010
				R _{Slab}	0.174
		Total Resistance	0.326	Total Resistance	0.295
III.	1	R _{fluid-to-Src}	0.021	R _{fluid-to-lwall}	0.011
		R _{Src-to-Slab}	0.206	R _{Pipe}	0.010
				R _{Slab}	0.174
		Total Resistance	0.227	Total Resistance	0.195
	2	R _{fluid-to-Src}	0.011	R _{fluid-to-lwall}	0.001
		R _{Src-to-Slab}	0.206	R _{Pipe}	0.010
				R _{Slab}	0.174
	Total Resistance	0.217	Total Resistance	0.185	
	3	R _{fluid-to-Src}	0.010	R _{fluid-to-lwall}	0.000
R _{Src-to-Slab}		0.206	R _{Pipe}	0.010	
			R _{Slab}	0.174	
Total Resistance	0.216	Total Resistance	0.184		
IV.	1	R _{fluid-to-Src}	0.010	R _{fluid-to-lwall}	0.000
		R _{Src-to-Slab}	0.206	R _{Pipe}	0.010
				R _{Slab}	0.174
		Total Resistance	0.216	Total Resistance	0.184
V.	1	R _{fluid-to-Src}	0.010	R _{fluid-to-lwall}	0.000
		R _{Src-to-Slab}	0.206	R _{Pipe}	0.010
				R _{Slab}	0.174
		Total Resistance	0.216	Total Resistance	0.184
VI.	1	R _{fluid-to-Src}	0.013	R _{fluid-to-lwall}	0.001
		R _{Src-to-Slab}	0.206	R _{Pipe}	0.010
				R _{Slab}	0.174
		Total Resistance	0.218	Total Resistance	0.185

The relative error between the methods varies between 8.65 and 14.73%. It can, perhaps, be more clearly understood by first looking at the steady-state resistances. Table 3.4 is the summary of thermal resistances for each case. An electrical analog of the heat transfer through the pipe and slab is given in Figure 3.17. Because cases considered are

two-dimensional, temperatures labeled in Figure 3.17 are mean or average temperatures. Each resistance in Table 3.4 is calculated by dividing the heat flux by the corresponding temperature difference. The basis of these resistances is the surface area of the slab.

Notations are defined as follows.

$R_{\text{fluid-to-lwall}}$: convective resistance at the inside pipe wall, $[\text{K}\cdot\text{m}^2/\text{W}]$, used for the BFC-FV model.

R_{Pipe} : conductive resistance caused by the pipe wall, $[\text{K}\cdot\text{m}^2/\text{W}]$, used for the BFC-FV model.

$R_{\text{Slab+Air}}$: sum of conductivity resistance of the slab (not including pipes), and the convective resistance at the slab surface, $[\text{K}\cdot\text{m}^2/\text{W}]$, used for the BFC-FV model.

R_{Slab} : conductive resistance of the slab (not including pipes), $[\text{K}\cdot\text{m}^2/\text{W}]$, used for the BFC-FV model.

$R_{\text{fluid-to-Src}}$: sum of convective resistance at the inside pipe wall and conductive resistance caused by the pipe wall, $[\text{K}\cdot\text{m}^2/\text{W}]$, used for the QTF model.

$R_{\text{Src-to-Slab}}$:conductive resistance of the slab (not including pipes), $[\text{K}\cdot\text{m}^2/\text{W}]$, used for the QTF model.

$R_{\text{Src-to-Slab+Air}}$:sum of conductive resistance of the slab (not including pipes), and convective resistance at the slab surface, $[\text{K}\cdot\text{m}^2/\text{W}]$, used for the QTF model.

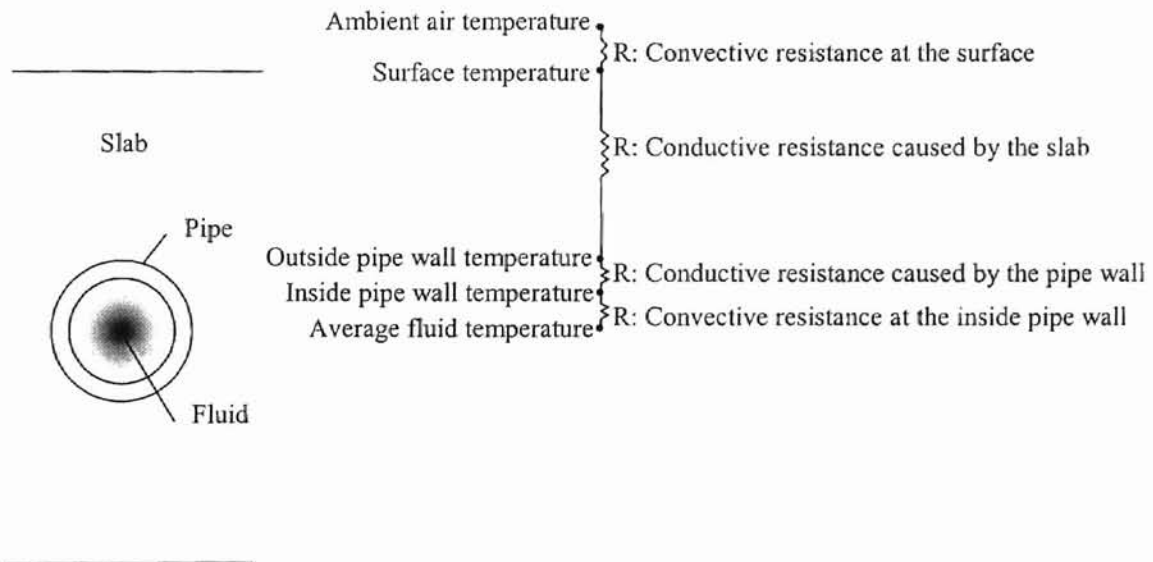


Figure 3.17: Electrical analog of heat transfer through the pipe and slab

For each case, $R_{fluid-to-Src}$ from the QTF model, which is the sum of convective resistance at the inside pipe wall and the conductive resistance caused by the pipe wall, almost exactly matches the sum of $R_{fluid-to-llwall}$ and R_{Pipe} obtained from the BFC-FV model. It demonstrates the accurate calculation of the heat transfer between the fluid and the outer pipe wall. However, as can be seen in category I, there is nearly a 15% discrepancy between $R_{Src-to-Slab+Air}$ and R_{Slab} . These should match exactly. Also, as can be observed from category II to VI in Table 3.4, the conductive resistances ($R_{Src-to-Slab}$ and R_{Slab}) differ in the two models, with 0.206 (K-m²/W) (1.170 F-ft²/BTU) for the QTF model and 0.174 (K-m²/W) (0.988 F-ft²/BTU) for the BFC-FV model. In the QTF model, the resistance is set by the transfer functions developed by the QTF calculator. It implies there are inaccuracies in the transfer functions generation.

In an attempt to reduce the errors, the tests were repeated using transfer functions generated with a more refined internal grid. However, these transfer functions did not improve the calculation. Another possible explanation of the error is the way in which the two-dimensional geometry is interpreted in the "QTF calculator". In the "QTF calculator", the pipe diameter is not required as an input for the two-dimensional problem. The source is defined between two layers, which are measured from the slab surfaces to the center of the pipe. The mixed geometry problem in this kind of system has not been described accurately. Also, other causes may be possible, such as mathematical calculation related to the matrix inverse and root finding.

The error of the conduction resistance is fixed once the material is selected for simulations. The different relative error shown in Table 3.3 can be explained by the relative importance of the conduction resistance error in the total resistance. For instance, cases in category I have lower relative error compared to other tests, because with the consideration of the convective resistance at the slab surface, the total resistance is higher, and it makes the conductive resistance error less important, and so gives a lower relative error. For cases in category III, with increasing convective heat transfer coefficient at the fluid side, the convective resistance becomes lower and lower, and it leads to lower total resistance and higher relative error as shown in Table 3.3 and 3.4.

Another point to be noticed is the effect of the convective heat transfer coefficient in the fluid side. As can be observed from cases in category III, the relative error doesn't change much once the convective heat transfer coefficient at the inside pipe wall is over 3400 [W/m²-K]. It implies that the convective resistance diminishes and becomes negligible as the flow rate increases. This can be observed directly from cases in category V and VI.

One possible way to check the accuracy of the NTU method used in the calculation of the source temperature and heat flux is the comparison between Case 3 in Category III and Case 1 in Category IV. One difference in test conditions is that the former specifies the fluid temperature and the latter sets the inlet fluid temperature. Then, for the Case 1 in Category IV, the NTU method is used to obtain the outlet fluid temperature and the heat transfer rate at the outer pipe wall. A large flow rate is used in

Category IV to make the average fluid temperature close to the fluid temperature for Case 3 in Category III. The relative error for these two cases are close as can be seen from Table 3.3. This example implies the NTU method doesn't impose extra error in the simulation.

3.5. Summary

A design and simulation tool for modeling the performance of a bridge deck heating system has been developed. The model (the QTF model) has been developed based on the transfer function method. According to the transfer functions provided, the model can solve the slab heat transfer problem for one-dimensional or two-dimensional geometry.

For applications that can be considered as one-dimensional, the QTF model presents accurate solutions as compared with analytical solutions from the literature and the ASHRAE Analytical Test Suite. For applications considered as two-dimensional, such as heat sources at discrete intervals, the results obtained from the QTF model match well with those from the FD model and the BFC-FV model in the case of the fixed heat flux input at the source location. However, in the case of hydronic heating systems with heat exchange fluid circulated in the embedded pipe, the discrepancy is obvious. The steady state flux obtained from the QTF model is always lower than results provided by other models. This has been shown to be caused by inaccuracies in the transfer functions provided by the QTF calculator.

Further research is suggested in the following areas:

- A more accurate transfer function calculator is desirable.
- Optimization of the source temperature calculation. Several methods may be tried besides the currently used NTU method.
- Additional validation of the model, using data collected under a wider range of weather conditions (i.e. rain, snow, and ice conditions), would be useful. A preliminary investigation is reported in the next chapter.

4. Validation of the QTF Model by Experimental Data

4.1. Introduction

The previous chapter describes the development of a new bridge deck model (the QTF model) based on the time series method, and the model is validated through analytical solutions and model comparisons. The work described in this chapter is to validate the model by experimental data.

The QTF model depicting the OSU bridge deck system is simulated for heating and recharge cases. A detailed description of the bridge deck system is given in the next section. Experimentally measured inlet fluid temperature and mass flow rate are used as inputs in simulations. For the recharge case, comparisons of top surface temperatures, exit fluid temperatures, and heat transfer rate are given. For the heating case, results are compared to the experimental measurements of the surface temperature and the exit fluid temperature. This study is intended for establishing a better understanding of the performance of the QTF model in simulations with real parameters and weather conditions.

4.2. Previous Work

Continuous work and studies on transient simulations of hydronic heating systems have been done in Oklahoma State University by using the finite difference bridge deck model developed by Chiasson (2000).

Ramamoorthy (2001) discussed the performance of a hydronically heated bridge deck system that is heated with a hybrid ground source heat pump system. The system is simulated and the performance studied in detail for a sample bridge deck located at Weatherford, OK. The simulation results for a few summer recharge set point temperatures are presented. The advantages of using the bridge deck during summer for recharging the ground is quite evident from simulation results. Storing the heat extracted from bridge deck surface during summer raises the ground temperature, and makes it available for use in winter for bridge deck heating. The study also shows that the system modeling and simulation approach is a powerful tool to study and analyze the system performance of several possible designs. Bridge deck heating systems have high initial cost; their optimal design and operation is of paramount importance. Using the system simulation approach, the performance of such systems and different control strategies could be easily simulated and analyzed, and a cost efficient design solution can be achieved.

Ongoing research at Oklahoma State University focuses on the development of a bridge deck heating system to eliminate preferential icing. The heating system is hydronic, and makes use of a ground source heat pump system, which recovers energy stored in the earth, and uses it to heat the fluid circulated through the bridge deck. The heating system automatically makes use of local and remote weather stations to forecast potential icing conditions. The automatic nature of the controls has given rise to the informal name "Smart Bridge". Initial research was done on a test bridge deck, which is described in more detail in the following section, along with an experimentally calibrated

numerical model. Several critical parameters have been more carefully measured (Progress Report, OSU Geothermal Smart Bridge, 2001). For instance, the measured density of the sample concrete was 2324 kg/m^3 at moisture content of 24% of total saturation, and the density from oven-dry to saturated condition varies about 6%. The thermal properties of the bridge deck were recomputed, taking into account two factors – the double-T thermal mass and the rebar embedded in the bridge deck. As a first order approximation, the double-T thermal mass was treated as a uniform layer of concrete 3.8 inches (97 mm thick). The rebar was accounted for by mass weighting the conductivity, specific heat and density. The resulting simulations match the experimental results more closely.

The following section describes the bridge deck system under investigation, the weather data source, and experimental data used in the model validation.

- OSU Bridge System

The experimental bridge heating system comprises a bridge deck with embedded heat exchanger pipe loops, a single water-to-water heat pump, a six-borehole vertical ground loop heat exchanger, along with circulating pumps and control system.

The experimental bridge deck is 18.3m (60 ft) long by 6.1m (20 ft) wide, but only half (9.2m*6.1m) is heated. Bridge deck thickness is 0.254m (10 inch). The pipe work consists of 10 fluid circuits laid in a serpentine configuration perpendicular to traffic flow on the bridge. E-PexB Pipe from WattsHeatway is embedded. Nominal pipe diameters are commonly 19.05mm (0.75 inch). The tubing is 0.0762m (3 inch) beneath the bridge surface measured from the surface to the pipe center with pipe spacing of 0.3048m (1 ft).

The specific heat of concrete used in the simulation is 889 J/kg-K, and the density is 2474 kg/m³.

The vertical closed-loop ground source heat exchanger installation is comprised of 6 boreholes with a diameter of 0.13 m (5.25 in) that are in a 2 by 3 configuration with 7.62 m (25 ft) spacing. Each borehole contains an HDPE U-bend pipe loop with nominal diameter of 25 mm (1 in), and is grouted with a mixture of 4020 sand and bentonite.

The nominal cooling capacity of water-to-water heat pump used in the system is 35 KW (10 tons) with the design output temperature of the fluid in the range 38-55°C (100-130°F). The working fluid is a mixture of water and propylene glycol, and circulated at a rate of approximately 1.3 l/s (21 GPM) through the ground-loop system.

The bridge anti-icing system has initially been operated with on-off control of the heating system. The objective has been to maintain the bridge surface temperature in the range of 4.4-5.5°C in case of risk of icing or snowfall. In recharge mode, it is switched on when the surface temperature is higher than 32.2°C (90°F) and switched off when the temperature falls to 31.1°C (88°F).

- Weather Data

The Oklahoma Mesonet is a collaborative project between Oklahoma State University and the University of Oklahoma. The Mesonet is a network of 114 weather stations distributed throughout Oklahoma. The measurements are packaged into "observations" every 5 minutes, then the observations are transmitted to a central facility every 15 minutes, 24 hours per day year-round. Nearly real-time weather data is available to customers, including schools, over the internet. The Stillwater Mesonet

Station is about 1 mile from the medium-scale heated bridge deck. Its data is assumed as same as that at the experimental site.

Weather data is rearranged and contained in a boundary variable file for simulations in the HVACSim+ environment. The data set has information about solar radiation, dry-bulb and dew point temperatures, precipitation, weather indicator, wind speed, and solar angle. The sky temperature required for the system simulation is calculated using the available weather data.

- Experimental data

Experimental measurements of mass flow rate and inlet temperature of the heat exchange fluid are used as inputs for the model validation. The simulation results of the top surface temperatures and the exit fluid temperatures are compared against the measured data. A point worth noticing is that thermocouples used to measure the surface temperature are just slightly below the slab surface. They actually reflect the temperature slightly below the top slab surface, which is expected to be higher than the top surface temperature in the winter heating mode and lower in the summer recharge mode.

4.3. System Simulation Results and Discussion

The bridge deck system under investigation is the OSU bridge deck. In the following section, a brief examination of the thermal resistance error caused by the transfer functions is given. This is followed by a detailed study of the simulation results with real weather conditions. The system is simulated with two events. One is for the recharge case from 8/1/2000 19:06:00 to 8/14/2000 08:51:06, and the other is snow event of Dec.30, 2001 for heating case.

4.3.1. Thermal Resistance Error

The error caused by the transfer functions calculation is examined with simple boundaries. The top and bottom surfaces are maintained at 10°C, while the average fluid temperature of 40°C and a constant convective heat transfer coefficient of 340.0 W/m² is specified at the boundary of inside pipe wall. Test results and error analysis are listed in Table 4.1 and 4.2.

Table 4.1

Comparison of Simulation Results of OSU Bridge Deck under Simplified Boundary Conditions

Test Condition		Comparison Model	Results			Conclusion
				Comparison Model	QTF	
Surface Temperature [°C]	10.0	BFC-FV model	Steady State Flux at the Outer Pipe wall [W/m ²]	417.62	380.86	Relative error in steady state flux: 8.8%
Fluid Temperature [°C]	40.0		Outer Pipe Wall Temperature [°C]	28.08	--	
Heat Transfer Coefficient at the Inside Pipe Wall [W/m ² -K]	340.0		Source Temperature [°C]	--	29.31	

Table 4.2

List of Thermal Resistances in the Numerical Simulation of OSU Bridge Deck [K-m²/W]

(Notation is consistent with that described in section 3.4.2.2)

QTF Model		BFC-FV Model	
R_fluid-to-Src	0.028	R_fluid-to-outer pipe wall	0.028
R_Src-to-Slab	0.051	R_Slab	0.043
Total Resistance	0.079	Total Resistance	0.071

The results show that the QTF coefficient calculation over-predicts the thermal resistance of the bridge deck. In turn, this results in errors in the simulation.

4.3.2. Summer Recharge

Simulation results obtained from the QTF model and the FD model are plotted against experimental data in Figure 4.1 and 4.2. Figure 4.1 shows the comparison of the top surface temperatures, and the exit temperature of heat exchange fluid is plotted in Figure 4.2. Time steps used in the simulations are 6 min/step for the FD model and 15 min/step for the QTF model.

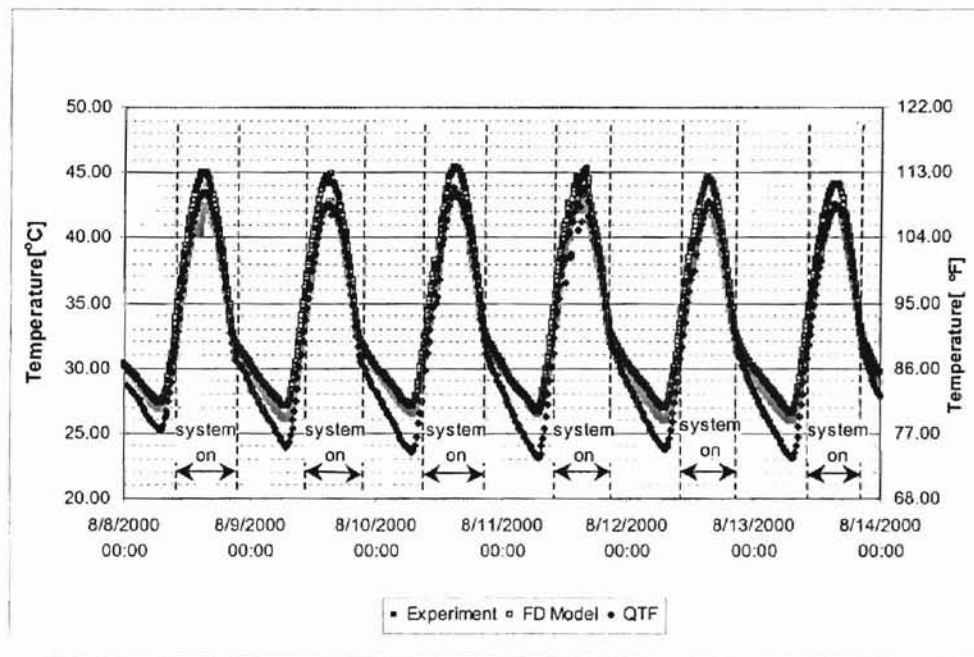


Figure 4.1: Comparison of experimental data and model predictions for top surface temperatures in summer recharge mode

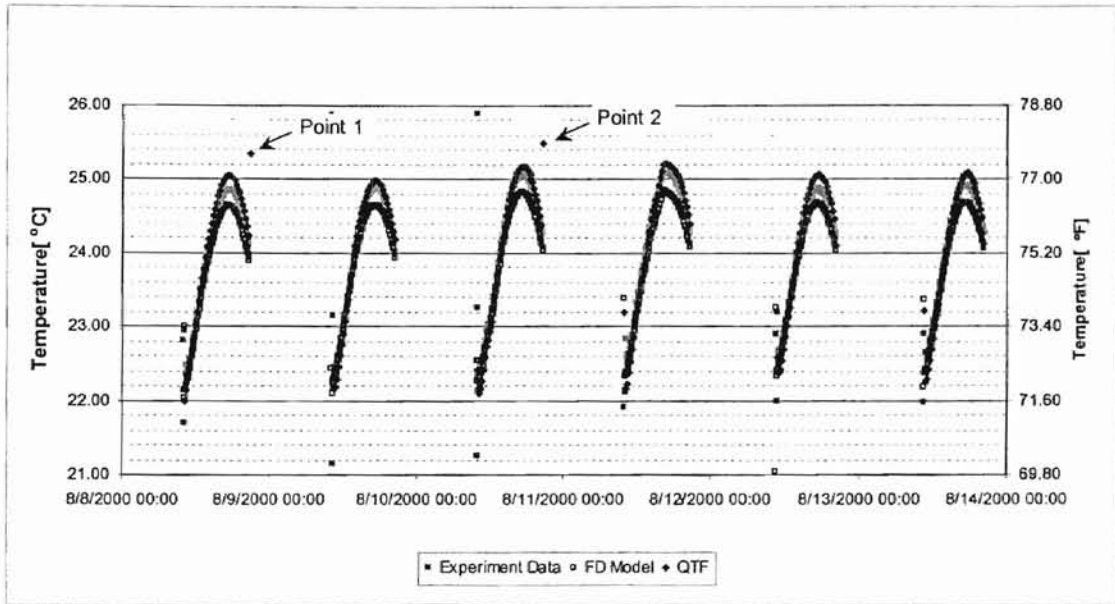


Figure 4.2: Comparison of experimental data and model predictions for exit fluid temperatures in summer recharge mode

As can be seen from Figure 4.1, the predictions of the top surface temperature obtained from numerical models agree well. The maximum temperature difference is about 3.5°C , occurring at the minimum daily temperature. The temperature difference is significantly less when the system is on.

The QTF model shows a good prediction of the exit fluid temperature as can be found from Figure 4.2. It's easy to observe that at Point 1 and Point 2 labeled in Figure 4.2, the QTF model over-predicts the exit fluid temperature. These two points depict the last time step of the intermittent system operations. The over-prediction is caused by the inconsistent time step used in the QTF model and the boundary file. The measuring interval in time is 6 min in this case, much shorter than 15 min/step used in the QTF model. The system was turned off before Point 1 or Point 2 occurs, which shows in the

boundary file that the mass flow rate of the fluid becomes zero. Under this circumstance of discontinuous change in the mass flow rate, the MODSIM generates a new flow rate by interpolation, which is lower than the actual flow rate. In the case we studied, with this low flow rate, the flow in the pipe is laminar, not as turbulent as it should be. Thus, it retards the heat transfer at the inside pipe wall, and the temperature of pipe wall tends to approach the temperature of the surface in contact with bridge deck. It over-predicts the temperature at the source location, and so over predicts the exit fluid temperature. To further demonstrate the phenomenon, the mass flow rate is artificially modified by maintaining it as a constant value until time of Point 1 or Point 2. The comparison of exit fluid temperatures and the top surface temperature are re-plotted in Figure 4.3 and Figure 4.4. With the modified flow rate, the over-predictions of the exit fluid temperature disappear, and the predictions of the top surface temperature right after the system turns off are increased about 0.13°C , though, it is difficult to observe from Figure 4.4.

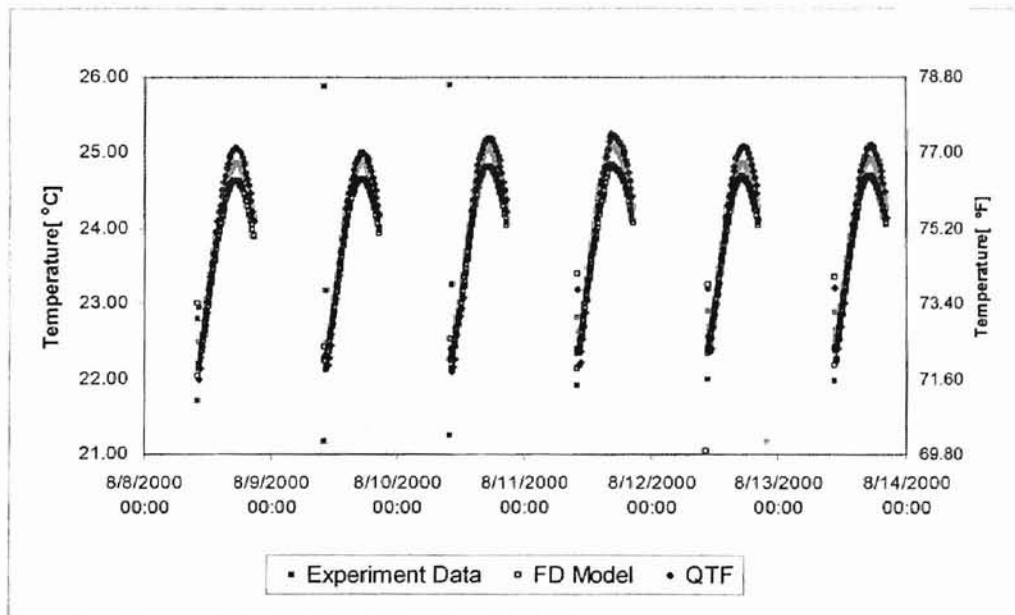


Figure 4.3: Comparison of experimental data and model predictions for exit fluid temperatures in summer recharge mode (with modified mass flow rate)

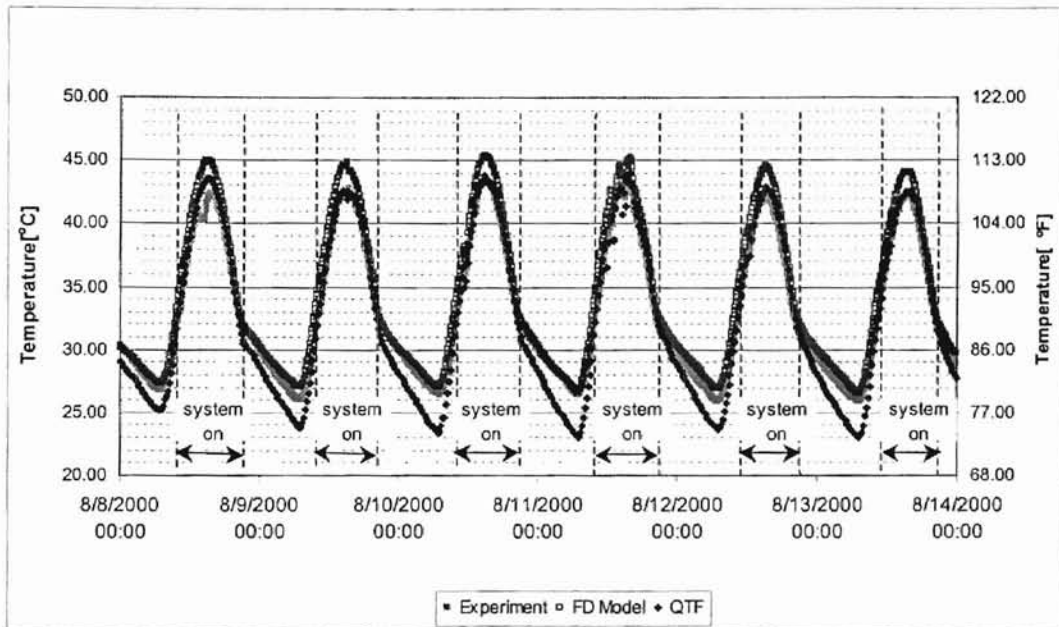


Figure 4.4: Comparison of experimental data and model predictions for top surface temperatures in summer recharge mode (with modified mass flow rate)

The inconsistency in the time step may be solved by picking a QTF time step that is an integral number of measurement time steps, or shortening the time step used in the transfer functions generation while maintaining stability. The instability was noted whenever the Fourier number exceeded a value of 0.3 for the sublayer defined as the region between the source plane and the closest surface boundary (Strand 1995). The instability could be caused by the Laplace solution or the method of back substitution for determining the source temperature (Strand 1995). For the cases we studied, the minimum interval of time step is nearly 15 minutes. It's decided by the physical properties of the material, and highly sensitive to the heat capacity. With a large heat capacity, like heavyweight concrete, a larger interval of time step is required to ensure the stability. 15 minutes per step is almost the minimum interval in time that can be used for

this bridge deck. An easy way to check the two-dimensional transfer functions is the test case described in the section 3.4.2.1. Besides this test, other fundamental tests, such as the summation of the transfer functions, are required.

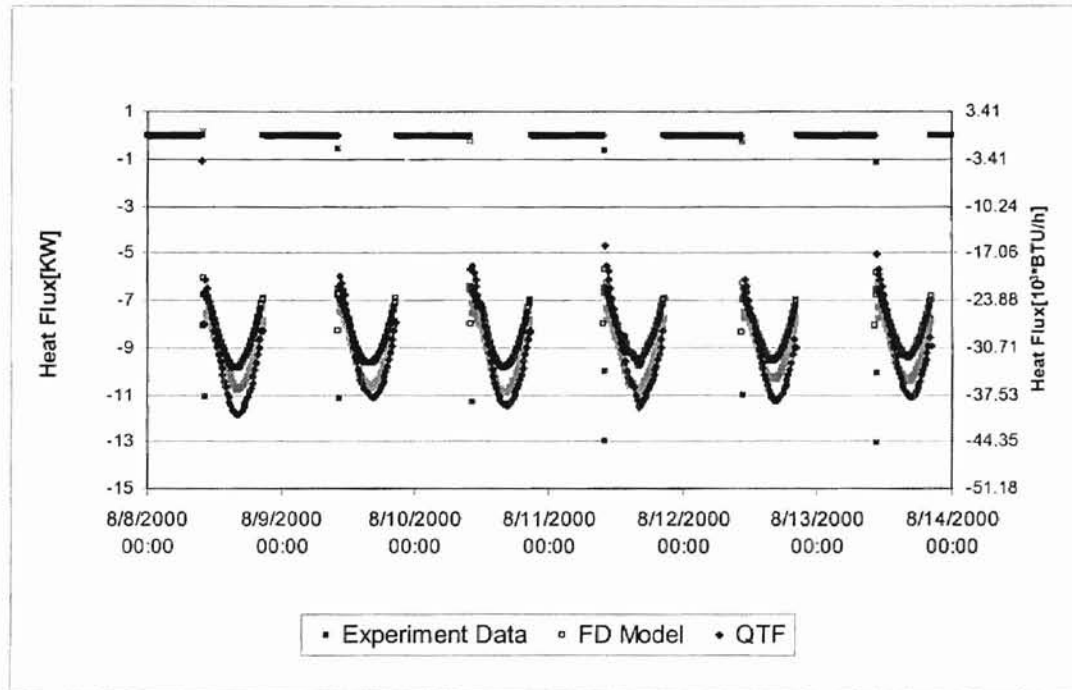


Figure 4.5: Comparison of experimental data and model predictions for heat transfer rates in summer recharge mode (with modified mass flow rate)

Figure 4.5 shows the comparison of heat transfer rates of the heat exchange fluid. Figure 4.6 shows the percentage error of the QTF predictions to experimental data of heat transfer rates of the heat exchange fluid. As stated in the previous section, the time interval used in the QTF model is 15 minute per step, much larger than that used in the measurement – 6 minute per step. To obtain the relative error varying with time, a linear interpolation is applied to the measured data. However, as can be observed from Figure 4.5, the measurements fluctuate dramatically when the system starts. The linear

interpolation may not be valid at system startup, and it results in larger percentage error at the beginning of system starts. Most relative error is within the range $\pm 10.0\%$.

Generally, the QTF predictions show a good agreement with the measurements. The cumulative percentage error is around 2.4% for the period shown in the figures.

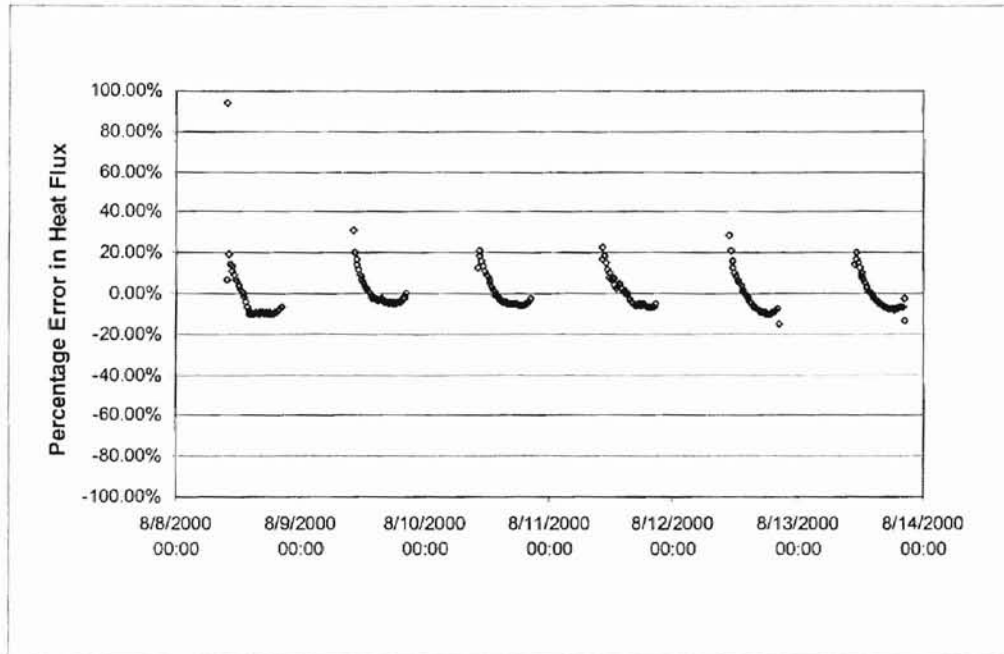


Figure 4.6: Percentage error of the QTF predictions to experimental data on heat transfer rates in summer recharge mode (with modified mass flow rate)

4.3.3. Winter Heating

Weather data for a winter heating event are plotted in Figure 4.7. The snow precipitation rate is given as equivalent mm of water. As accurate precipitation data in freezing conditions is not available from the automated experimental bridge site, the snow precipitation plotted is the average over time (only the total precipitation for the snow event is available). Simulations start from 12/24/2001 00:00.

(a) SI Units

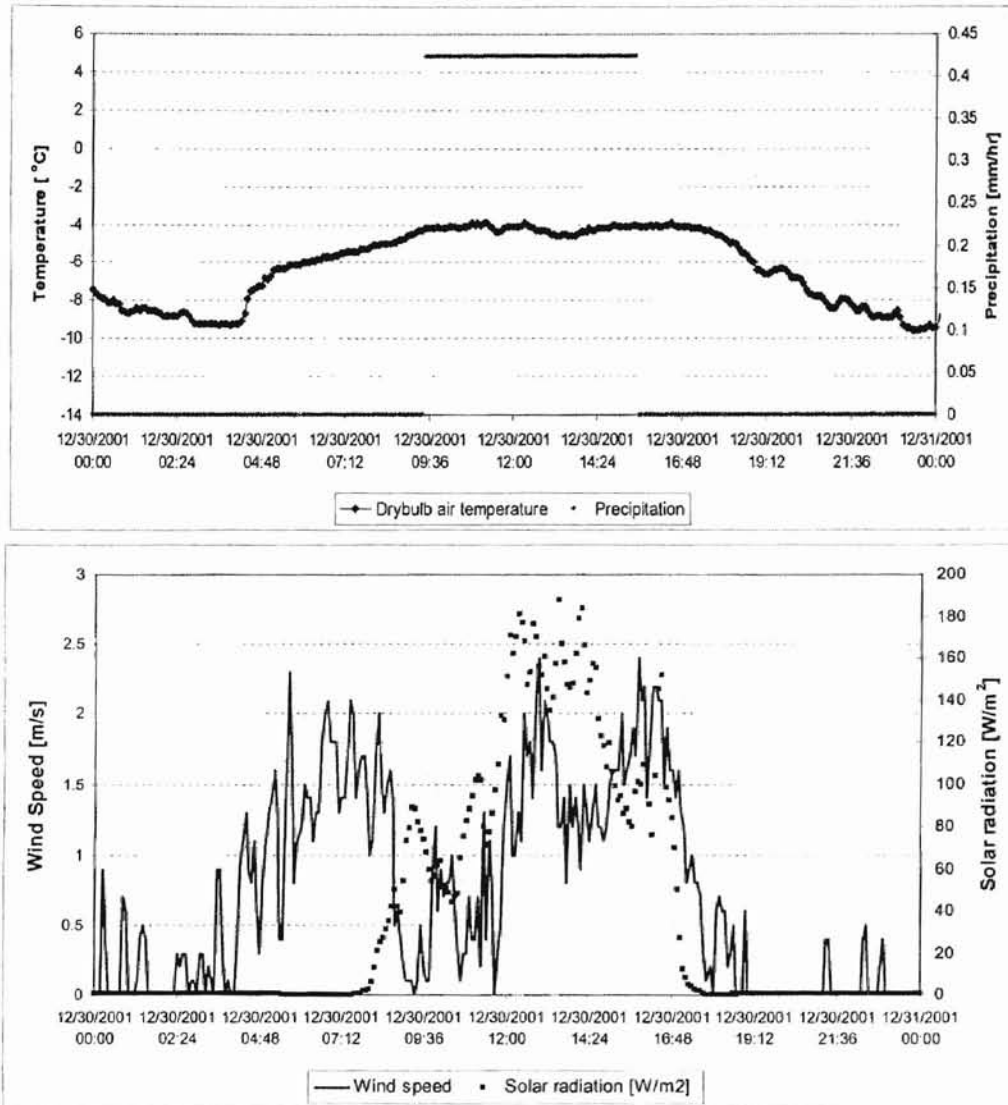


Figure 4.7 (a): Weather information for snow event of Dec.30, 2001 (SI Units)

(b) IP Units

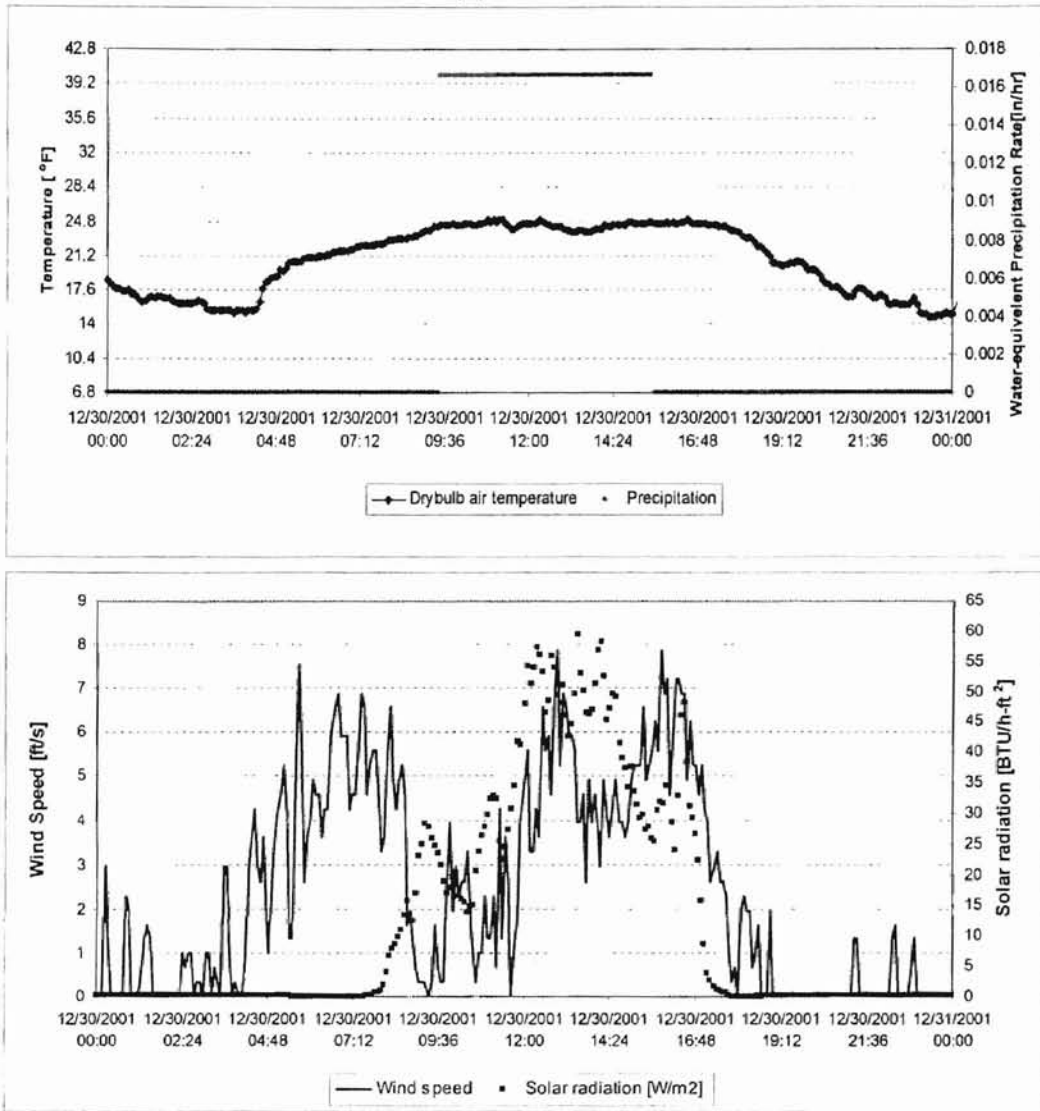


Figure 4.7 (b): Weather information for snow event of Dec.30, 2001 (IP Units)

In the simulation, the QTF model uses an estimated value of 0.8 for the snow albedo. This value as stated in Chapter 3 is recommended for a new snow surface. The whole simulation takes around three minutes, much less than time (over 12 minutes) needed for a similar case simulated using the BFC-FV model. Simulation results obtained from the QTF model are plotted against experimental data and the results from the FD model. In the following section, initial simulation results are given. It's followed by the

discussion of possible corrections and the presentation of results after making individual modification. Last come the final results with recommended corrections. Time interval is 5 min/step for the measurement and 15 min/step for the QTF model.

Initial simulation results

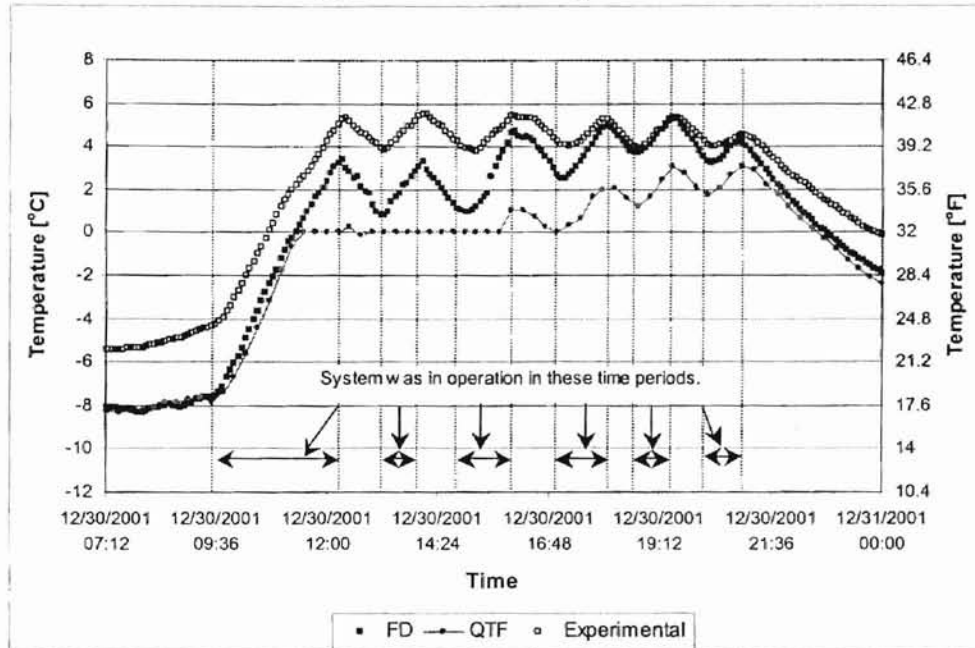
Figure 4.8 shows the initial simulation results. The discrepancy in temperature between the experimental measurements and the numerical predictions are obvious. However, at the beginning of storm and several hours after storm, the results obtained from the QTF model agree with those from the FD model. One possible cause of the initial discrepancy is the inaccuracy of weather data shared by two numerical models, like sky temperature. Inaccuracy in calculating the convection and radiation occurring at the surfaces is probably another cause. Two numerical models use different formulas for the convection and radiation calculation on the slab surfaces. There have been many different methods published for calculating the convective coefficient, with much disparity among them. Identifying the best correlation for the bridge deck heating case may require more future work.

After the storm starts, one cause of the discrepancy in temperature between the numerical solutions and the experimental measurement is the assumed constant snow precipitation (rather than actual time-varying snow precipitation). Another possible cause is that the experimental temperature measurements are made slightly below the slab surface, and are expected to be higher than the top surface temperature in the winter.

However, there is a big difference between the numerical solutions after the surface temperature reaches the freezing point. The restriction in the QTF model, that the surface temperature would be maintained at the freezing point when snow, ice, or snow slush was melting on the surface, makes the surface temperature keep as constant (0°C) for a period. After the surface is clean of snow and slush, the top surface temperature obtained for the QTF model creeps up. While in the FD model, without the restriction to maintain the surface at the freezing when the slab was covered by snow or ice, the surface temperature creeps up continuously. The surface temperatures fluctuate with the intermittent system operations as shown in Figure 4.8 (a).

The numerical solution on the exit fluid temperature obtained for the QTF model agrees well with the experimental measurements as can be observed from Figure 4.8 (b).

(a) Slab surface temperature



(b) Exit fluid temperature

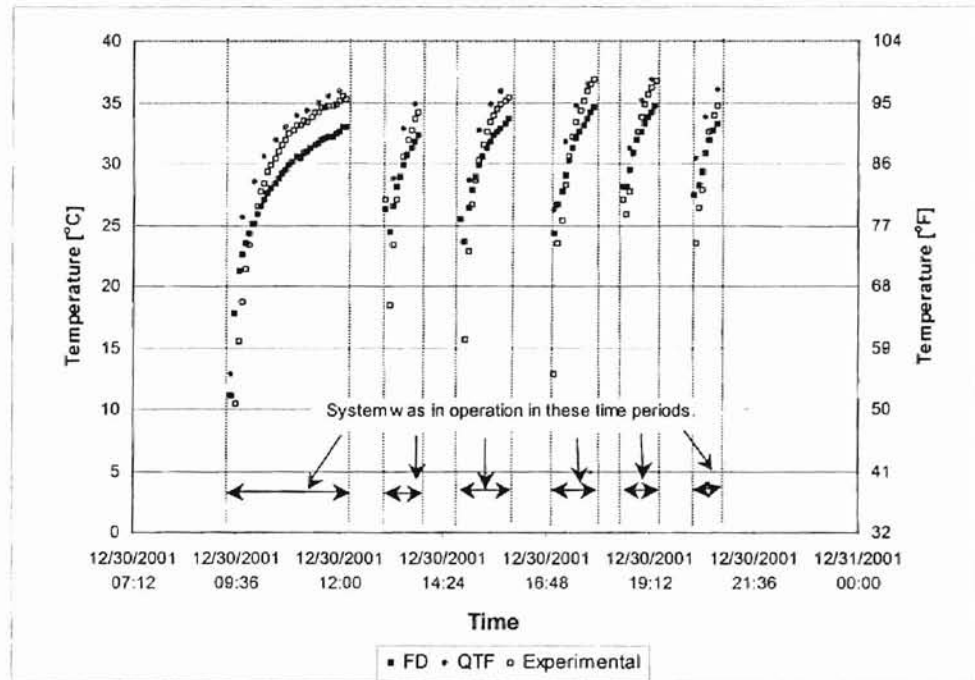


Figure 4.8: Comparison of initial model predictions against experimental data in winter heating case (snow event of Dec.30, 2001, snow albedo=0.8)

Possible corrections and simulation results

Several corrections are considered in the following section. These include the correction of sky temperature, the estimation of the value of snow albedo, and the thermal properties of saturated slab surface.

As described in Chapter 3, sky temperatures are calculated based on other available weather data, such as dry-bulb air temperature, humidity ratio, cloud cover factor, etc. However, the cloud cover fraction is not easy to measure accurately. The cloud cover data used in the validation is obtained by combining cloud cover data from the National Virtual Data system with the data from the Oklahoma Mesonet (Liu *et al.* 2002). Inaccuracies in estimating the sky temperature lead to deviations in the surface temperature calculation especially during nights when long-wave radiation has a greater proportion in the heat transfer rate occurring at the surfaces. The modified sky temperatures used in the following simulations are calculated by the Brown sky temperature model with the assumption that from 24 hours before the snow event till the end of the storm, the cloud fraction is assumed as 1.0.

Snow albedo (snow reflectance) determines the proportion of solar radiation absorbed by the snow/slush. The estimated value of snow albedo used in this case is 0.8 assuming a new snow surface covering the slab during precipitation. This approximation is not necessarily accurate at the end of the snow-melting process, when the slab surface is warm enough to melt the precipitation as soon as it falls on the slab, and the surface is covered by the slush. Another lower estimation of snow albedo, 0.38, is used to illustrate

the effect of snow albedo estimation. This lower estimation of snow albedo makes the snow surface have the same absorptance as slab surface. Besides two estimations, a time varying snow albedo calculated by the QTF model is used for further analysis.

The following section also describes the effect of the change in the physical properties of the slab when it's saturated. During the snow-melting process, the slab surface may be wet and saturated. The conductivity and specific heat of the concrete in saturated condition are different from values of dry concrete. For instance, for the material currently used, the specific heat varies between 898 and 1037 J/kg-K when it's at oven-dry, normally dry, and saturated conditions; the change is over 10%.

The correction of physical properties is achieved by switching transfer functions generated by different inputs properties in the simulation. (This is a rough approximation; it doesn't correctly account for the history). An estimation of time required for the surface to reach saturated is used. When the surface is wet for 45 consecutive minutes, the slab surface is considered saturated, and the set of transfer functions generated by using the saturated concrete properties are used in the simulation. Once the slab surface is dry, the set of transfer functions generated by using the concrete properties under the dry condition are restored.

The following section shows the results after correction.

- Correction in the sky temperature

The improvement is obvious as can be found from Figure 4.9. It demonstrates that the prediction of sky temperature plays a significant role in calculating the long-wave radiation with the environment. This, in turn, affects the prediction of surface temperature. A good estimate of sky temperature before the storm hits improves the surface temperature prediction during that period, and with better temperature and flux histories, the surface temperature prediction during the storm is improved. Future improvements in measurement and predicting the sky temperature would be useful.

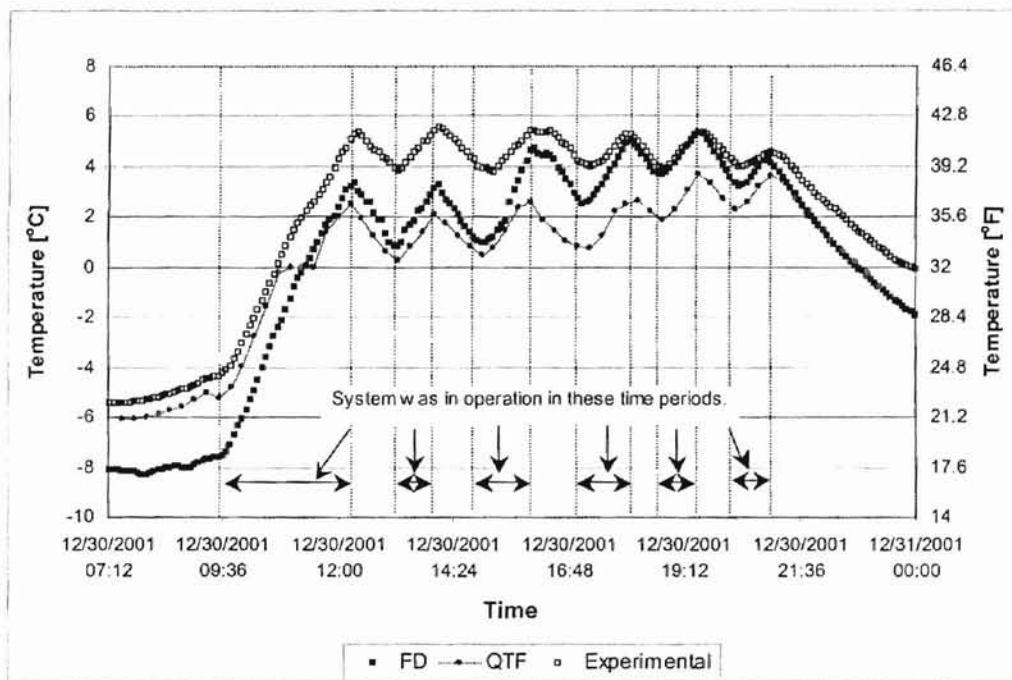


Figure 4.9: Effect of the sky temperature correction on the top surface temperature predictions in winter heating mode (snow event of Dec.30, 2001, snow albedo=0.8)

- Sensitivity to snow albedo

As described in Chapter 3, there are two ways to set the value of snow albedo in the QTF model. One is to use a constant estimate of the snow albedo, and the other is to calculate a time varying snow albedo by following the procedure described in the section 3.2.2.1.

Figure 4.10 shows the top surface temperature distribution under a lower constant snow albedo with sky temperature correction. Comparing Figure 4.9 and 4.10, it's easy to observe that with a lower snow albedo, the prediction of the top surface temperature obtained from the QTF model shifts up. It can be explained by the larger portion of solar radiation that has been absorbed by the snow surface with a lower snow reflectance. It demonstrates that the prediction of top surface temperatures is sensitive to the value of snow albedo.

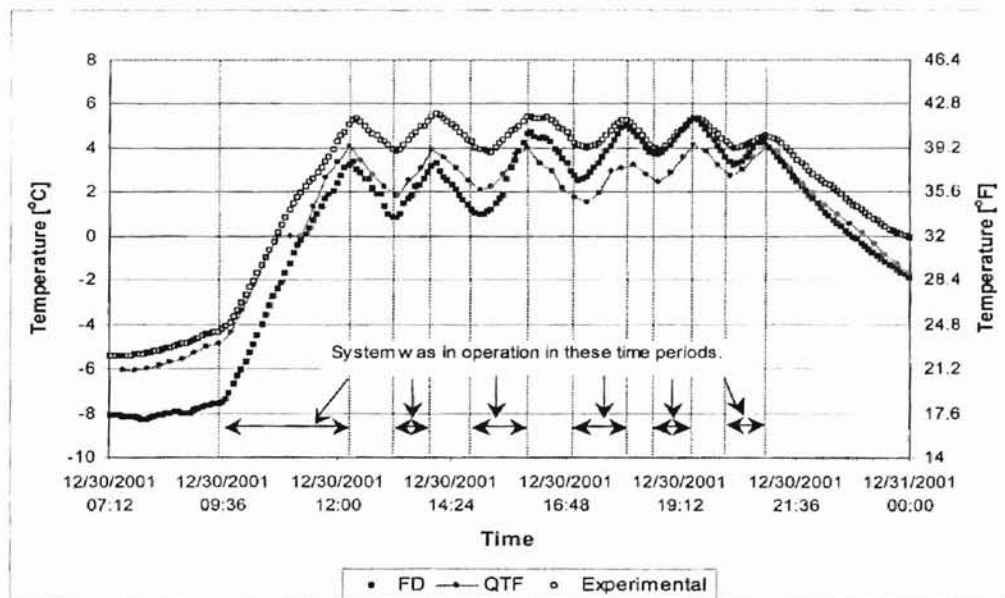


Figure 4.10:Effect of the value of snow albedo on the top surface temperature predictions in winter heating mode (snow event of Dec.30, 2001, snow albedo=0.38, with sky temperature correction)

Figure 4.11 shows the top surface temperature distribution under a time varying snow albedo with sky temperature correction. No obvious difference in the QTF results can be observed from Figure 4.10 and 4.11, except that it requires less time to clear the snow with a time varying snow albedo. It implies that for a snow slush surface, the value of 0.38 may not be a good estimation, and the actual value is lower. The similarity of the two results also implies the snow precipitation is not high enough to accumulate a new snow surface. From this analysis, the method of time varying snow albedo is preferable, unless a good estimation of snow albedo available.

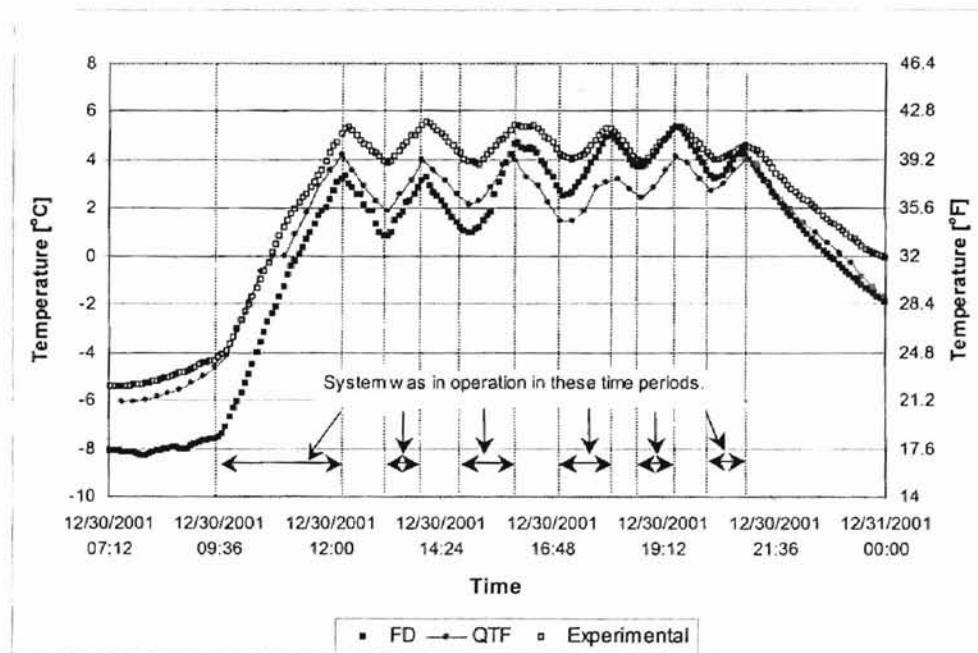


Figure 4.11: Comparison of experimental data and model predictions for slab surface temperatures in winter heating mode (snow event of Dec.30, 2001, time varying snow albedo, with sky temperature correction)

- Effect of wet slab surface

Figure 4.12 shows the effect of saturated surface condition. The temperature fluctuation during the storm is more obvious as compared with Figure 4.8 (a). The larger heat capacity implied in the transfer functions of saturated slab may over-estimate the energy that has already been stored in the slab, and leads to a better snow-melting rate. However, use of the saturated properties for the entire history is not consistent with the reality. Future work on finding a more reasonable way to account for the effect of physical property changes of the slab may be useful.

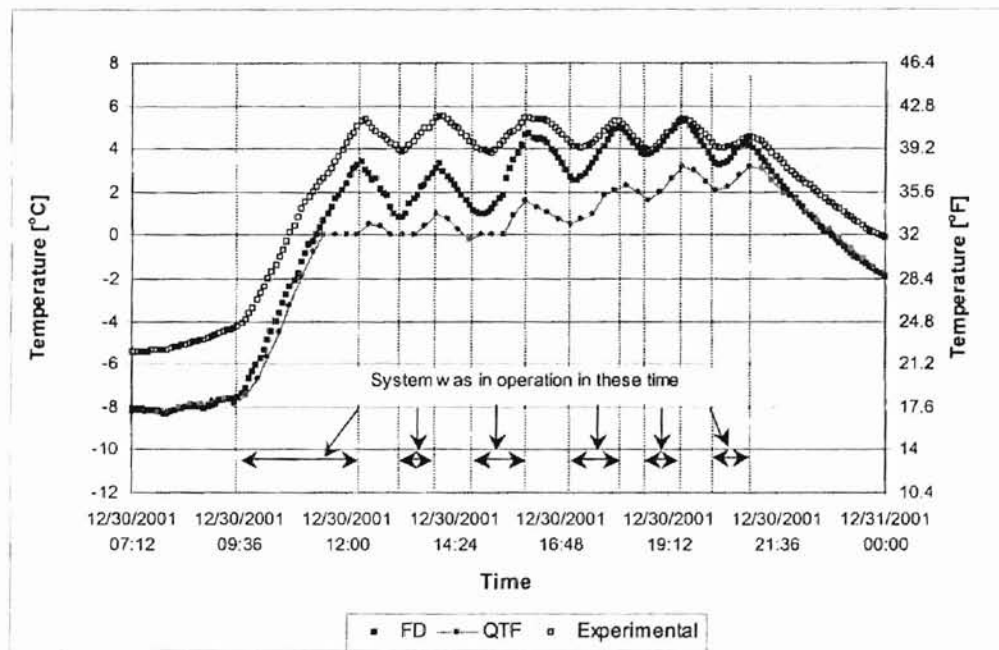


Figure 4.12: Comparison of experimental data and model predictions for slab surface temperatures in winter heating mode (snow event of Dec.30, 2001, estimated snow albedo = 0.8, no sky temperature correction, with consideration of saturated surface condition)

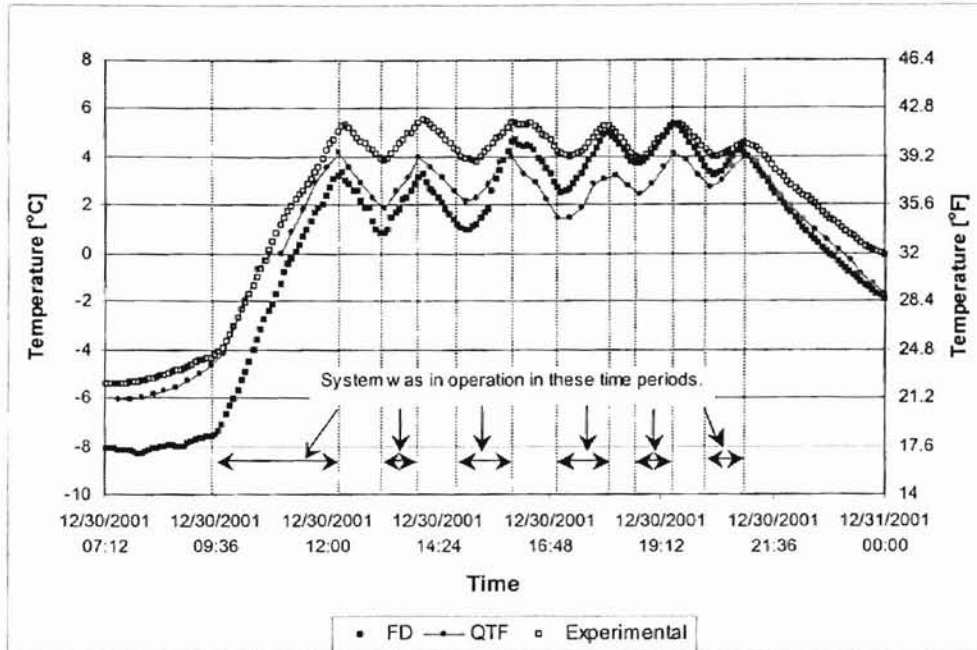
Final results

Figure 4.13 serves as the final simulation results with the consideration of the correction in the sky temperature and a time varying snow albedo. The improvement is obvious as compared with Figure 4.8.

The surface temperature obtained from the QTF model agrees with the measurements when there is no precipitation. Also, a good agreement can be observed before the surface temperature reaches the freezing point after the storm starts. The discrepancy during snow precipitation is obvious, and as stated in the previous section, it may be caused by the make-up snow precipitation data and the location of thermocouples. After the storm, the temperature comes to a new low at around 17:00. It can be explained by the fact that the unit cloud cover assumption is ended with the storm, and a larger radiation loss occurs at the surface. Without the correction of the sky temperature, the predictions from the QTF model tend to agree with those from the FD model.

The exit fluid temperature predictions agree well with experimental data, and it implies a good agreement in the heat transfer rate in the heat exchange fluid side. As can be observed from Figure 4.13 (b), the start/stop times of the bridge heating don't quite match the experimental data. This is caused by the large time step used in the QTF model.

(a) Slab surface temperature



(b) Exit fluid temperature

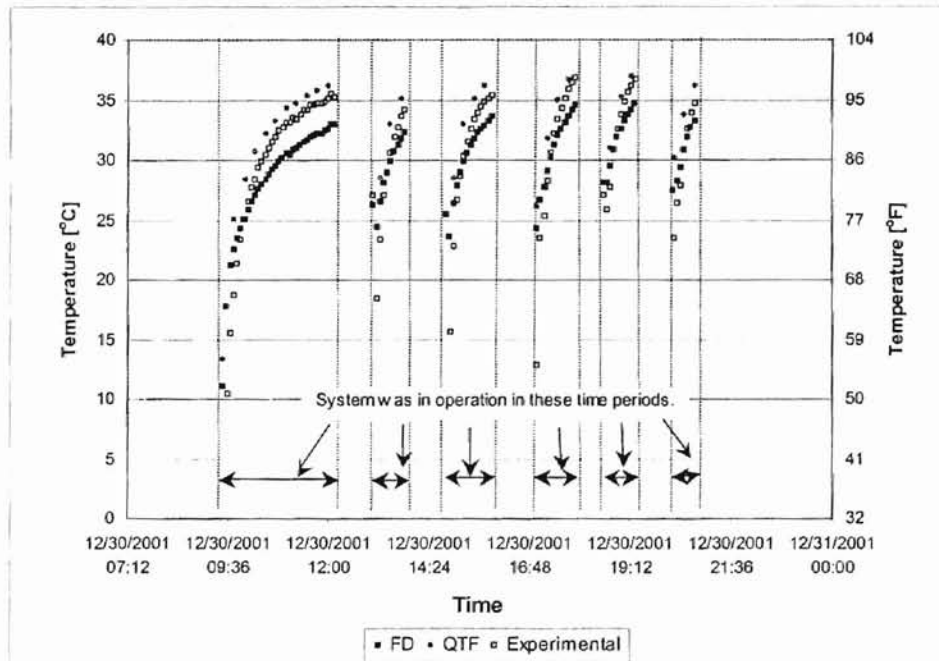


Figure 4.13:comparison of experimental data and model predictions in winter heating mode (snow event of Dec.30, 2001, time-varying snow albedo, with the sky temperature correction and no consideration of saturated surface condition)

4.4. Summary

In this study, the QTF model is validated by the experimental data for winter heating and summer recharge two cases. The bridge deck heating system under investigation is the medium-scale bridge deck in OSU. Within the limited scope of the study, the following specific conclusions can be drawn:

1. For summer recharge cases, the QTF model predicts the behavior of the bridge deck system quite well. Some jumps of exit fluid temperature may occur when the time step used in the QTF model is not consistent with the time interval of time-varied boundary information, such as mass flow rate, the inlet fluid temperature and precipitation. The QTF model tends to under-predict the surface temperature at nighttime.
2. Winter heating cases are relatively complex because of the complex boundary conditions that occur with precipitation. Some estimated snow/slush properties are used in the simulation. The prediction of the exit fluid temperature generally agrees well with experimental data. The prediction of the surface temperature by the QTF model has obvious discrepancies with the experimental data. It may be caused by inaccuracy in weather data, the different thermal properties of the slab surface in saturated condition, and the estimated value of snow albedo used in the simulation. The study finds that the snow-melting process is sensitive to the snow albedo.
3. The QTF model has advantages and disadvantages. The QTF model has a higher computational efficiency compared to the BFC-FV model, and validation results agree well with experimental data. However, the transfer

functions are generated by another program in advance. The limitation is that, for the QTF model, the time step must be fixed in the simulation to be the same as that used in the transfer functions generation. The variable time step is not allowed in the application of the QTF model. Limited by the transfer functions, the QTF model can't provide detailed two-dimensional temperature and flux distributions. Only average values are available.

This work opens a number of areas for further study. The validation in this work is not sufficient to draw a general conclusion. Further research is suggested in the following areas:

- Additional work in sky temperature estimation would be useful.
- Additional experimental work in snow-melting cases is required. These may include the measurement of snow albedo, the sky temperature, detailed record of surface conditions (i.e. dry, wet, snow/slush), and thermal properties of slab surface in saturation.
- Additional validation of the QTF model, using experimental data and a wider range of transient weather condition, would be useful.
- The inconsistency in the time step may be solved by picking a QTF time step that is an integral number of measurement time steps, or shortening the time step used in the transfer functions generation while maintaining stability.
- Validation of the QTF model for other related applications, such as modeling the performance snow melting systems in pavement, would be useful.

5. Conclusions and Recommendations

5.1. Conclusions

As the size and the number of applications of hydronic and electric-cable snow-melting systems increase, economic design and optimization become increasingly important. Considerable savings in cost and effort could be realized if the performance of such systems could be easily simulated and analyzed. The system modeling and simulation approach is a powerful tool to study and analyze the system performance of several possible designs. Various system configurations, component sizes, and different control strategies could be studied using the system simulation approach to arrive at cost efficient design solutions. Both short and long-term system performance could be easily simulated using validated numerical models.

This study uses the simulation approach to analyze the applications of hydronic and electric-cable snow-melting systems. The challenges associated with the analysis originate from the transient nature of weather and the intermittent operation of systems. The objectives of this study were threefold: (1) to examine the effects of different parameters on transient system performance, (2) to develop a design and simulation tool for modeling the transient performance of a hydronic and electric-cable snow-melting systems by time series method (QTFs), and (3) to validate the transient QTF model by experimental data.

Chapter 2 of this thesis has presented a parametric study of hydronic and electric-cable snow-melting systems. The effects of two phenomena on the transient snow-melting system behavior have been investigated. One is back and edge losses, and the other is transient design conditions and operation of the snow-melting system. The studied parameters include pipe spacing, pipe depth, pipe diameter, insulation level, soil conductivity, location, and storm. The transient load requirements are not closely correlated to the steady-state loads. More than any other factor, the transient behavior is most sensitive to the storm itself, and then to pipe spacing. As the tubes are placed deeper, the effect of spacing is less important. The heat flux requirements at the source location are almost insensitive to the soil conductivity and the insulation level. Insulation is useful for reducing back losses.

Chapter 3 of this thesis has described the development and validation of a model (the QTF model) for simulating the transient performance hydronic and electric-cable snow-melting systems by time series method (QTFs). The QTF model has been coupled to HVACSim+ environment. The simulation results are compared with the analytical solution, and the results from other software. It's found that the transfer functions calculator has inaccuracies in generating the transfer functions, which leads to 8%~15% error in the steady state flux in the simulation.

Chapter 4 discusses the validation of the QTF model developed in Chapter 3 by experimental data obtained from a medium-scale bridge deck located at OSU. The simulations have been done under real transient weather conditions with operation and

construction parameters from a working system. Within cases that have been studied, the QTF model gives good predictions on the exit fluid temperature with maximum error of around 0.3°C (0.54°F). For the surface temperature, the simulation results agree with the experimental data, except for the situation of snow precipitations. The maximum error in the case of summer recharge is 3.5°C (6.3°F), occurring when the system is off. When system is on, the error is significant less, and the QTF model gives accurate predictions on the surface temperature. The cumulative error of the energy recharged to the ground is around 2.4% compared to the experimental data. For winter heating case, the surface temperature predictions agree with the experimental measurements after the correction of the sky temperature is applied. However, there is a big difference (around 2°C (3.6°F)) in surface temperature predictions during the snow precipitation. This difference implies a different surface condition on the slab. The assumed constant snow precipitation rate is one cause of this difference. Another possible cause is that the experimental temperature measurements are made slightly below the slab surface, and are expected to be higher than the slab surface temperature in the winter heating cases. Results show that the snow-melting process is sensitive to the snow albedo estimate. More experimental work is needed for validation of surface condition in snow-melting cases.

5.2. Recommendations

Though the work presented in this thesis is a step towards a better understanding of transient performance of performance hydronic and electric-cable snow-melting systems, its scope is limited. Further research is suggested in the following areas:

- Additional experimental work on snow-melting cases would be helpful.

- Additional work on sky temperature estimation with consideration of cloud cover data would be helpful.
- Additional validation of the QTF model, using experimental data and a wider range of transient weather condition, would be useful.
- Validation of the QTF model to other applications, such as modeling the performance snow melting systems in pavement, would be useful.

REFERENCES

- ASHRAE Handbook — Fundamentals, 1993. Atlanta, GA: American Society of Heating Refrigerating and Air-conditioning Engineers Inc.
- ASHRAE Handbook — Applications, 1999. Atlanta, GA: American Society of Heating Refrigerating and Air-conditioning Engineers Inc.
- ASHRAE Toolkit for Building Load Calculations —Manual, 2001. Atlanta, GA: American Society of Heating Refrigerating and Air-conditioning Engineers Inc.
- Brown, D. 1996. Development of an improved meteorological preprocessor and applied dispersion model. Ph.D. dissertation, University of Illinois at Urbana-Champaign, Department of Mechanical and Industrial Engineering
- Chapman, W.P., 1952. *Design of Snow Melting Systems*. Heating and Ventilating, Vol. 49(4), pp: 96-102.
- Chapman, W.P., 1952. *Design of Snow Melting Systems*. Heating and Ventilating, Vol. 49(11), pp: 88-95.
- Chapman, W.P. and S. Katunich, 1956. *Heat Requirements of Snow Melting Systems*. Heating, Piping & Air Conditioning, Vol. 28(2), pp: 149-153.
- Chapman, W.P., 1957. *Calculating the Heat Requirements of Snow Melting Systems*. Air Conditioning, Heating and Ventilating, Vol. 54(8), pp: 81-96.
- Chiasson, A. 2000. *Advances in Modeling of Ground-Source Heat Pump Systems*. M.S. Thesis. Oklahoma State University. Stillwater, OK. (Also available at http://www.hvac.okstate.edu/pdfs/chiasson_thesis.pdf).
- Clark, D.R., 1985. *HVACSim+ Building System and Equipment Simulation Program – Reference Manual*. National Bureau of Standards. NBSIR 84-2996.
- Gnielinski, V. 1976. *New equations for heat and mass transfer in turbulent flow pipes and ducts*. International Chemical Engineering, Vol. 16, pp: 359-367.
- Gordon, W.J. and Hall, C.A. 1973. *Construction of curvilinear coordinate systems and applications to mesh generation*. International Journal for Numerical Methods in Engineering, Vol. 7(4), pp. 461-477.
- Incropera, F.P., and D.P. Dewitt. 1996. *Introduction to Heat Transfer*, pp: 332-334. New York: Wiley & Sons
- Kilkis I. B. 1994a. *Design of embedded snow-melting systems. Part 1, Heat requirements - an overall assessment and recommendations*. ASHRAE Transactions, Vol. 100, Part 1, pp: 423-433.
- Kilkis I. B. 1994b. *Design of embedded snow-melting systems. Part 2, Heat transfer in the slab - a simplified model*. ASHRAE Transactions, Vol. 100, Part 1, pp: 434-441.
- Kondo, J., and T. Yamazaki 1990. *A Prediction Model for Snowmelt, Snow Surface Temperature and Freezing Depth Using a Heat Balance Method*. Journal of Applied Meteorology 29:375-384.

- Kusuda, T., P.R. Achenbach 1965, *Earth Temperature and Thermal Diffusivities at Selected Stations in the United States*. ASHRAE Transactions, Vol. 71, pp: 61-76.
- Leal, M.R.L.V., P.L. Miller. 1972. *An Analysis of the Transient Temperature Distribution in Pavement Heating Installations*. ASHRAE Transactions, Vol. 78, Part 2, pp: 61-66.
- Liu, X, S.J. Rees, J.D. Spitler. 2002. *Simulation of a Geothermal Bridge Deck Anti-icing System and Experimental Validation*. Submitted to the TRB 82nd Annual Meeting.
- Luikov, A.V. 1968. *Analytical heat diffusion theory*. New York: Academic Press.
- Potter, W.G. 1967. *Electric snow melting systems*. ASHRAE Journal 9(10), pp: 35-44.
- Ramamoorthy, M. 2001. *Applications of hybrid ground source heat pump systems to buildings and bridge decks*. M.S. Thesis. Oklahoma State University, Stillwater, OK. (Also available at http://www.hvac.okstate.edu/pdfs/Ramamoorthy_Thesis.pdf).
- Ramsey, J.W., H.D. Chiang, R.J. Goldstein, 1982. *A study of the incoming long-wave atmospheric radiation from a clear sky*. J. Appl. Meteorol. 21, pp: 566-578.
- Ramsey, J.W., M.J. Hewett, T.H. Kuen, S.D. Petersen. 1999, *Updated Design Guidelines for Snow Melting Systems*. ASHRAE Transactions. 105(1), pp:1055-1065.
- Ramsey, J.W., M.J. Hewett, T.H. Kuen, S.D. Petersen. T.J. Spielman, A. Briefer, (1999), *Development of Snow Melting Load Design Algorithms and Data for Locations Around the world* (ASHRAE 926-RP), Final Report. Atlanta: American Society of Heating Refrigerating and Air conditioning Engineers Inc.
- Rees, S.J., J.D. Spitler, X. Xiao. 2002. *Transient analysis of snow-melting system performance*. ASHRAE Transactions, 108(2). In press.
- Schnurr, N.M., D.B. Rogers. 1970. *Transient Analysis of Snow Melting Systems*. ASHRAE Transactions, Vol. 77, Part 2, pp: 159-166.
- Schnurr, N.M., M.W. Falk. 1973. *Heat Transfer Design Data for Optimization of Snow Melting Systems*. ASHRAE Transactions, Vol. 76, Part 2, pp: 257-263.
- Sparrow, E.M., J.W. Ramsey, E.A. Mass, 1979. *Effect of finite width on heat transfer and fluid flow about an inclined rectangular plate*. Journal of Heat Transfer Vol.101, n 2, pp: 199-204.
- Spitler, J.D., S.J. Rees, D. Xiao. 2002. *Development of an Analytical Verification Test Suite for Whole Building Energy Simulation Programs - Building Fabric (RP-1052)*, Final Report, Atlanta, GA: American Society of Heating Refrigerating and Air-conditioning Engineers Inc.
- Spitler, J.D., S.J. Rees, X. Xiao, M. Chulliparambil. 2001. *Development Of A Two-Dimensional Transient Model Of Snow-Melting Systems, And Use Of The Model For Analysis Of Design Alternatives (RP-1090)*, Final Report, Atlanta, GA: American Society of Heating Refrigerating and Air-conditioning Engineers Inc.
- Spitler, J.D., (2001), Progress Report, Aug. 2001. Oklahoma State University Geothermal Smart Bridge Research Project.

- Stone, H.L. 1968. *Iterative Solution of Implicit Approximations of Multidimensional Partial Differential Equations*. SIAM Journal of Numerical Analysis. Vol.5, No.3, pp: 530-558.
- Strand, R.K. 1995, *Heat source transfer functions and their application to low temperature radiant heating systems*, Ph.D. dissertation, University of Illinois at Urbana-Champaign, Department of Mechanical and Industrial Engineering.
- Strand, R.K., Pedersen, Curtis O. 1997, *Implementation of a radiant heating and cooling model into an integrated building energy analysis program*, ASHRAE Transactions, v 103, n 1, 1997, pp 949-958.
- Tarboton, D. G. and C. H. Luce, 1996. *Utah Energy Balance Snow Accumulation and Melt Model (UEB)*. Utah Water Research Laboratory and USDA Forest Service Intermountain Research Station.
- Thomson, J.F., Waris, Z.U.A., and Mastin, C.W. 1985, *Numerical Grid Generation-Foundations and Applications*. Elsevier Science Publishing Co., Inc.
- Vansant, J.H. 1983. *Conduction heat transfer solutions*. Lawrence Livermore National Laboratory, University of California. UCRL-52863 Rev.1.
- Walton, G.N. 1981. *Passive solar extension of the Building Loads Analysis and System Thermodynamics (BLAST) program*. Technical Report, United States Army Construction Engineering research Laboratory, Champaign, IL.
- Walton, G.N. 1983. *Thermal analysis research program reference manual*. National Bureau of Standards. NBSSIR 83-2655.
- Williamson, P.J. 1967. *The estimation of heat outputs for road heating installations*. Transport Road Research Laboratory (UK): Report LR77. pp: 63.

APPENDIXES

Appendix A: Description of the QTF model in *TYPAR.DAT*

```
548 'QTF MODEL'  
0 0 11 2 22 ! Numbers of SAVED, Diff. Eq., XIN, OUT, PA  
3 'Tamb[C]'  
3 'Tsky [C]'  
3 'Inlet Fluid Temperature [C]'  
4 'Humidity Ratio [kg Water/kg Dry Air]'  
4 'Wind Speed [m/s]'  
4 'Wind Direction [Degree]'  
4 'Solar Gain [W/m2] '  
4 'Solar Zenith Angel [Degree]'  
4 'Snow Precip(Precipitation) [mm/h]'  
4 'Rain Precip(Precipitation) [mm/h]'  
4 'Inlet Mass Flow Rate [kg/s]'  
#  
3 'Exit Fluid Temperature' [C]'  
6 'PipeFlux' [W/Circuit]'  
#  
4 'Latitude'  
4 'Longitude'  
4 'TimeZone'  
4 'Surface Facing'  
4 'Surface Tilt'  
4 'Ground Reflect'  
4 'Surface Emittance'  
4 'Surface Absorptance'  
4 'Number of Circuit'  
4 'null(for future use)'  
4 'Fluid Type' '1 for water, 2 for Propylene Glycol'  
4 '% WT. OF Propylene Glycol in solution used' '%'  
4 'Pipe Length per Circuit' [m]'  
4 'Pipe Spacing' [m]'  
4 'Pipe Outside Diameter' [m]'  
4 'Bridge Width' [m]'  
4 'Bridge Length' [m]'  
4 'Thermal Conductivity of Pipe' [W/m-K]'  
4 'Thickness of Pipe Wall' [m]'  
4 'Insulation at the Bottom 1/yes, 0/no'  
4 'Source Type, 1 for temp. control, 2 for flux control'  
4 'Source Flux [W/m2]'
```

✓

VITA

Xia Xiao

Candidate for the Degree of

Master of Science

Thesis: MODELING OF HYDRONIC AND ELECTRIC-CABLE SNOW-
MELTING SYSTEMS FOR PAVEMENTS AND BRIDGE DECKS

Major Field: Mechanical Engineering

Biographical:

Personal Data: Born in Nanchang, P.R.China, Jan. 31, 1978, the daughter of Yuli Jia and Zhizhen Xiao.

Education: Received Bachelor of Science Degree in Thermal Engineering from Tsinghua University, P. R. China, in May, 2000; Completed the requirements for Master of Science degree at Oklahoma State University in December 2002.

Experience: Employed by the Oklahoma State University from August 2000 to August 2002 as research assistant.

Professional Membership: ASHRAE